12-15-2006

The Mechanical Thermal and Microstructural Behaviors of the Strip Silicates Reinforced Epoxy-based Nanocomposites

Man Wai Ho
University of New Orleans

The Mechanical Thermal and Microstructural Behaviors of the Strip Silicates Reinforced Epoxy-based Nanocomposites

A Dissertation

Submitted to the Graduate Faculty of the
University of New Orleans
in partial fulfillment of the
requirements for the degree of

Doctor of Philosophy
in
Engineering and Applied Science

by

Man Wai Ho

B.Sc. The Chinese University of Hong Kong, 1999
M.Phil. The Chinese University of Hong Kong, 2001

December, 2006

Acknowledgements

I would like to express my sincere gratitude to my major supervisor Prof. David Hui from Department of Mechanical Engineering in The University of New Orleans and co-supervisor Prof. Alan Kin-Tak Lau from Department of Mechanical Engineering in The Hong Kong Polytechnic University for granting me a great deal of freedom, directions in research and financial support throughout my Ph.D. studies. I am indebted to Prof. Dickon Hang-Leung Ng from Department of Physics in The Chinese University of Hong Kong for his recommendation to my overseas education.

My thanks are sent to my classmates Eunice Wai-Yin Tam, Javier Garcia Barros and Stefano Bietto for their help in my coursework studies and the joys of life in US. My gratitude is extended to Mr. Wan and Mr. So from Industrial Center (IC), Mr. Jeremy Yeung from Materials Research Center (MRC) and technicians from Mechanical Engineering Project Laboratory in The Hong Kong Polytechnic University for their technical supports and instrumentation.

I would like to give my special thanks to Mr. Yuk-Lim Wong and Mr. Hua-Xiang Zheng from Metairie, Louisiana for their kindness hospitality for my stay in their homes to finish my Ph.D. dissertation after Hurricane Katrina. I would like to further special thank Mrs. Selina Tsang from Metairie, Louisiana and Sum-So from Hong Kong for their unconditioned help in every aspect.

Finally, I want to express my deepest gratitude to my dearest family in Hong Kong for their endless love and care, especially to my mother for her unlimited support and continuous encouragement that have given me the power to complete my research work.

Thank you very much and I love you all.

Table of Contents

List of Figures

Abstract

Ten different sets of epoxy samples with compositions from 0wt% to 8wt% nanoclay were prepared by mechanical stirring and then casting to mold dog-bone shape samples for tensile and other tests. A gradual trend of changes upon mechanical, thermal and microstructural behaviors were investigated.

Introduction of strip silicates inside the epoxy matrix contributed to higher tensile strength, flexural strength and Vickers' hardness. From tensile tests, the ultimate tensile strength of samples from 0wt% to 8wt% nanoclay ranged from 42MPa to 46MPa. The epoxy samples with 1wt%, 4wt% to 6wt% nanoclay had a stepwise increase in the ultimate tensile strength of 5% when compared with a pure epoxy sample. In general, samples with nanoclay content below 1wt% were ductile, while samples with nanoclay content from 2wt% to 6wt% were in the ductile-brittle transition and developed higher strength than the pure epoxy sample. However, samples with nanoclay content above 7wt% were brittle and the ductility drastically dropped by more than 70% for 8wt% nanoclay sample and the failure was catastrophic.

On the other hand, from X-Ray Diffractometry (XRD), it was shown that there was no nanoclay peak shifting in the epoxy matrix. Moreover, it was further verified by Dynamic Mechanical Analyzer (DMA), Thermomechanical Analyzer (TMA) and Thermogravimetric Analyzer (TGA) that there was no significant change of elastic modulus, glass transition, thermal expansion and decomposition temperature in the nanoclay-epoxy samples when compared with that of pure epoxy. Finally, it was found from Scanning Electron Microscopy (SEM) that as the nanoclay content in the epoxy samples increased, the fracture surfaces were rougher, irregular in shape and broken down into tiny pieces with stress whitened sharp edges. A lot of white spots or

white lines which believed to be the nanoclay (strip silicates), were found coming out from the fracture surfaces.

As a result, strip silicates reinforced epoxy composites with compositions at 4wt% to 6wt% nanoclay content showed enhanced mechanical properties. However, for ease of casting, the nanoclay content should be kept below 5wt%. Finally, a model is deduced from all the experimental results, which is called a “net” model.

Chapter 1

Layered Silicates (nanoclay) and Epoxy

1.1 Introduction to layered silicates (nanoclay)

Nanocomposites are the trend of the 21st century in engineering materials, which have aroused a lot of interest in aerospace and automotive industries. In specific, clay-polymer nanocomposites are a new class of materials, which combine inorganic and organic matters together to revolutionize today's industrial world. In 2002, General Motors (GM) teamed up with Southern Clay Product to produce a nanocomposite TPO-based step-assist for 2002 GMC Safari and Chevrolet Astro vans that assists passengers in stepping into and out of the vehicle.

Clay has a lot of impact in our daily lives, from a common name for the soils in which we grow crops on the Earth, to the bowls and plates used in kitchens, to the high technology ceramic materials covering the space shuttles. Therefore, clays are utilized in various applications from all walks of life and are an inexpensive form of material.

Natural clays are most commonly formed by the in situ alteration of volcanic ash 85 - 125 million years ago under marine or alkaline lake conditions. The instability of the volcanic ash made changes when contacted with the available marine chemistry. The most important factor in the formation of the clay was the availability of sufficient magnesium in the marine sediment environment, ensuring chemical and structural changes took place throughout the deposits' entire geologic history. Bentonite is a rock name of the clay ore, which consists of smectite clay and

impurities such as gravel, shale, limestone, etc. The interesting fraction of the Bentonite ore is the smectite clay.

Smectite clay is purified from the Bentonite ore. Now, there are billion tons of Bentonite ores in Montana, Wyoming and Dakotas. The unique characteristic of Smectite that sets it apart from other minerals is its ability to disperse and swell in water, thus controlling the rheology of the water system in which it is used. There are many different species of Smectite. The most common two of the greatest commercial importance and value are Montmorillonite and Hectorite. Commercial availability of Hectorite is very limited, while Montmorillonite deposits are vast. Montmorillonite is the Dioctahedral species of Smectite clay, which is classified as Magnesium Aluminum Silicate, while Hectorite is the Trioctahedral species of Smectite clay, which is classified as Magnesium Silicate. The difference in their chemical compositions leads to a difference in crystal shape. Montmorillonites have a sheet morphology, whereas, Hectorite have a lath or strip morphology.

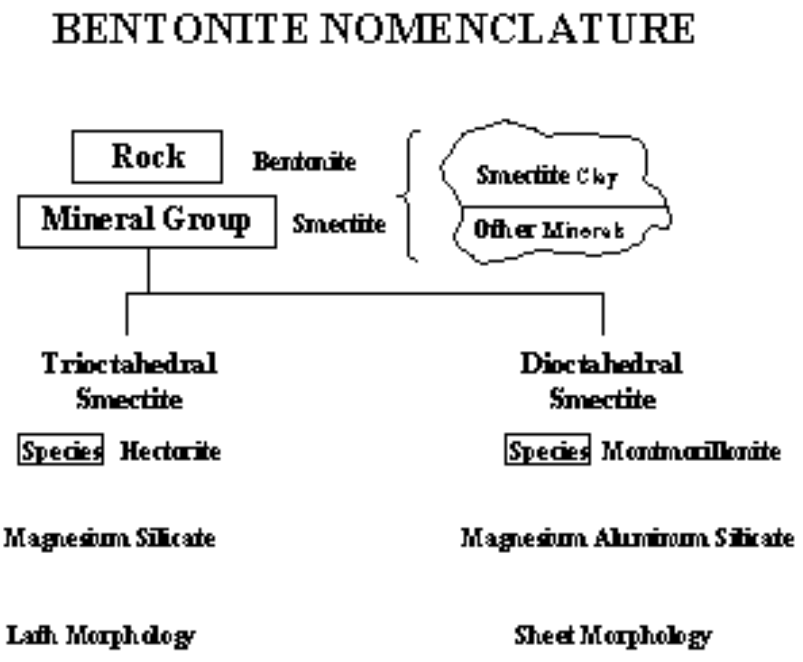

Figure 1.1 The nomenclature of Bentonite.

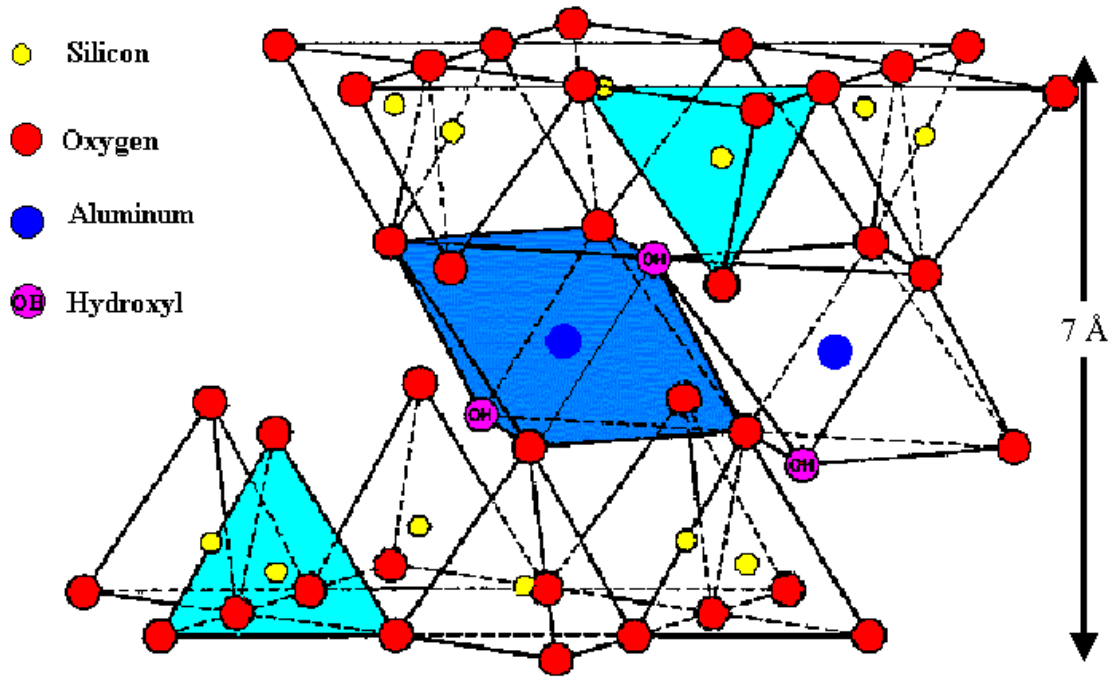

Figure 1.2 The atomic structure of clay.

Clays have a sheet structure consisting of 2 types of layers, the silica tetrahedral and the alumina octahedral layers. Silica is the dominant constituent in clays, with Alumina being essential. The silica tetrahedral layer consists of SiO_4 groups linked together to form a hexagonal network of the repeating units of the composition Si_4O_{10}. On the other hand, the alumina octahedral layer consists of cages of close packed oxygens or hydroxyls, where the octahedrally coordinated aluminum atoms are situated equidistantly inside from the six oxygens or hydroxyls. The two tetrahedral layers sandwich the octahedral layer, sharing their apex oxygens together. Therefore, the apex oxygen has 12 coordination numbers, while the hydroxyl ions in the cage situated at each top center of the silica hexagonal network, has 9 coordination numbers. Thus, these 3 layers form one clay sheet.

If the octahedral positions are occupied by alumina, it is called the inert mineral pyrophyllite. Therefore, a phenomenon of isomorphous substitution plays an extremely important role to the structure of clays. If the trivalent aluminum is replaced by a divalent magnesium or iron II, there will be a net negative charge in the crystal. The excess negative charge is compensated on the clays' surface by cations that are too large to be accommodated in the interior of the crystal. The edge of the crystal has a few positive charges thus attracting negatively charged ions or molecules. The result is a polyionic, supercharged nano-wafer that is unique in the world of minerals.

Smectite clay becomes so unique and commercially important because of its special shape, size, and charge. Smectite crystals have a shape of flat thin sheet structure. They are irregular in overall shape and can be up to 1,000 nm in length. However, the side view dimension of the crystal is only 0.9 nm in thickness. As a result of this special morphology, the total surface area can be as large as about 750 square meters per gram. Moreover, this extremely large surface area allows Smectite to have a large effect on the rheology of the water even with a small amount of it.

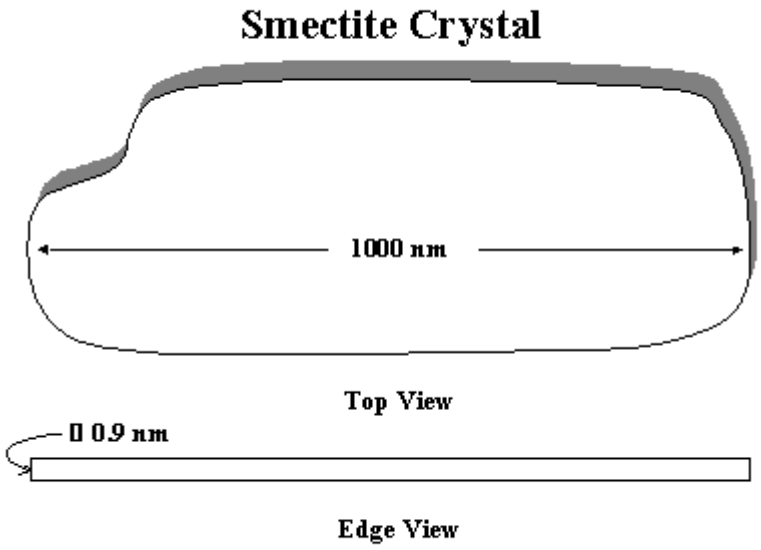

Figure 1.3 The particle shape of clay.

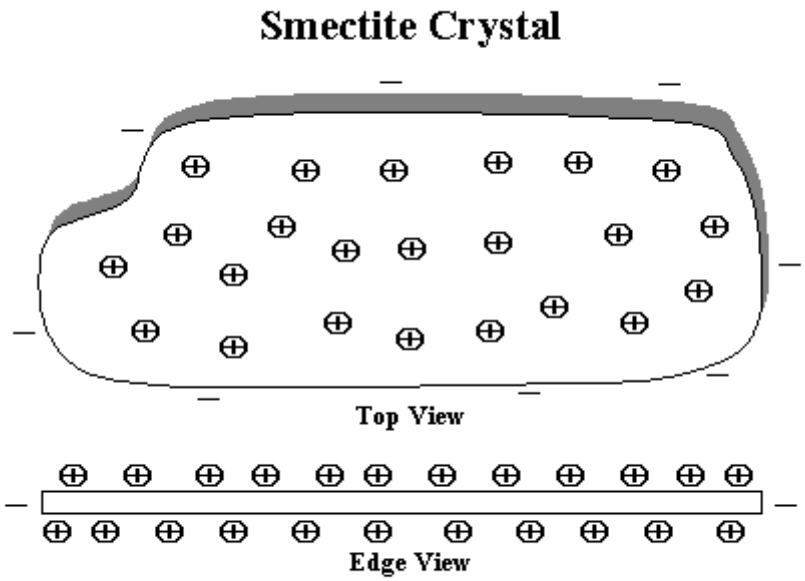

Figure 1.4 The particle charge of clay.

Each Smectite crystal has a large amount of net negative charges, so it tends to attract cations on its surface, such as Calcium or Sodium ions. If the majority of these cations are Sodium, it is commonly called Sodium Montmorillonite. If the majority of the ions on the clay surface are Calcium, it is then called Calcium Montmorillonite. The net negative charge is located inside the crystal itself. Therefore, cations that are too large to be embedded inside the sheet layer are attracted to the surface of the particle in an effort to neutralize the charge. The edge of the crystal has a few positive charges thus attracting negatively charged ions or molecules. The cations on the clay surface can be easily exchanged for other cations. A measure of this capacity is commonly known as the cation exchange capacity (CEC) and is usually expressed as milliequivalents of cations per hundred grams of clay.

In order to make the clay into organoclay, this can be achieved by reacting organ-cationic surfactants, such as a quaternary ammonium (onium) chloride, with smectite Clay. This mechanism is something like a soap. As the cationic head group of the onium molecule

preferentially replaces the Sodium cation on the clay layer surface, the organic tail will radiate away from the surface and make the interlayer spacing larger. The modified clay then changes from hydrophilic in nature to organophilic. The organically modified clay is able to impart various rheological characteristics to organic polymer, solvents and oil. Under well-defined experimental conditions, the intercalation of polymer molecules within the layers is easy.

The large surface area ($750m^2/g$) and high aspect ratio (70-150) of the clay contribute to its enormous benefits. Nanoclay can be employed in the preparation of polymer-clay nanocomposites. Typical performance advantages, taken from the open literature, with the introduction of nanoclay into the plastics when compared with traditional reinforcing agents are as follows:

1) Polymer with nanoclay will develop similar increase in modulus and tensile strength at 3-5% loading compared to 20-60% loading of conventional reinforcing agents such as kaolin, silica, talc, and carbon black. Implicit advantages resulted in lighter plastic parts with greater transparency.
2) Particle shape is known to affect plastic barrier properties. Nanoclay is a nanoparticle with an anisotropic, plate-like or strip-like, high aspect-ratio morphology. It is this morphology that leads to the improved permeation barrier for liquids and vapors through a tortuous path mechanism. With the addition of nanoclay, the plastic will have increased barrier properties to moisture, solvents, chemical vapors, gases such as O_2 and flavors.
3) With the addition of nanoclay, the plastic will have increased dimensional stability at low reinforcement loading, dramatic decreases in coefficient of thermal expansion (CTE) values have been reported, and moreover, the plastic will have a higher heat distortion temperature. Only a few percent loading of nanoclay will increase the temperature at

which the plastic will begin to soften. This property is critical, for example, in under-the-hood automotive applications.

4) Nanoclay can improve polymer upon recycling performance, the thermoplastic polymer will be more recyclable. Fiberglass products, on the other hand, typically cannot be recycled for the same application, since the fibers are damaged during the recycling process.
5) Due to the colloidal nature, high surface area, and surface treatability of nanoclay, it can serve as an active site to fix dyes into plastic. The plastic will be dyed easier.
6) Nanocomposites offer a new flame-retardant approach. The improved flame retardancy as measured by Cone Calorimetry shows a decrease in the Peak Heat Release Rate. A decrease in smoke and an increase in char formation are observed. National Institute of Standards and Technology (NIST) has formed a consortium to study the flammability of polymer-clay nanocomposites.
7) The appearance of painted parts is improved compared to conventional reinforced parts. It is because the nanocomposite particles are much smaller than traditional reinforcing agents so the plastic surface is much smoother, reduced static is observed in cling film using nanocomposites.

Therefore, these super-charged nanoparticles providing a variety of benefits to all classes of plastics at very low loadings.

1.2 Introduction to epoxy

Epoxy resin is defined as any molecule which has one or more epoxide groups consisting of an oxygen atom bonded to two carbon atoms. It is a versatile resin, with the addition of a wide selection of curing agents and additives, can achieve various applications such as coatings, adhesives, reinforced plastics, civil structures and electrical insulation. The physical forms of epoxy resin range from low viscous liquid, semi-solid to solid, which can provide fabricators with flexibility in working conditions. Epoxy resins, upon curing, show many favorable characteristics such as:

1) Excellent adhesion to most materials
2) Dimensional stability
3) Very little shrinkage
4) Resistance to most chemicals
5) Electrical insulation
6) Strong tensile strength

Moreover, in a wide range of applications, epoxy resins out perform thermoplastics because of their low viscosity at room temperature. Thus melting is not required. On average, liquid resins have less than one repeating unit per molecule while solid resins have more than two. Liquid resins have higher epoxide content and thus form denser cross-linking structure upon curing, which lead to higher chemical and thermal resistance in their final use. Viscosity of liquid resins is lowered by addition of diluents to achieve higher filler loading in their formulations. Diluents are added even to reduce the tendency for liquid resins to crystallize during transportation and storage. The solid bisphenol A epoxy resins have high densities of hydroxyls for curing with phenolic resins, isocyanates and amino resins than those of liquid

bisphenol A epoxy resins. Most low molecular weight solid resins have softening and caking characteristics at elevated temperature and pressure, due to their low melting points. Major applications include adhesives, industrial coatings, moldings, flooring and electrical insulation. The structure of epoxy resin of a low-molecular-weight polymer with epoxide groups at each end is shown below:

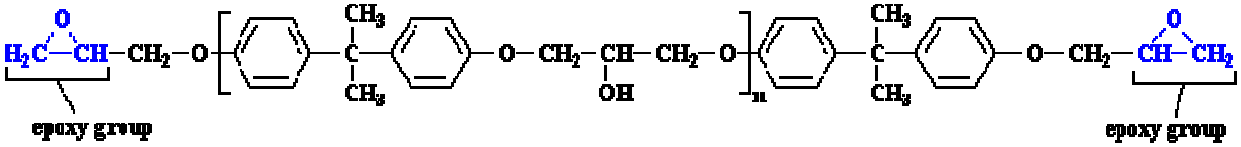

Figure 1.5 The structure of epoxy resin.

In these prepolymers n can be as high as 25, but the liquid epoxy adhesive is more likely a small molecule with two epoxy groups as shown below:

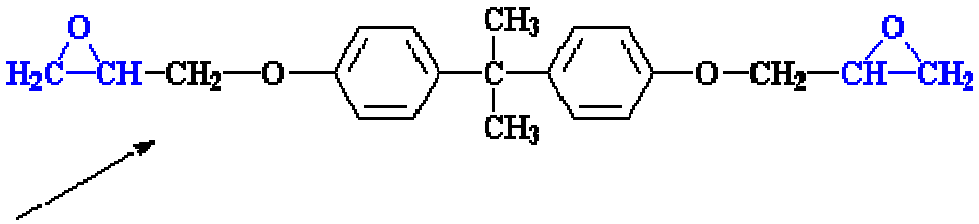

This is a small molecule diepoxy. You can think of it as the polymer shown above with a degree of polymerization of one. Some other diepoxy small molecules are shown below.

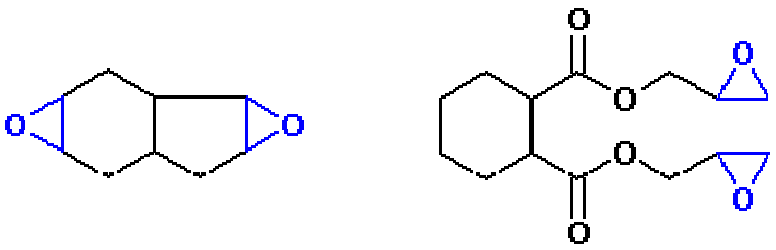

Figure 1.6 The structure of small molecule epoxy resin.

If the two-part epoxy adhesive is two tubes of liquid, than the diepoxy is probably one of the small molecules. The bigger prepolymers are solids at room temperature. If n is as high as 25,

the diepoxy is a hard plastic at room temperature. This type of diepoxy has to be heated and melted before it can be mixed with the other part of the two-part epoxy mix.

Polyamide is the most popular epoxy curing agent for ambient systems. These curing agents are generally made by reaction of dimer acids and amines. Polyamide curing agents are less toxic than aliphatic amines and provide better flexibility owing to longer chains of polymers. The second part of the two-part epoxy mix is a diamine as shown below:

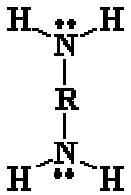

Figure 1.7 The structure of diamine.

When the two parts are mixed together, the diepoxy and the diamine react and join end to end in a ratio that 1 diamine joins with 4 different other diepoxies, in such a way that links up all the diepoxy and diamine molecules together as shown below:

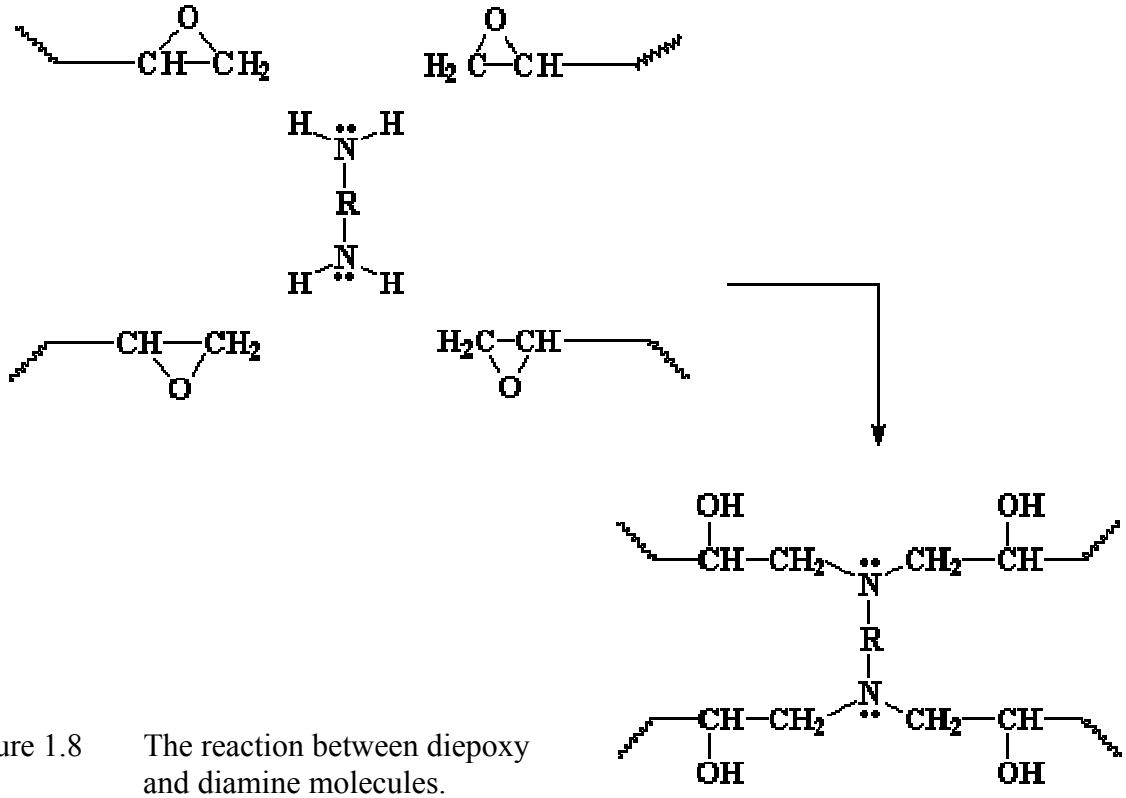

Figure 1.8 The reaction between diepoxy and diamine molecules.

As the reaction goes on and on, the diepoxy and diamines are not linear polymers anymore. Instead, it's a cross-linked network with enormous amount of heat energy given up. The cross-linked structure is shown below:

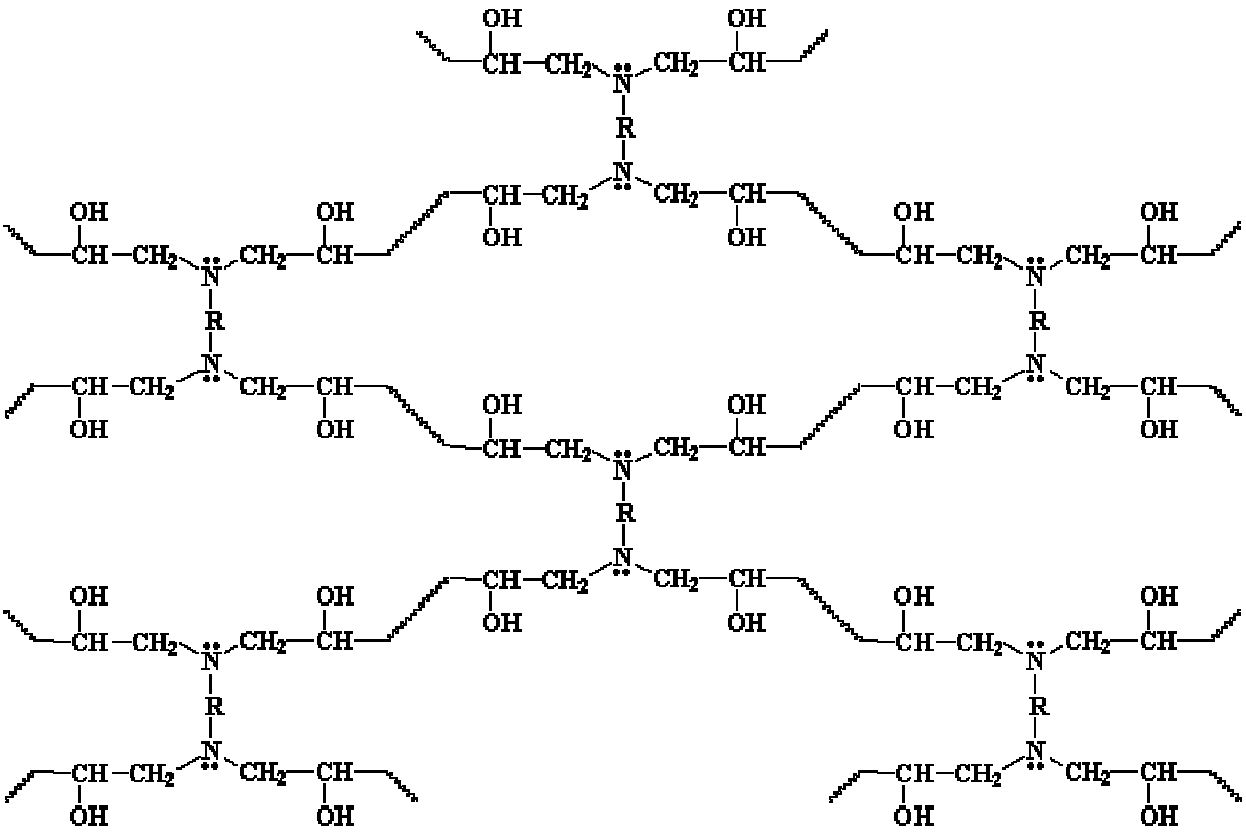

Figure 1.9 The cross-linked network structure of epoxy.

All the diamines and all the epoxy molecules have become one big molecule. When this happens, the result is a hard substance that can be very strong, but not processable. It cannot be molded into shape, or even melted. This is why the two parts do not come already mixed together before any application. If they do, they will be a solid chunk, and cannot be used as an adhesive.

Chapter 2

Literature Review

2.1 Introduction

Polymer-layered silicate nanocomposites are a new class of composites which introduce nanoclay into the polymer [1]. Recent research by Kojima and coworkers from Toyota Central Research and Development Laboratories discovered that, even at low nanoclay content below 5wt% [1-6], the composites will have much improved thermal (stability, fire retardancy), barrier (gas, vapor transmission) and mechanical (tensile strength, Young's and flexural modulus) properties when compared with those of pure polymer or conventional (microscale) composites. They showed that montmorillonite cation-exchanged with 12-aminolauric acid was swollen by ε-caprolactam which polymerized in the interlayer of montmorillonite to form a new intercalated compound producing nylon 6-clay hybrid (NCH) nanocomposites [7-9].

However, this kind of polymer-layered silicate nanocomposites still can't compete with the traditional fiber reinforced composites in the high filler range, as the mechanical properties achieved in the best clay/polymer nanocomposites are much lower than the conventional fiber reinforced composites with a high fiber volume fraction. But it is impossible to produce a nanocomposite with high nanoclay content. As in complete exfoliation state, the surface area of the reinforcing nanoclay will increase hundreds or thousands of times. Such a huge increase in

surface area may result in an inability for polymer molecules to wet the nanoclay surface. Therefore, the high performance fiber reinforced composite still has its own market.

On the other hand, when focusing on low filler content, polymer-layered silicate nanocomposites exhibit better reinforcement than conventional fiber reinforced composites. T. D. Fornes and D. R. Paul showed that the clay/nylon-6 nanocomposites have a higher efficiency in improving the Young's modulus than the glass fiber reinforced nylon-6 composites in the filler loading up to 10 wt% [10]. It is clear that the clay/polymer nanocomposites have advantages over the fiber reinforced composites in terms of lighter components. In the low filler loading range, polymer-layered silicate nanocomposites have the potential to replace traditional fiber reinforced composites.

2.2 Characterization of layered silicates

When the polymer is unable to intercalate between the silicate sheets, a phase-separated composite is obtained, whose properties stay in the same range as traditional microcomposites. However, when the polymer chain is intercalated between the silicate layers, then a well ordered multilayer morphology is built up with alternating polymeric and inorganic layers and is called an intercalated structure. Under well defined experimental conditions, such as the organo-modified nanoclay, modified oligomers and the miscibility between the modified oligomers and the matrix polymer chains, the intercalation of polymer molecules within the nanoclay layers is easy [11-12]. Unfortunately, there was a phenomenon reported that the silicate layers would have a tendency to re-aggregate together during the fabrication process [13-18]. On the other hand, if the silicate layers are completely and uniformly dispersed in a continuous polymer matrix, an exfoliated or delaminated structure is obtained. Two complementary techniques, X-Ray

Diffractometry (XRD) and Transmission Electron Microscopy (TEM), can be used to characterize this type of structure. XRD is used to identify the intercalated structures. In intercalated nanocomposites, the intercalation of the polymer chains usually increases with the interlayer spacing, when compared with the spacing of the organoclay alone, the diffraction peak will shift towards the lower angle values. For exfoliated nanocomposites, no diffraction peaks are visible in the XRD diffractograms either because of too large spacing between the layers or the nanocomposite does not present any ordering. Then, TEM is used to characterize the nanocomposite morphology. Besides these two well defined structures, there is another intermediate morphology where both intercalation and exfoliation structures coexist. In this case, a broadening of the diffraction peak will be observed in XRD and TEM will be employed to define the overall structure.

2.3 Fabrication of nanocomposites

There are four feasible processes to fabricate polymer-layered silicate nanocomposites.

2.3.1 Exfoliation-adsorption

In exfoliation-adsorption, the layered silicate is exfoliated into single layers using a polymer soluble solvent. Owing to the weak forces between the layered silicates, the layers can be easily dispersed in a solvent, then the polymer can attach onto the delaminated sheets. When the solvent is evaporated, the sheets reassemble and sandwich the polymer to form an ordered multilayer structure. Wu and Lerner had successfully intercalated poly-ethylene oxide (PEO) in sodium montmorillonite and sodium hectorite by dispersion in acetonitrile, and allowed one or two polymer chains stoichiometrically bonded between the silicate layers so that the interlayer spacing increased from 0.98 to 1.36 and 1.71 nm, respectively [19]. However, the exfoliation-

adsorption technique will give quite different results depending much upon the polymer matrix. For each type of polymer, the right kind of layered clay, organic modifier and solvent must be used.

2.3.2 In situ intercalative polymerization

In situ intercalative polymerization requires layered silicate to be swollen within the liquid monomer, so the polymer formation can occur between the intercalated sheets. Polymerization can be initiated either by heat or radiation, by the diffusion of a suitable initiator or by an organic initiator or catalyst fixed through cationic exchange inside the interlayer before the swelling step by the monomer. The Toyota research group was the first team to study the polymer-layered silicate nanocomposites. They studied the ability of Na-montmorillonite organically modified by ω-amino acid ($^{+}H_3N$-$(CH_2)_{n-1}$-COOH, with n = 2, 3, 4, 5, 6, 8, 11, 12, 18) to be swollen by the ε-caprolactam monomer (melting temperature = 70^{o}C) at 100^{o}C and subsequently to initiate its ring opening polymerization to obtain nylon-6-based nanocomposites [7-9,20]. A clear difference occurred in the swelling behavior between the montmorillonite with relatively short (n<11) and long alkyl chains, indicating that a larger amount of monomer could be intercalated for longer alkyl chains.

2.3.3 Melt intercalation

The layered silicate is mixed with the polymer matrix in the molten state for melt intercalation. Under these conditions and if the layer surfaces are sufficiently compatible with the chosen polymer, the polymer can crawl into the interlayer space and forms either an intercalated or an exfoliated nanocomposite. In this technique, no solvent is required. Vaia and Giannelis had

studied polystyrene (PS) as the matrix for dispersing different types of clays [21]. The nanocomposites were synthesized by statically annealing a palletized, intimately mixed modified silicate in PS under vacuum at 170^{o}C, a temperature well above the PS glass transition, without any mixing or shearing [22].

2.3.4 Template synthesis

In template synthesis, the layered silicates are formed in situ in an aqueous solution containing the polymer and the silicate building blocks. Based on the self-assembly forces, the polymer aids the nucleation and growth of the inorganic host crystals and gets trapped within the layers as they grow. The typical method for in situ hydrothermal crystallization of a polymer/hectorite nanocomposite consists in refluxing for 2 days a 2 wt% gel of silica sol, magnesium hydroxide sol, lithium fluoride and the desired polymer in water. XRD patterns proved the formation of a polymer/hectorite intercalated nanocomposite. Moreover, the interlayer spacing varied linearly with the weight percentage of polymer in synthetic poly-vinylpyrrolidone (PVPyr)-hectorite clay nanocomposites [16].

2.4 Properties

2.4.1 Mechanical properties

2.4.1.1 Tensile properties

Y. Kojima et al. had shown that low filler content of about 5 wt% introduced in nanocomposite could drastically increase the Young's modulus of the samples. Nylon-6-based nanocomposites obtained by in situ intercalative polymerization of ε-caprolactam in 5.3 wt% protonated ε-caprolactam modified montmorillonite (L-NCH) [23] and 4.1 wt% Na-

montmorillonite (one-pot-NCH) [24] gave out Young's modulus of 2.04 and 2.25 GPa respectively when compared with commercial nylon-6 Young's modulus of 1.11 GPa.

He also demonstrated that the difference in the extent of exfoliation, as observed for nylon-6-based nanocomposites synthesized by in situ intercalative polymerization of ε-caprolactam using Na-montmorillonite and various acids, strongly influenced the measured Young's modulus values [24]. It was observed that the variation of the XRD peak intensity (I_m) was inversely related to the amount of exfoliated layers in the nanocomposite. For an increase in the I_m values, a parallel decrease in the Young's modulus was observed, indicating that exfoliated layers were the main factor responsible for the stiffness improvement, while intercalated particles, having a less important aspect ratio, played a rather minor role.

L.M. Liu et al. had shown the relationship of the Young's modulus at room temperature of nylon-6 nanocomposites obtained by melt intercalation as a function of the filler weight content of organic modified montmorillonite [25]. There was a constant and large increase in the Young's modulus of the nanocomposites up to 10 wt% of nanoclay addition. However, the Young's modulus seemed to level off above that threshold. That changes exactly corresponded to the phenomenon from totally exfoliated structure (below 10 wt%) to partially exfoliated-partially intercalated structure (10 wt% or more) as determined by XRD and TEM analyses.

2.4.1.2 Impact properties

The nylon-6-based nanocomposites did not have much reduction in the impact properties. Y. Kojima et al. had measured the impact properties for nylon-6-based nanocomposites prepared by in situ intercalative polymerization of ε-caprolactam using protonated aminododecanoic acid-exchanged montmorillonite [9]. The Izod impact strength was reduced from 20.6 to 18.1 J/m

when 4.7 wt% of nanoclay was incorporated. Similarly, for the same nanoclay content, the Charpy impact strength dropped from 6.21 kJ/m^2 to 6.06 kJ/m^2.

Moreover, L.M. Liu et al. also showed the Izod impact strength of the melt-intercalated of nylon-6 in octadecylammonium-exchanged montmorillonite nanocomposites did not decrease much over a relatively large range of filler content [25].

This relatively good resistance to impact, together with a high Young's modulus, good flexural modulus and a remarkable enhancement of the increase in the heat distortion temperature from 65^{o}C for pure nylon-6 to more than 150^{o}C for nanocomposites, have allowed this material to replace glass fiber reinforced nylon or poly-propylene in the production of timing belt covers of automotive engines [26].

2.4.2 Thermal properties

2.4.2.1 Dynamic mechanical analysis

Dynamic mechanical analysis (DMA) measures the response of a given material to a cyclic deformation as a function of the temperature. The deformation is usually tension or three-point flexion. DMA results are expressed by three main parameters: (i) the storage modulus (E'), corresponding to the elastic response to the deformation; (ii) the loss modulus (E''), corresponding to the plastic response to the deformation and (iii) tan δ, the (E'/E'') ratio, useful for determining the occurrence of molecular mobility transitions such as the glass transition temperature (T_g).

Noh and Lee studied DMA analysis to track the temperature dependence of the storage modulus upon the formation of an intercalated PS nanocomposites [27]. No significant difference in E' could be seen in the investigated temperature range, indicating that intercalated

nanocomposites did not strongly influence the elastic properties of the matrix. On the other hand, the shift and broadening of the tan δ peak towards higher temperatures for the nanocomposite indicated an increase in the glass transition temperature together with some broadening of this transition. This behavior had been ascribed to the restricted segmental motions at the organic-inorganic interface neighborhood of intercalated compositions.

However, Messersmith and Giannelis studied DMA analysis on epoxy nanocomposites exfoliated within cross-linked matrices showed much improvement of the storage modulus, especially above T_g [28]. For epoxy matrix below T_g, there was a 58% increase in modulus from the dispersion of 4 vol.% montmorillonite with the formation of a well-ordered exfoliated nanocomposite. At 40^{o}C, E' equaled to 1.55 and 2.44 GPa for the unfilled cross-linked matrix and the nanocomposite, respectively. But above T_g, at 150^{o}C, the storage modulus improved from 11 to 50 MPa for the unfilled and filled epoxy, respectively.

In general, the storage elastic modulus appears to be substantially enhanced at temperatures above T_g for exfoliated nanocomposites filled with layered silicates of high aspect ratio. A possible explanation for such an improvement could be the creation of a three-dimensional network of interconnected long silicate layers, strengthening the material through mechanical percolation.

2.4.2.2 Thermal stability

The thermal stability of a material is usually studied by thermogravimetric analysis (TGA) where the sample mass loss due to volatilization of degraded by-products is monitored as a function of temperature. When heating up the sample under an inert gas flow such as nitrogen or

helium, a non-oxidative degradation occurs. On the contrary, when air or oxygen is used, an oxidative degradation of the sample is studied.

Burnside and Giannelis had measured the thermal stability of cross-linked poly-dimethylsiloxane (PDMS) by TGA under nitrogen flow in which 10 wt% of organomontorillonite was exfoliated [29]. When compared to the unfilled cross-linked PDMS, TGA showed a drastic shift of the weight loss of the nanocomposite towards higher temperature, with stabilization as high as 140^{o}C at 50% weight loss. It was because the cyclic silicates hindered the diffusion of the volatile decomposition products in exfoliated nanocomposites.

On the other hand, S. J. Wang et al. synthesized nanocomposites based on cross-linked PDMS using slightly different operating conditions to produce mainly intercalated structures [30]. In this case, the increase in thermal stability for a nanocomposite intercalated with 8.1 vol% of organomontmorillonite was limited to about 60^{o}C at 50% of weight loss.

2.4.2.3 Thermal expansion coefficient

Thermomechanical analysis (TMA) measures the linear coefficient of thermal expansion (CTE) of a given material as a function of the temperature. Y. Yang et al. showed that the thermal expansion coefficient of poly(imide)-based nanocomposites with hexadecylammonium cation exchange montmorillonite could be strongly reduced from 3.6x10^{-5} K^{-1} to 1.96x10^{-5} K^{-1} and 1.55x10^{-5} K^{-1} when 1 wt % and 10 wt% of nanofiller was dispersed, because of the high aspect ratio of the exfoliated silicate layers [31].

2.4.2.4 Flame retardancy

S. Zhang gave a review of flame retardant properties on polypropylene with layered silicates nanocomposites [32]. Gilman also reviewed the flame retardant properties of nanocomposites in detail [33]. The main bench-scale method used to measure the flame retardant behavior of a material is Cone calorimetry. In a typical experiment, the sample was exposed to a given heat flux (often taken as 35 kW/m^2) and the heat release rate (HRR) as well as the mass loss rate (MLR) were recorded as a function of time. It is worth noting that the reduction of the peak HRR is the most clear-cut evidence for the efficiency of a flame retardant. Moreover, gas and soot production are also measured. Comparison between nylon-6 and nylon-6 with 5 wt% exfoliated montmorillonite showed a 63% reduction in the peak HRR for the nanocomposite. Experiments carried out in a radiative gasification apparatus had determined that the flame retardant effect of nanocomposites mainly arose from the formation of char layers obtained through the collapse of the exfoliated and the intercalated structures [34]. This multilayered silicate structure may act as an excellent insulator and mass transport barrier, slowing down the escape of the volatile decomposition products as observed in nylon-6 but also in thermoset nanocomposites [35].

Moreover, S. Duquesne et al. also showed that the rate of degradation of Ethylene Vinyl Acetate (EVA) was affected by the presence of organo-modified nanoclay. On heating, the clay formed a barrier on the surface of the material, which slowed down the evolution of degradation products, resulting in a decrease of the HRR but a similar value of total heat release THR [36].

2.4.3 Gas barrier properties

T. Lan et al. measured the permeability of carbon dioxide in the partially-exfoliated poly(imide)-based nanocomposite films prepared by curing $CH_3(CH_2)_{17}NH_3^+$ montmorillonite-poly(amicacid) at 300^oC [37]. They showed that the high aspect ratio characteristic of the exfoliated nanocomposite films had highly reduced the gas permeability.

K. Yano et al. on the other hand measured the effect of water permeability on both partially and totally exfoliated poly(imide)-based nanocomposites [38], using organoclay with different layer lengths. A relatively good agreement between the experimental values and the corresponding theoretical curve was achieved. As the length of the clay increased, the relative permeability decreased drastically. That is, the barrier properties are related to the dimension of the clay platelets; the higher the aspect ratio of clay, the lower the permeability coefficient of the resulting nanocomposites.

2.4.4 Miscellaneous properties

2.4.4.1 Cryogenic cycling

J. F. Timmerman et al. showed that layered silicates used as nanoparticle fillers in a low concentration, such as 5wt% in fiber-reinforced epoxy composites, significantly reduced the transverse cracking in symmetric carbon fiber epoxy laminates as a response to cryogenic cycling [39]. Therefore, nanoclay can be used to modify traditional fiber-reinforced composite materials and enhance their resistance to thermal cycling induced stresses.

2.4.4.2 Memory effect in liquid crystal

Kawasumi et al. showed that when Na-montmorillonite ion-exchanged with 4-(4'-cyanobiphenyl-4-oxy) butyl ammonium (CBAM) or 4-cyano(4'-biphenyloxy) undecylammonium (CBUM) was homogeneously dispersed in nematic liquid crystal phases 4-pentyl-4'-cyanobiphenyl (5CB) and nematic TFALC, a cell of the liquid crystalline composite (LCC) containing this organoclay scattered light strongly [40-41]. Upon the application of a low frequency electrical field, the liquid crystal showed a strong dielectric anisotropy, becoming aligned parallel to the electric field and the cell became transparent. This forced a similar alignment of the clay which minimized scattering and increased transparency. The clay layers then appeared to act as anchors, as they prohibited the reformation of a random matrix, leading to a semi-transparent memory state which remained for months after the electric field was turned off. More recent liquid crystal work has indicated that the application of a high frequency field can erase the memory state and return the nanocomposite to the original opaque state wherein the clay is randomly dispersed. Future applications could include adjustable light-controlling glass, erasable optical storage devices and thermo-optical sensors.

2.4.4.3 Nucleating effect on crystallization

Z. Wu et al. investigated that the nucleating effect of nylon 1212/montmorillonite nanocomposite prepared by melt intercalation using differential scanning calorimetry (DSC) [42]. They found that the overall crystallization time t_c and the induction time t_i were strongly influenced by the addition of montmorillonite and the cooling rate. The crystallization time t_c of nylon 1212 decreased from 3.08 min to 0.69 min as the cooling rate increased from 5°C/min to 40°C/min and those for the nanocomposite decreased from 0.9 min to 0.07 min respectively. The

induction time t_i decreased monotonously with the increase of the cooling rate for both nylon 1212 and the nanocomposite. These data implied that, with the addition of montmorillonite, nylon 1212 had a higher crystallization rate and smaller induction time.

When montmorillonite was exfoliated in the nanocomposite and the silicate layers were uniformly dispersed in the nylon 1212 matrix, the nylon began to crystallize in the presence of montmorillonite, with crystals also growing on the surface of the silicate layers. These silicate layers served as seeds for the growth of spherulite. As the spherulites grew, they might be confined by each other and the silicate layers as well, so they were fine and uniform, but not as big as those in pure nylon 1212. Therefore, montmorillonite could serve as an effective nucleating agent.

Chapter 3

Methodology and Instrumentation

3.1 Introduction

In this work, casting method was employed to produce the dog-bone shape samples for tensile and other tests. It is well known that casting is the most convenient and inexpensive way to make finished products that do not require further machining and moreover gives a smooth final surface. A good molding is a minimum requirement.

3.2 The making of Silicone mold

Silicone rubber was found inert to the epoxy, since epoxy won't stick to the silicone rubber after it was cured. Therefore, the making of a silicone mold is the first step in the casting sequence. An aluminum bar of the exact size, shape and thickness of the desired mother dog-bone shape sample was wired cut into the shape as shown below in Figure 3.1. The dimensions are 100mm in length, 12.5mm in width and 2mm in thickness. The gage length is 30mm.

Figure 3.1 The dog-bone shape of the sample.

The silicone rubber of model KE-13 with hardener CX-32-1482 from Shin-Etsu Chemical Co. Ltd. was poured in between 2 pieces of acrylic plates where the piece of dog-bone shape Aluminum bar was adhered firmly inside. The acrylic plates were used for support purpose. One day later, the silicone rubber, which was white in color, would be cured and could be taken out for usage. A photo of the acrylic plates and the silicone mold are shown below in Figure 3.2.

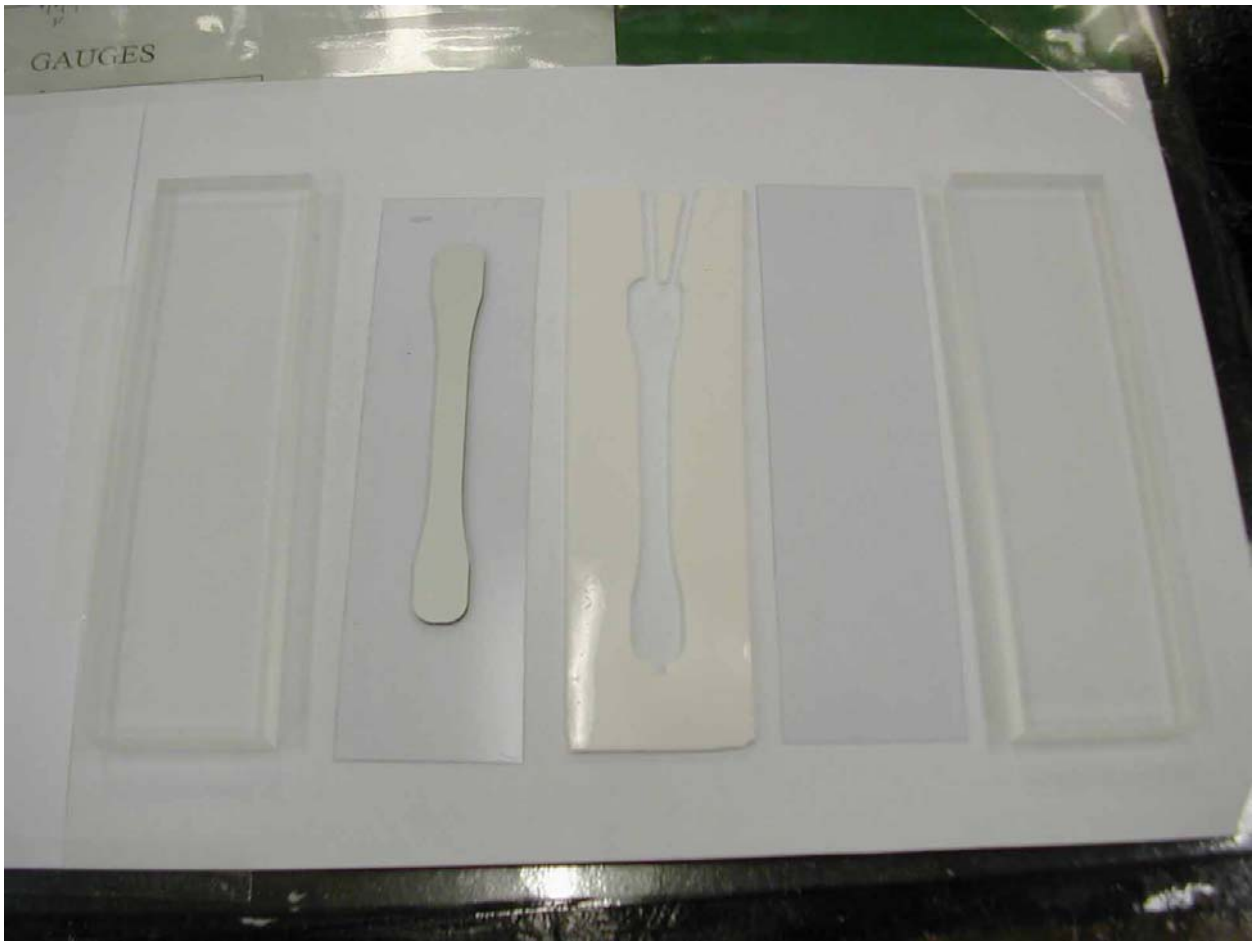

Figure 3.2 The acrylic plates and the silicone mold for casting.

3.3 The making of nanoclay-epoxy samples

For the samples, the epoxy resin Araldite®GY 251 and the hardener HY 956 from CIBA-GEIGY were chosen and mixed in the ratio of 4:1 by weight. The nanoclay was courtesy from

Southern Clay Products Garamite 1958. A total of 10 different nanoclay-epoxy compositions were prepared in order to capture any trends in the changes of the mechanical, thermal and microstructural properties. Those compositions were pure epoxy (that is 0wt% nanoclay), 0.5wt%, 1wt%, 2wt%, 3wt%, 4wt%, 5wt%, 6wt%, 7wt% & 8wt% nanoclay in epoxy.

The nanoclay was firstly introduced into the epoxy resin and mixed well with a glass rod before subjected to mechanical stirring at 500rpm for 1 hour. The mechanical stirrer was from IKA RW 20 DZM.n. as shown in Figure 3.3.

Figure 3.3 The mechanical stirrer and its propeller.

Secondly, the nanoclay-resin mixture was poured into a beaker and heated up in a sonication water bath at 50^{o}C to lower the viscosity. Then it was subjected to a vacuum in order to remove trapped air bubbles caused by mechanical stirring. When degassing inside a vacuum flask, occasional shaking and rocking the flask helped get rid of the air bubbles easier and faster.

Figure 3.4

The sonication bath (left) and the vacuum flask with mechanical pump (right).

The sonication bath and the vacuum flask with mechanical pump are shown above in Figure 3.4. As the process continued, 9 different nanoclay-resin compositions from 0.5wt%, 1wt%, 2wt%, 3wt%, 4wt%, 5wt%, 6wt%, 7wt% & 8wt% nanoclay with resin were prepared. The mixture colors changed from very pale brown to deep brown as the nanoclay content increased. Moreover their viscosities also increased accordingly, as shown in Figure 3.5. The higher nanoclay content resin's residue still remained sticking around the inner glass wall, unlike the ones with less nanoclay content.

After the mixture was cooled down inside the glass, the appropriate amount of hardener was added and mixed well with the nanoclay-resin mixture, and ready to be transferred to the silicone mold. Two pieces of transparencies as shown in Figure 3.2 were inserted between the acrylic plates and the silicone mold for anti-sticking purpose between the acrylic plates and the epoxy. Finally the whole liquid mixture was poured inside the dog-bone shape silicone molds for

self curing and forming as shown in Figure 3.6. The samples were taken out from the molds after 12 hours as shown in Figure 3.7 and room temperature cured for 1 week before subjected to various testing. Therefore, casting is a convenient method for production of multiple samples. The whole experimental setup with mechanical stirrer, sonication bath, vacuum flask and silicone molds are shown in Figure 3.8. Moreover, the dog-bone shape samples of the 10 different nanoclay-epoxy compositions from 0wt%, 0.5wt%, 1wt%, 2wt%, 3wt%, 4wt%, 5wt%, 6wt%, 7wt% & 8wt% nanoclay in epoxy are shown in Figure 3.9.

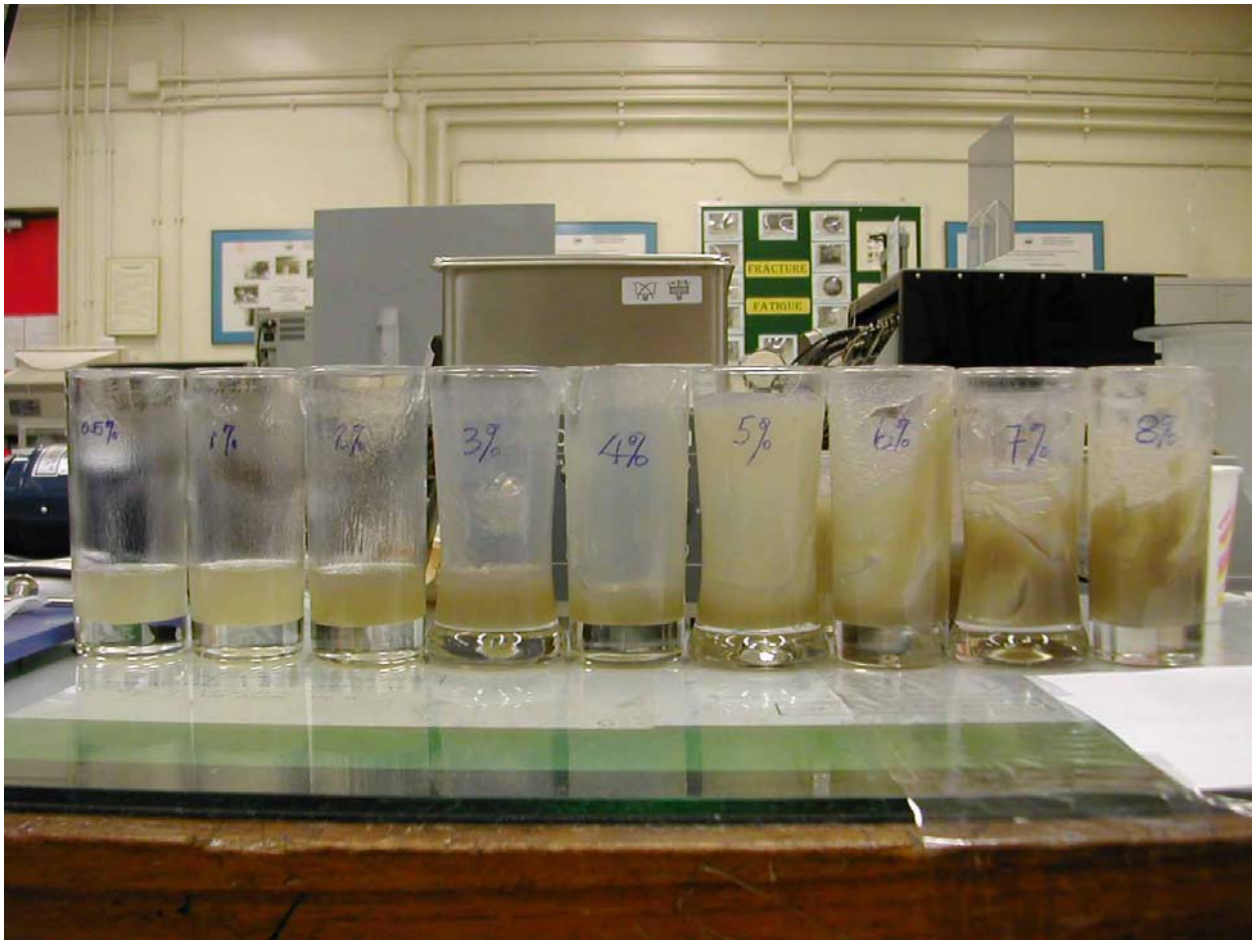

Figure 3.5 Nine different nanoclay-resin mixtures from 0.5wt%, 1wt%, 2wt%, 3wt%, 4wt%, 5wt%, 6wt%, 7wt% & 8wt% nanoclay with resin were prepared. Note the color and the viscosity of the nanoclay-resin mixtures.

Figure 3.6 The nanoclay-epoxy mixture was poured inside the dog-bone shape silicone molds for self curing and forming.

Figure 3.7 Dog-bone shape samples were taken out from the silicone molds after 12 hours.

Figure 3.8 The experimental setup of making nanoclay-epoxy samples.

Figure 3.9

The dog-bone shape samples of the 10 different nanoclay-epoxy compositions from 0%, 0.5wt%, 1wt%, 2wt%, 3wt%, 4wt%, 5wt%, 6wt%, 7wt% & 8wt% nanoclay in epoxy.

3.4 Characterization methods

Several different characterization instruments were employed to study the mechanical, thermal and microstructural behaviors of the nanoclay-epoxy samples. They will be discussed in further detail in Chapters 4, 5 & 6 respectively. For the investigations of the ultimate tensile strength, the flexural strength and the microhardness value of the nanoclay-epoxy samples, tensile test, 3-point bending test and microhardness test were employed respectively. For the investigations of the storage modulus in tension or bending, glass transition, the coefficient of linear thermal expansion (CTE) and the weight loss as a function of temperature of the nanoclay-epoxy samples, DMA, TMA and TGA were employed respectively. For the investigations of the microstructural behavior and the quantity or distribution of nanoclay inside the nanoclay-epoxy samples, XRD and SEM were employed respectively.

3.4.1 Mechanical Analysis

3.4.1.1 Tensile Test

MTS Instron loading machine Alliance RT/50 was employed for tensile tests at a crosshead speed of 2mm/min. Tensile tests were performed on all 10 sets of nanoclay-epoxy samples and 5 samples from each set were tested for averaging. The MTS Instron loading machine is shown in Figure 3.10. Moreover, 3-point bending tests were also performed in the same machine with only the change of the tensile grips to 3-point bending grips. The crosshead speed was also set at 2mm/min. However, only 1 sample from each set was tested due to the limited number of the remaining samples. The samples before tensile testing and the samples after 3-point bending tests are shown in Figure 3.11.

Figure 3.10 The MTS Instron loading machine for both tensile and 3-point bending tests.

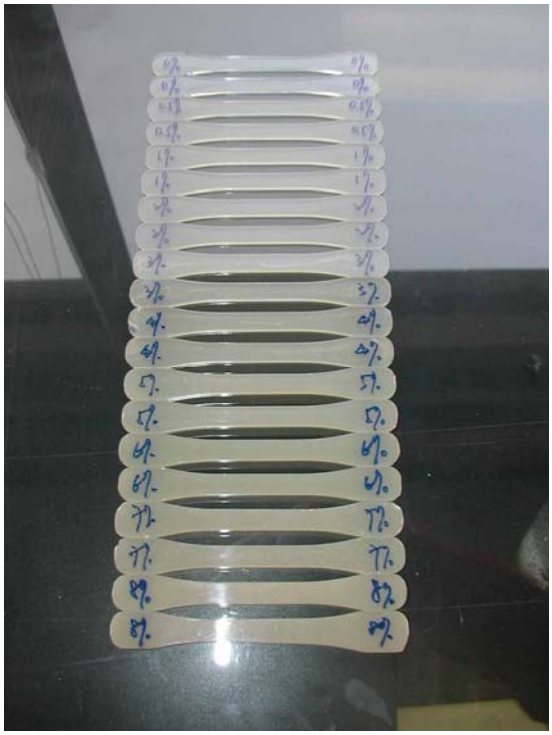

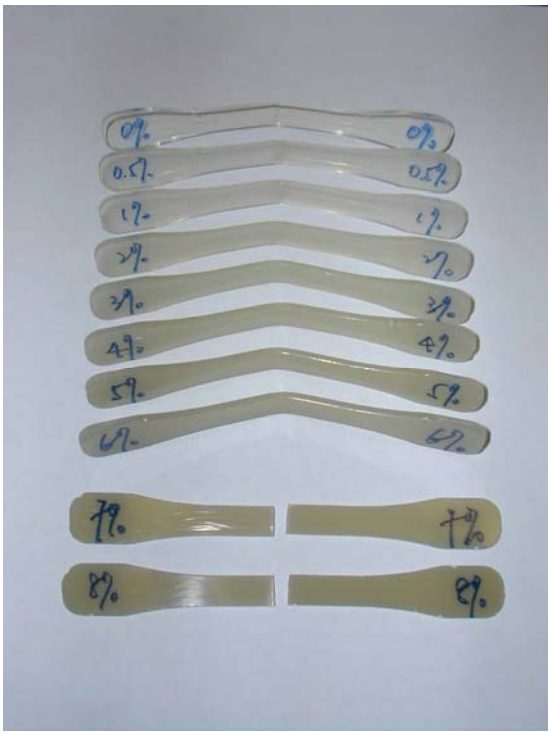

Figure 3.11 The nanoclay-epoxy samples before tensile testing (left) and the samples after 3-point bending (right).

3.4.1.2 Vickers' Hardness Test (HV)

The microhardness tester FM-7E from Future Technology, Tokyo Japan was employed for the Vickers' hardness tests. The microhardness tester FM-7E is shown in Figure 3.12. Hardness is a measure of the resistance of a material to a localized plastic deformation. Ten measurements for each set of samples were averaged. Each indentation was set at 50 gf for 15 seconds. The sample being tested should be polished to give a mirror-like surface for accurate measurement. It has two types of indentors, one for Vickers hardness and the other one for Knoop hardness measurement. The Vickers' hardness indentor was used in this experiment. The material of the indentor is diamond, which has a right pyramidal shape with an apex of 136^{o}. The Vickers' hardness value (HV) can be calculated by measuring the length of both the diagonals of the square base made by the diamond indentor. The equation is given by

$$HV = \frac{2 \times F \times \cos 22^{\circ}}{D^2} = \frac{1.854 \times F}{D^2}$$

where F is the loading force and D is the average value of the length of the diagonals. Hardness value has a dimension of N/m^2, but the unit is usually omitted because hardness is a comparison measurement.

Figure 3.12 The Vickers' hardness tester.

3.4.2 Thermal Analysis

3.4.2.1 Dynamic Mechanical Analysis (DMA)

The Pyris Diamond DMA Dynamic Mechanical Analyzer manufactured by Perkin Elmer is shown in Figure 3.13. A photo of the samples after being tested by DMA is shown in Figure 3.14. The length of the sample being tested was about 30mm, which was just the gage length of the dog-bone shape sample. The sample was scanned from 25^{o}C to 140^{o}C, at a heating rate of 2^{o}C/min to ensure even heating. Oscillating frequencies at 1 Hz, 2Hz, 5Hz & 10Hz were applied at the same time. Both tensile and 3-point bending tests were performed by DMA. A schematic diagram of the structure of DMA is shown in Figure 3.15.

Figure 3.13 The Dynamic Mechanical Analyzer (DMA).

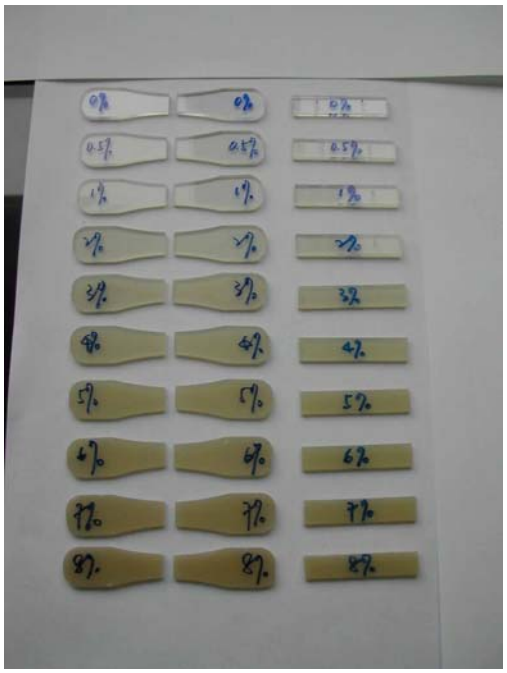

Figure 3.14

A photo of the samples after being tested by DMA

DMA is a computer-controlled dynamic mechanical force analyzer which applies an oscillating force, causing a sinusoidal stress to a sample. In return, the loaded sample generates a sinusoidal strain, which is analyzed by DMA as a function of temperature. By measuring both the amplitude of the deformation at the peak of the sine wave and the lag between the stress and strain sine waves, quantities such as the modulus, viscosity, and damping can be calculated.

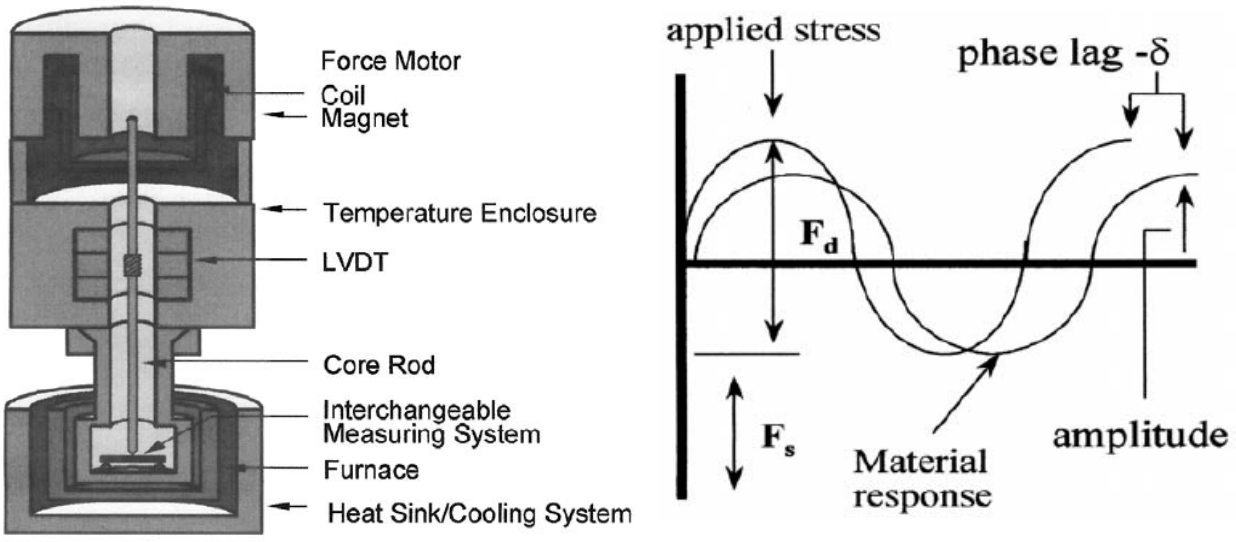

Figure 3.15 A schematic diagram of the structure of DMA and its mathematical principles.

The ratio of stress to strain in the initial linear portion of a typical stress–strain curve is the Young's modulus (*E*), which is a measurement of the material's stiffness. However, the modulus is dependent on both the temperature and the applied stress. The traditional mechanical tensile test is usually done at room temperature. That's why the need for DMA for material strength analysis at elevated temperature is critically important.

The dynamic modulus measurement in DMA calculation is not exactly the same as that for the Young's modulus in a typical stress–strain curve. In DMA, a complex modulus (*E**) is the square root of both the elastic modulus (*E*′) square plus the loss modulus (*E*") square. The elastic modulus (*E*′), and the imaginary (loss) modulus (*E*") can be calculated from the material response to the sinusoidal stress. These different moduli allow better characterization of the material, because the ability of the material to return or restore energy (*E*′), the ability to lose energy (*E"*), and the ratio of these effects (tan delta), which is called damping, can be examined.

Moreover, DMA can measure the glass transition temperatures when a material changes from glassy to rubbery by a drop in the elastic modulus even though the transitions are too faint to be detected by Differential Scanning Calorimeter (DSC) or Thermal Mechanical Analyzer (TMA). Therefore, DMA is much more sensitive than these techniques and can easily measure transitions not apparent in other thermal methods. This sensitivity allows the DMA to detect the glass transition (T_g) of highly crosslinked thermosets or even thin coatings.

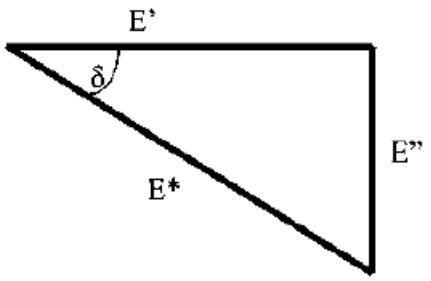

$$E^* = E' + iE''$$
$$\tan\delta = E''/E'$$
$$\eta^* = E^*/\omega$$

Figure 3.16 The calculation of the complex modulus in DMA.

3.4.2.2 Thermomechanical Analysis (TMA)

The TMA 7 Thermal Mechanical Analyzer manufactured by Perkin Elmer is shown in Figure 3.17. The TMA 7 is a computer-controlled thermal mechanical analyzer, which measures the coefficient of linear thermal expansion (CTE), extension, flexure, penetration or dilatometry of a material as a function of temperature. The internal structure of TMA is very similar to DMA as TMA provides a static force to measure the dimensional changes and the use of a quartz tube as the probe because of its very low thermal expansion and the high stiffness at elevated temperature. The sample was scanned from 25^{o}C to 200^{o}C with a static force of 100mN at a heating rate of 10^{o}C/min. The size of the sample was a thin square of 5mm in length and 2mm in thickness.

Figure 3.17 The Thermomechanical Analyzer (TMA).

3.4.2.3 Thermogravimetric Analysis (TGA)

The TGA Thermogravimetric Analyzer Jupiter STA 449 C manufactured by Netzsch is shown in Figure 3.18. The TGA is a computer-controlled thermogravimetric analyzer with a microbalance inside, which measures the weight loss of a material as a function of temperature. The weight of the sample was about 20 mg for each TGA analysis. The sample was scanned from 25^{o}C to 600^{o}C at a heating rate of 10^{o}C/min. TGA is the simplest thermal analysis instrument. It measures the weight loss of a sample as a function of temperature. TGA can be used to detect the heat decomposition temperature, or even the kinds of elements which are evaporating during heating, if it is connected with a mass spectrometer for elemental detection.

Figure 3.18 The Thermogravimetric Analyzer (TGA).

3.4.3 Microstructural Analysis

3.4.3.1 X-Ray Diffractometry (XRD)

Since the finished surface of the sample was shiny plane after casting, the whole sample was subjected to XRD 2θ scanning from 5^o to 80^o, at a step size of 0.04^o for 1 second. The diffractometer from Philips Xpert XRD System equipped with a rotating anode x-ray generator with a maximum output at 60kV & 60mA is shown in Figure 3.19. The installed anode target is copper (Cu) which generates $K\alpha_1$ radiation with a wavelength of 1.540598 Å with Ni filter attached at the shutter. Sample in bulky size was put on a sample holder and then was placed onto the platform of the diffractometer. The X-ray diffractograms were obtained with the generator set at a voltage of 40kV and a current of 30mA.

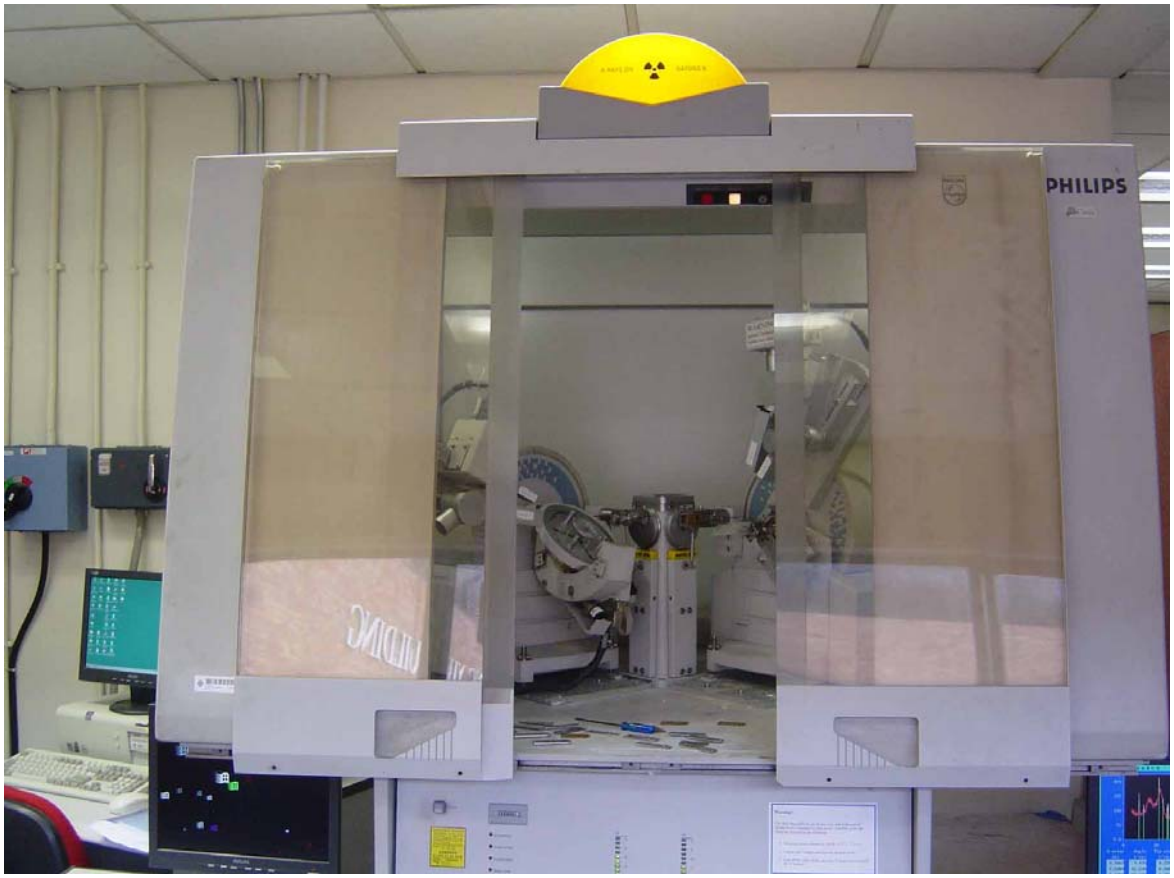

Figure 3.19 The X-Ray Diffractometer (XRD).

3.4.3.2 Scanning Electron Microscopy (SEM)

The fracture surface of the sample after tensile test was cut out and gold coated before being subjected to SEM microstructural investigation. The SEM from Leica Stereoscan 440 is shown in Figure 3.20. The maximum magnification can be reached at 300,000X. Energy Dispersive X-ray spectroscopy (EDX), Electron Backscattered Diffraction (EBSD) are equipped within the SEM to determine the types and quantities of elements down to Boron. Moreover, it can perform real time monitoring of tensile and compressive behavior of a sample. The tensile stage is a 5kN capacity and the heating facility is up to 800^{o}C. The Tungsten filament was operating at 20kV with the probe current set at about 50pA for SEM imaging, while the probe current set at about 400pA for EDX analysis.

Figure 3.20 The Scanning Electron Microscope (SEM).

Chapter 4

Mechanical Analysis

4.1 Introduction

Before a material is applied for real product, the mechanical properties such as the tensile strength, flexural strength, yield strength, Young's modulus, Vickers' hardness and the thermal properties such as the glass transition temperature, melting point, thermal expansion etc. should be obtained in order to fully utilize the material. In Chapter 4, the mechanical test results (tensile test, 3-point bending test and Vickers' hardness test) of the nanoclay-epoxy samples will be reported, while thermal test results will be discussed in Chapter 5.

4.2 Tensile test

Tensile test is the basic and vital measurement to obtain the mechanical parameters such as the tensile strength, yield strength and Young's modulus of a material. The yield strength is the stress that divides the elastic and plastic behavior of a material. After the material is stressed beyond the yield strength, the material will be permanently deformed. Tensile strength is the largest applied stress in a tensile test. If the material is loaded beyond the tensile strength, necking begins in ductile material. As the load continues rising, the necking region becomes narrower until fracture occurs at the breaking strength. Young's modulus is a measure of the

stiffness of the material, which is the initial linear portion of the slope of the stress-strain curve. Young's modulus is the ratio of initial stress to initial strain.

From the stress-extension curves of the epoxy samples as shown in Figure 4.1, the ultimate tensile strengths of all the samples with 0wt% to 8wt% nanoclay ranged from 42MPa to 46MPa. For epoxy samples with 0wt% to 1wt% nanoclay, they showed an obvious peak of ultimate tensile strength and went through necking with a tail before breaking. For epoxy samples with 2wt% to 6wt% nanoclay, the curves did show the peak of ultimate tensile strength, but they didn't go through significant necking before breaking. For epoxy samples with 7wt% & 8wt% nanoclay, they even broke at the peak tensile strength without any necking, which meant they were quite brittle. A magnified figure about the peak of the tensile strength region of the 10 compositions was shown at the top right hand corner in Figure 4.1.

The drop in the ultimate tensile strength for samples with 7wt% and 8wt% nanoclay was mostly due to the presence of big holes inside the nanoclay-epoxy samples. Those big holes were created when mixing the nanoclay-resin mixture with hardener. It was because as the nanoclay content increased, the mixture itself became too viscous and sluggish as shown in the photo in Figure 3.5. The increase in the nanoclay content in the resin increased the viscosity of the nanoclay-resin mixture. Once the hardener was added, big bubbles were easily created and trapped inside the sluggish mixture. When the samples were left inside the silicone mold for self curing and forming, the finished products would be full of bubbles. Later on, when it was tested under MTS loading machine, the bubbles inside couldn't withstand the load and might have initiated cracks that propagated throughout the sample. It is hypothesized that the presence of bubbles was the reason why those samples made of these two compositions showed lower ultimate tensile strength and the failure was brittle and catastrophic.

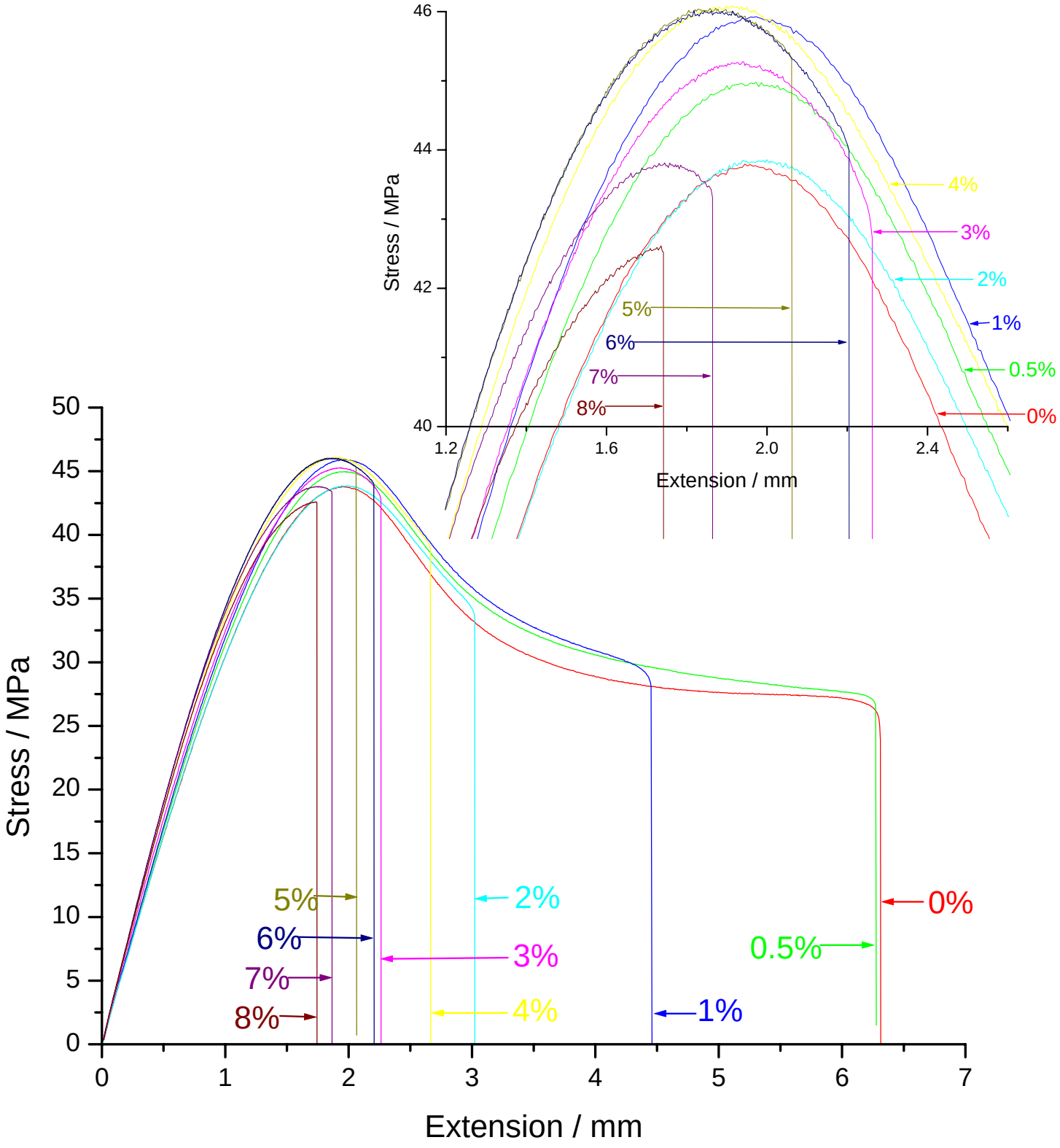

Figure 4.1 The stress-extension curves of epoxy samples with 0wt% to 8wt% nanoclay, tested at a crosshead speed of 2mm/min.

As the nanoclay content increased, the ultimate tensile strengths of the epoxy samples also increased when compared with that of pure epoxy sample. The increase in the strength of the epoxy samples must be due to the introduction of nanoclay, which hindered the molecular movement of polymer chains. The epoxy samples of 1wt%, 4wt%, 5wt% & 6wt% nanoclay showed an increment by 5% in the ultimate tensile strength when compared with that of pure epoxy sample. A graph of the ultimate tensile strength of samples as a function of weight percentage of nanoclay in epoxy from 0wt% to 8wt% was shown in Figure 4.2. However, the reason for the sudden drop in the ultimate tensile strength in 2wt% nanoclay was unknown. N. Sheng et al. found that 2wt% nanoclay is the critical exfoliated clay content above which matrix transcrystallization percolates [43]. The drop in the ultimate tensile strength in samples with 7wt% & 8wt% nanoclay was due to the bubbles inside the samples, as explained previously.

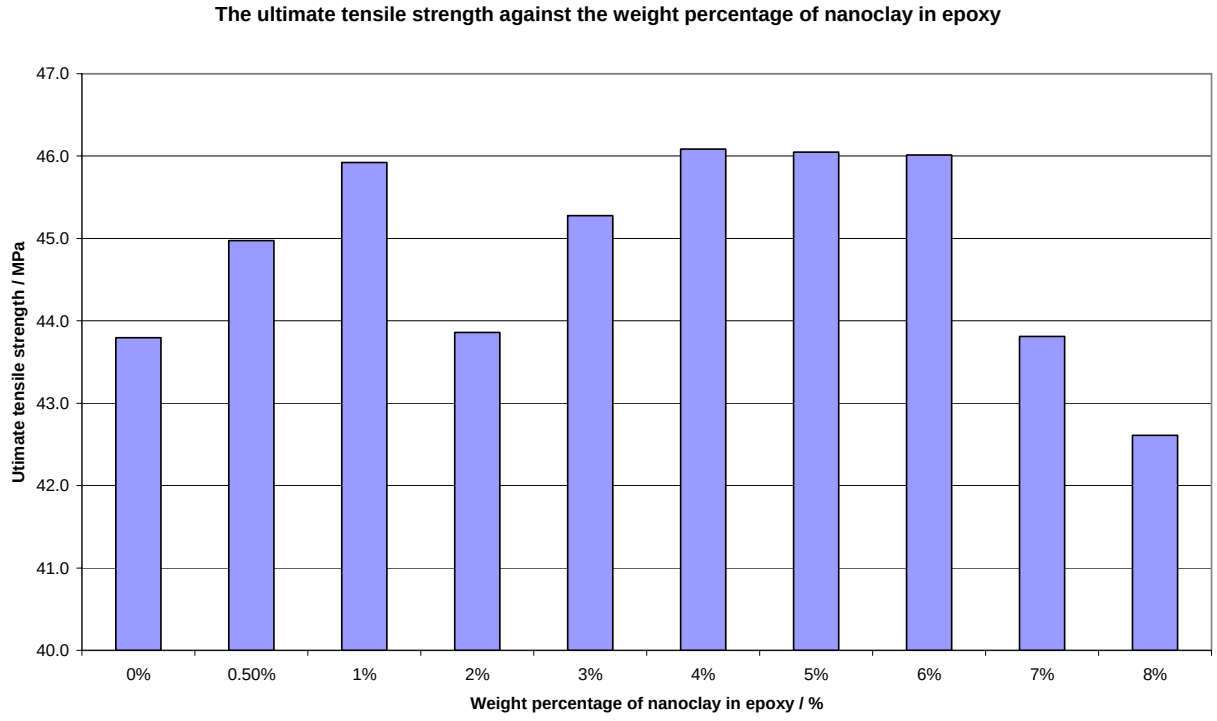

Figure 4.2 The ultimate tensile strength of samples as a function of weight percentage of nanoclay in epoxy from 0wt% to 8wt%.

A graph of the extension at the ultimate tensile strength of samples as a function of weight percentage of nanoclay in epoxy from 0wt% to 8wt% was shown in Figure 4.3. It showed a decreasing trend that as the nanoclay content increased, the extension decreased before arriving at the peak of the ultimate tensile strength. When combined with the results of the increased in the ultimate tensile strengths of the epoxy samples as the nanoclay content increased, the samples became stronger and stiffer. Or on the other way of saying, the samples with higher nanoclay content weren't as ductile as the samples with less nanoclay content. Moreover, T. X. Liu et al. also found the same behavior that the extension at yield decreased with increasing nanoclay content in polyamide 6 nanocomposites [44]. Again the exception was for the 2wt% nanoclay epoxy sample. On the contrary to the trend, the 2wt% nanoclay epoxy sample had longer extension before the peak of ultimate tensile strength, which meant it was softer.

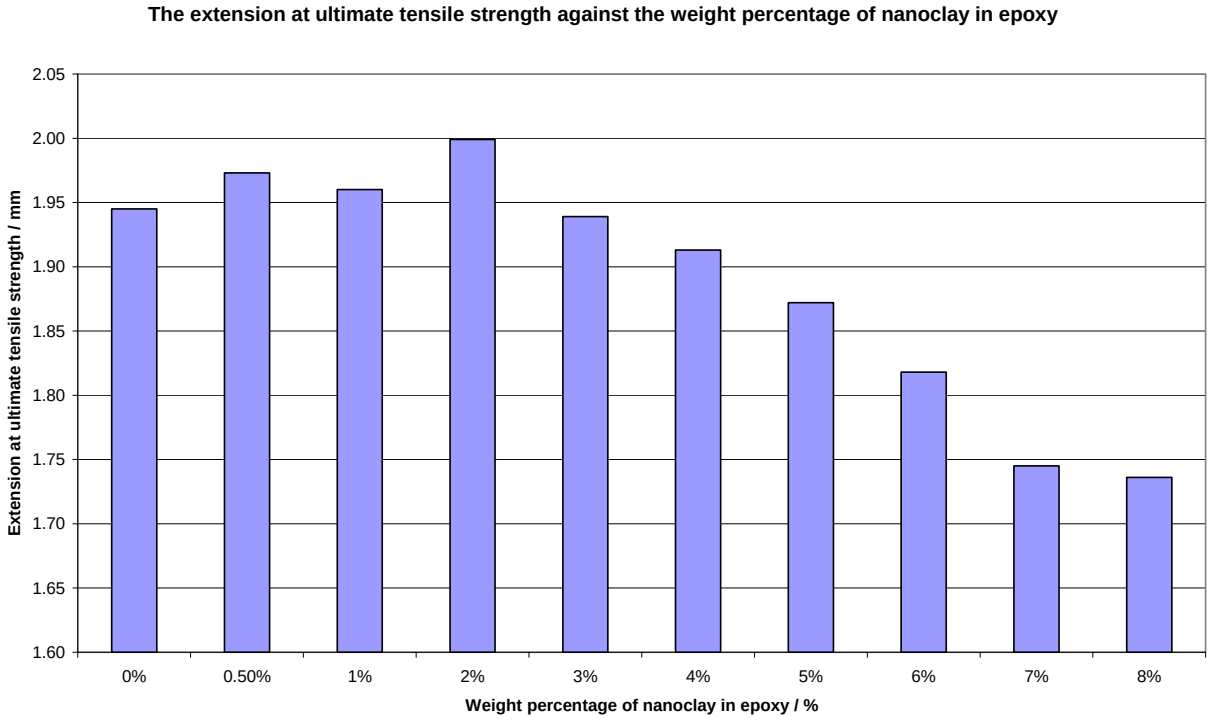

Figure 4.3 The extension at ultimate tensile strength of samples as a function of weight percentage of nanoclay in epoxy from 0wt% to 8wt%.

A graph of the elongation at break of samples as a function of weight percentage of nanoclay in epoxy from 0wt% to 8wt% was shown in Figure 4.4. It showed a decreasing trend that, as the nanoclay content increased, the elongation at break decreased. That meant the epoxy samples became less ductile. The ductility of the epoxy samples gradually dropped from 1wt% nanoclay. When comparing the elongation at break of pure epoxy sample with other nanoclay epoxy samples, the ductility dropped drastically by more than 70% for the 8wt% nanoclay sample and the failure was catastrophic. Similarly, M. F. Lai et al. also found in poly(ethylene terephthalate-co-ethylene naphthalate) PETN/Cloisite30B organoclay nanocomposites showed a higher tensile strength and modulus with increasing nanoclay content, but at the expense of reduced ductility [45]. Filler particles were believed to reduce the molecular mobility of polymer chains, producing a less flexible material with a higher tensile strength and Young's modulus.

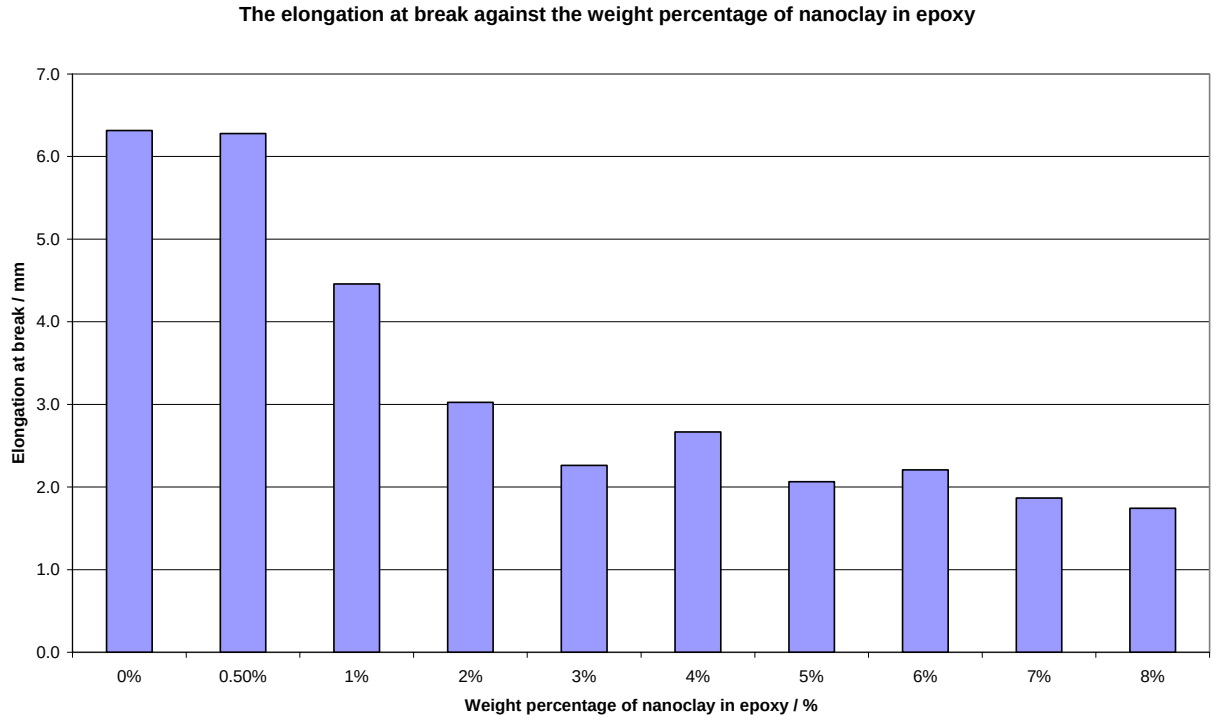

Figure 4.4 The elongation at break of samples as a function of weight percentage of nanoclay in epoxy from 0wt% to 8wt%.

4.3 3-Point Bending Test

In a ductile material, the stress-strain curve will show a peak of ultimate tensile strength, followed by a tail with necking, reducing the cross-sectional area before breaking as shown on the epoxy samples with 0wt% to 1wt% nanoclay in Figure 4.1.

However, in brittle materials such as the epoxy samples of 7wt% & 8wt% nanoclay in Figure 4.1, failure occurred at the ultimate tensile strength without necking. In the worst case, cracking even happened in the grips of the tensile testing machine before loading. In this situation, 3-point bending test needed to be employed. Flexural stress-deflection curves were obtained in the bending test, rather than the stress-strain curve in the normal tensile test. The results of the bending tests were similar to that of the stress-strain curves in tensile tests. Moreover, it was found that brittle materials failed at much higher compressive stresses than tensile stresses.

From the stress-deflection curves of the epoxy samples with 0wt% to 8wt% nanoclay content as shown in Figure 4.5, they all showed the same pattern with the compressive strength ranged from 61MPa to 67MPa, and the deflection curves went through a maximum peak and fading with a tail. Only the 7wt% & 8wt% nanoclay epoxy samples broke apart with a short tail, meaning that they were very brittle. As reflected from the real picture of the samples after the bending tests in Figure 3.11, the samples with 0wt% to 6wt% nanoclay content bended with a permanently deformed “V” shape, while the samples with 7wt% & 8wt% nanoclay content were completely torn apart. A magnified figure about the peak of the maximum deflection region of the 10 compositions was shown at the top right hand corner in Figure 4.5.

The flexural strength of samples against the weight percentage of nanoclay in epoxy from 0wt% to 8wt% was shown in Figure 4.6. The epoxy sample of 6wt% nanoclay showed the

largest flexural strength with an increment of 4.3% when compared with that of pure epoxy sample. And again 2wt% nanoclay sample showed a smaller compressive stress than the others, which was consistence with the tensile test results. The deflection at maximum stress of samples versus against the weight percentage of nanoclay in epoxy from 0wt% to 8wt% was shown in Figure 4.7.

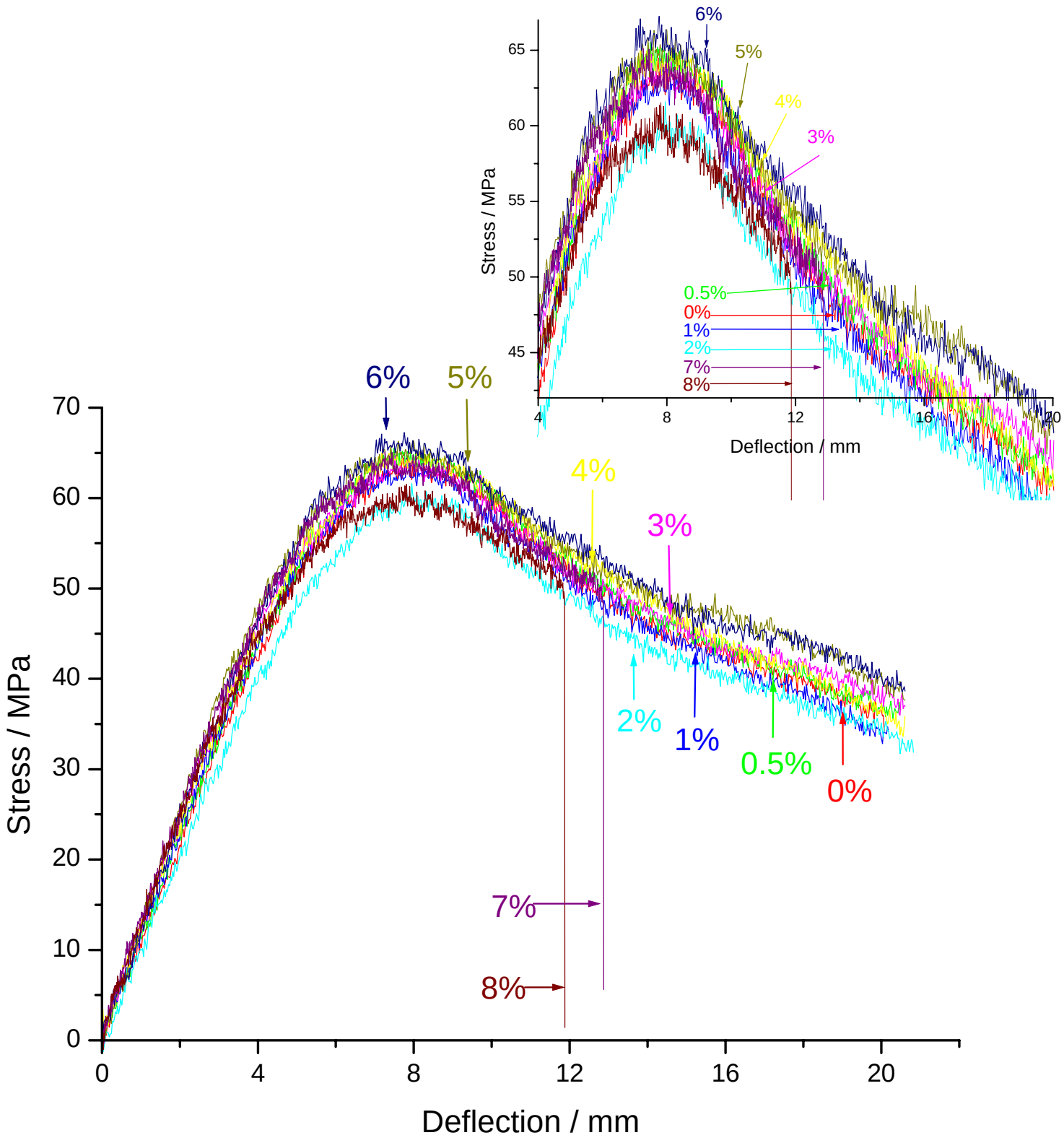

Figure 4.5 The stress-deflection curves of epoxy samples with 0wt% to 8wt% nanoclay, tested at a crosshead speed of 2mm/min.

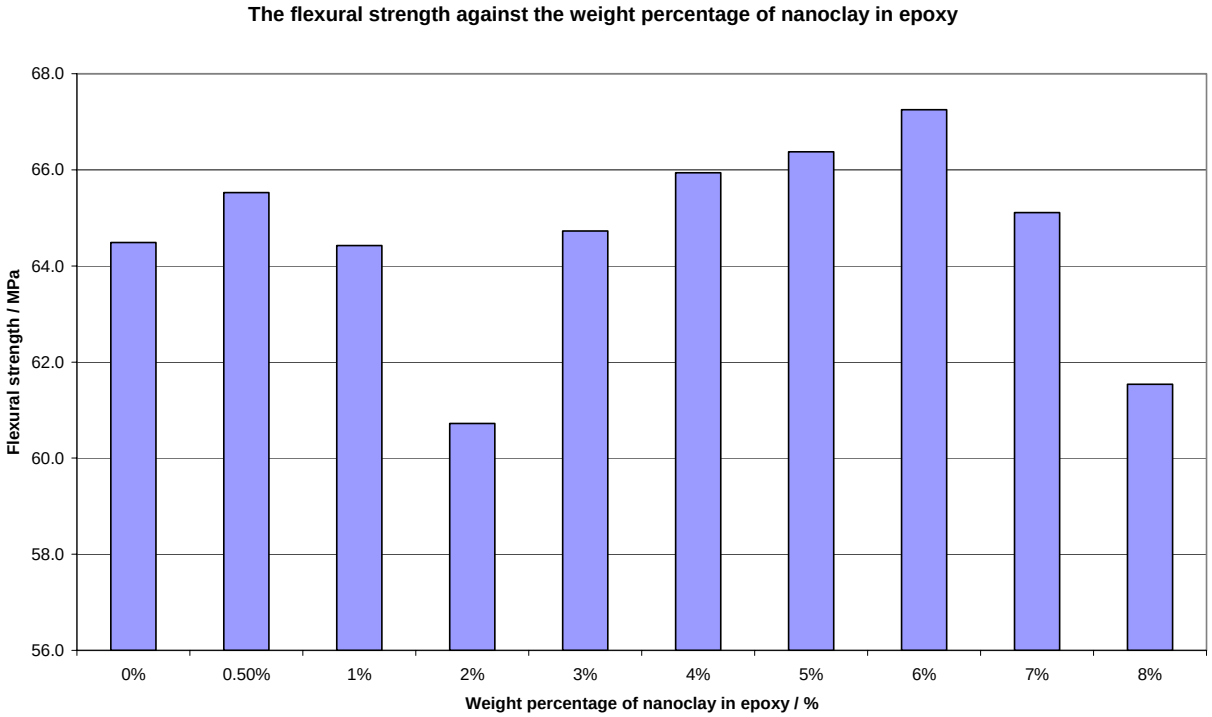

Figure 4.6 The flexural strength of samples as a function of weight percentage of nanoclay in epoxy from 0wt% to 8wt%.

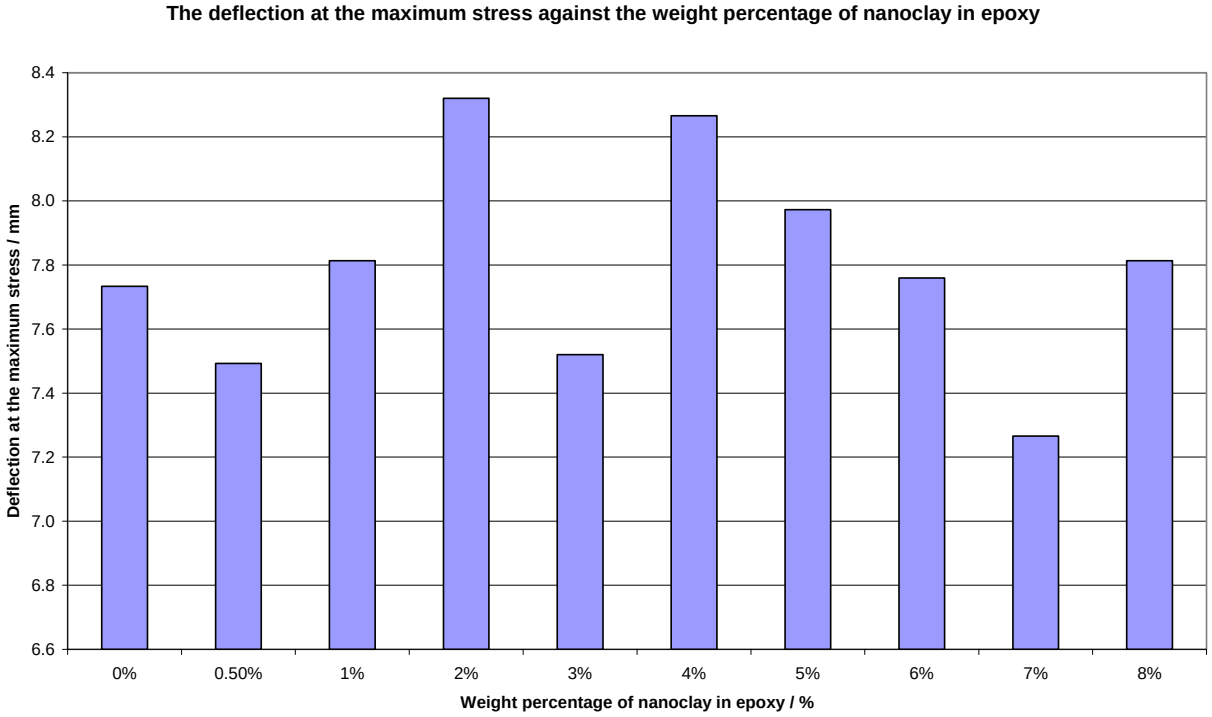

Figure 4.7 The deflection at maximum stress of samples as a function of weight percentage of nanoclay in epoxy from 0wt% to 8wt%.

4.4 Vickers' Hardness Test

A hardness test is a measure of the resistance to penetration on the surface of a material by a hard object. The Vickers' hardness measurements were similar to the results of the tensile tests, since there is a co-relationship between the hardness and the tensile strength in terms of mechanical property.

A graph of the Vickers' hardness value of samples as a function of weight percentage of nanoclay in epoxy from 0wt% to 8wt% was shown in Figure 4.8. The 5wt% nanoclay sample showed the largest HV value of 11.3 when compared with that of pure epoxy sample of HV 9.8, the increase in Vickers' hardness value was 15%. That meant 5wt% nanoclay sample was the hardest among all the compositions. And again 2wt% nanoclay sample showed a drop in the hardness value of HV 10.1. This result was consistent as illustrated in Figures 4.2 & 4.6 that 2wt% nanoclay sample was softer.

In conclusion, when analyzing the graphs from Figure 4.1 to Figure 4.4, samples with nanoclay content below 1wt% were ductile, while samples with nanoclay content from 2wt% to 6wt% were in between the ductile and brittle transition and developed higher strength than pure epoxy sample. However, samples with nanoclay content above 7wt% were brittle. Upon review of the results of all the mechanical tests (tensile tests, 3-point bending tests and Vickers' hardness tests), the compositions at 4wt%, 5wt% & 6wt% nanoclay content were feasible to produce with enhanced mechanical properties.

However, for the ease of casting and in order to mold samples with good mechanical properties, the nanoclay content should be kept below 5wt% to avoid viscosity-related casting problems [46].

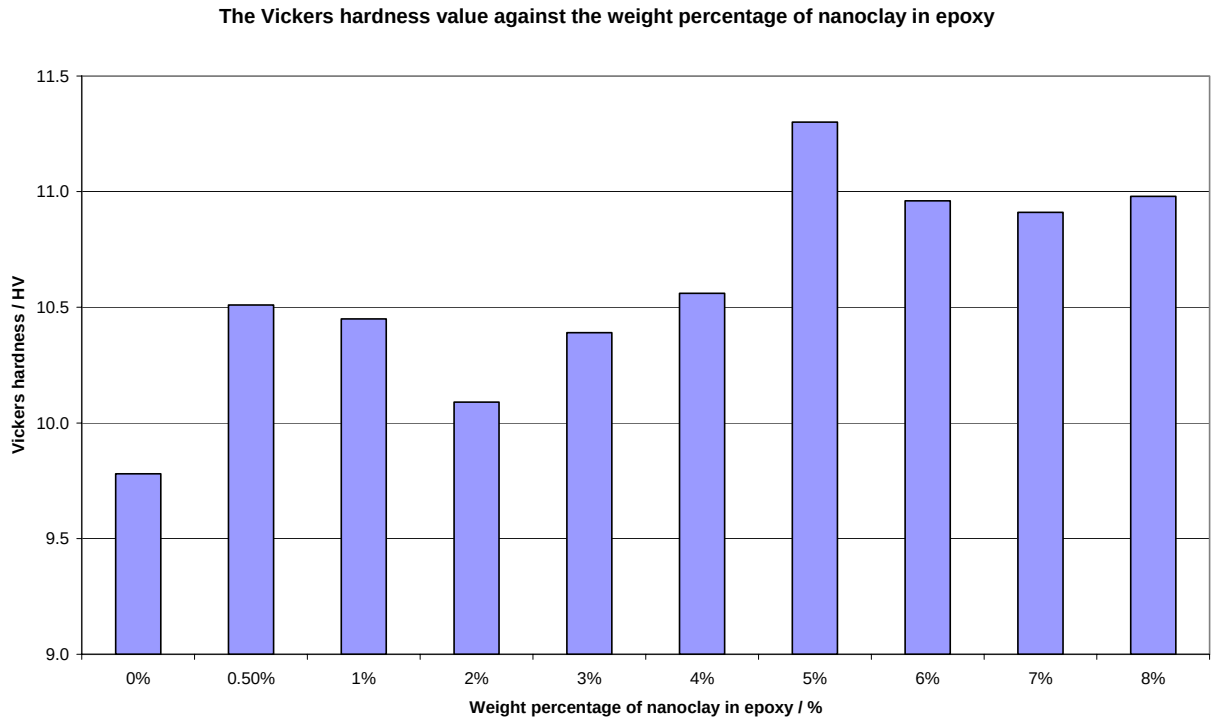

Figure 4.8 The Vickers' hardness value of samples as a function of weight percentage of nanoclay in epoxy from 0wt% to 8wt%.

Chapter 5

Thermal Analysis

5.1 Introduction

Thermal analysis of a material plays an important role in our daily lives. For an example, if a plastic cup of water is heating up in a microwave oven, will this plastic cup be rigid enough to withhold the water at elevated temperature? Or will this plastic cup decompose at this temperature, and so on? In this chapter 5, thermal analysis instruments such as Dynamic Mechanical Analyzer (DMA), Thermomechanical Analyzer (TMA) and Thermogravimetric Analyzer (TGA) will be employed to find out the glass transition temperature, elastic modulus, coefficient of linear thermal expansion and decomposing temperature respectively for the nanoclay-epoxy samples.

5.2 Dynamic Mechanical Analysis (DMA)

Dynamic Mechanical Analysis (DMA) is becoming more and more commonly used in the analytical laboratory as a tool rather than a research curiosity. It supplies information about the major transitions such as glass transition (T_g or alpha transition T_α) or as well as secondary (T_β or beta transition) and tertiary (T_γ or gamma transition) transitions, which are not readily identified by other methods. It also allows characterization of bulk properties such as elastic

modulus (*E'*, the ability to restore energy), loss modulus (*E"*, the ability to lose energy) and tan δ (damping, the ratio of *E"* / *E'*), which are directly affecting the material performance.

The glass transition (T_g) of a polymer is the change from the glassy to rubbery behavior where the polymer chains gain enough mobility to slide over each other. Therefore, T_g is assigned to be the gradual chain movement, whereas the beta transition (T_β) is assigned to be the other changes in molecular motions. The beta transition is often associated with the side chain or pendant group movements and can often be related to the toughness of a polymer. It is important to note that beta and gamma transitions are too faint to be detected in the differential scanning calorimeter (DSC) or Thermomechanical Analyzer (TMA).

In the following DMA results, T_g is considered to be the onset of the drop of the elastic modulus. It is because once the elastic modulus drops, that means the material is no longer strong enough to withstand the applied force, and ready to change from glassy to rubbery behavior. Therefore, the change in the slope of the elastic modulus signifies a glass transition. Since T_g only occurs in amorphous materials, on the other hand, in a completely crystalline materials, T_g cannot be detected. At glass transition, large segments of the chains start moving. When the temperature continues rising, large scale chains slippage occurs and the polymer flows, this is the melting temperature of the polymer T_m. However, in this case, after the T_g, nothing will happen for the epoxy samples. In fact, the epoxy samples begin to burn or degrade because epoxy is a thermoset, the cross-linking prevent the polymer chains from slipping each other. Therefore, cross-linked polymers don't flow.

5.2.1 Tensile Test in DMA

Tensile tests for the epoxy samples from 0wt% to 8wt% nanoclay measured in DMA with frequency scans at 1Hz, 2Hz, 5Hz & 10Hz as a function of temperature from 25^{o}C to 140^{o}C were shown in Figure 5.1 – Figure 5.4 respectively, all 10 curves showed the same tensile behavior.

It was found that the elastic modulus of the epoxy samples dropped at around 50^{o}C. A drop in the elastic modulus signifies a glass transition. When studied carefully with the magnified figure around the onset of the drop of the elastic modulus at the top right hand corner in each Figure 5.1 – Figure 5.4, the T_g of the epoxy samples took place at 45^{o}C. It was found that as the scanning frequencies increased, the epoxy samples appeared a bit stiffer by comparing the tails of the 10 compositions at each magnified figure at the top right hand corner in Figures 5.1 – 5.4. In the magnified figure scanned at 1Hz in Figure 5.1, the tails at 50^{o}C with elastic modulus of average 1x10^{9}Pa, while that in the magnified figure scanned at 10Hz in Figure 5.4, the elastic modulus at 50^{o}C was increased up to average 1.3x10^{9}Pa. Therefore, samples tested at higher frequencies seemed to be stiffer as the samples behaved stronger to try to resist the cyclic change.

Graphs of the elastic modulus of epoxy samples at 25^{o}C and the temperature of epoxy samples at which the elastic modulus dropped at 1x10^{9}Pa as a function of weight percentage of nanoclay in epoxy measured in DMA tensile mode at frequencies 1 Hz, 2Hz, 5Hz & 10Hz were shown in Figure 5.5 – Figure 5.8 respectively. 7wt% nanoclay sample showed the highest elastic modulus of 1.84x10^{9}Pa at 1Hz to 1.89x10^{9}Pa at 10Hz at 25^{o}C, while 2wt% nanoclay sample showed the lowest elastic modulus of 1.71x10^{9}Pa at 1Hz to 1.76x10^{9}Pa at 10Hz at 25^{o}C among all the compositions. When compared 7wt% nanoclay sample with 0wt% nanoclay sample with elastic modulus of 1.74x10^{9}Pa at 1Hz to 1.78x10^{9}Pa at 10Hz at 25^{o}C, the increment in the elastic modulus was 5.7% at 1Hz and 6.2% at 10Hz respectively.

5wt% nanoclay sample showed the best tensile performance upon elevated temperature among all the compositions. The temperature of 5wt% nanoclay sample at which the elastic modulus dropped at $1x10^9$Pa increased from 51°C to 53°C at scanning frequencies at 1Hz and 10Hz respectively, while 2wt% nanoclay sample showed the lowest tensile performance, where the temperature of 2wt% nanoclay sample at which the elastic modulus dropped at $1x10^9$Pa increased only from 48°C to 50°C at scanning frequencies at 1Hz and 10Hz respectively, which was about 3°C lower than that of 5wt% nanoclay sample.

In general, 7wt% nanoclay sample showed the highest elastic modulus at 25°C, 5wt% nanoclay sample showed the best tensile behavior upon elevated temperature above 50°C, while 2wt% nanoclay sample showed both the lowest elastic modulus at 25°C and the lowest tensile performance at elevated temperature among all the compositions. As the nanoclay content in the epoxy samples increased except at 2wt% nanoclay content, the elastic modulus at room temperature or even after glass transition T_g, the tensile performance also increased. It is stated above that the glass transition is associated with the gradual polymer chains movement. The increase in the elastic modulus of the epoxy samples was a result of the difficulty in the movement of the polymer chains. This may be explained by the nanoclay interrupted with the polymer chains in a certain extent, making the polymer chains difficult to move. Therefore, the tensile performance of the epoxy samples enhanced with the nanoclay content.

The results from tensile in DMA were consistent with those from tensile in MTS Instron loading machine done at room temperature in Chapter 4. Both tensile tests results showed that 5wt% nanoclay sample was stiffer, while 2wt% nanoclay sample was softer. Moreover, as the nanoclay content in the epoxy samples increased, the elastic modulus, the glass transition temperature and the tensile performance upon elevated temperature also increased.

5.2.2 3-Point Bending Test in DMA

On the other hand, 3-point bending tests for the epoxy samples from 0wt% to 8wt% nanoclay measured in DMA with frequency scans at 1Hz, 2Hz, 5Hz & 10Hz as a function of temperature from 25^{o}C to 140^{o}C were shown in Figure 5.9 – Figure 5.12 respectively, all 10 curves showed the same bending behavior.

The elastic modulus of the epoxy samples as shown in Figure 5.9 – Figure 5.12 dropped at around 40^{o}C. Similarly to tensile tests, as the frequency scan increased, the elastic modulus of the epoxy samples in the 3-point bending tests appeared a bit stiffer by comparing the tails of the 10 compositions at each magnified figure at the top right hand corner in Figures 5.9 – 5.12. In the magnified figure scanned at 1Hz in Figure 5.9, the tails at 42^{o}C with elastic modulus of average 3x10^{9}Pa, while that in the magnified figure scanned at 10Hz in Figure 5.12, the elastic modulus at 42^{o}C was increased up to average 3.7x10^{9}Pa. Therefore, samples tested at higher frequencies were stiffer as the samples behaved stronger to try to resist the cyclic change.

Graphs of the elastic modulus of epoxy samples at 25^{o}C and the temperature of epoxy samples at which the elastic modulus dropped at 1x10^{9}Pa as a function of weight percentage of nanoclay in epoxy measured in DMA bending mode at frequencies 1 Hz, 2Hz, 5Hz & 10Hz were shown in Figure 5.13 – Figure 5.16 respectively. 7wt% nanoclay sample showed the highest elastic modulus of 5.86x10^{9}Pa at 1Hz to 6.02x10^{9}Pa at 10Hz at 25^{o}C, while 0.5wt% nanoclay sample showed the lowest elastic modulus of 4.9x10^{9}Pa at 1Hz to 5.07x10^{9}Pa at 10Hz at 25^{o}C among all the compositions. When compared 7wt% nanoclay sample with 0wt% nanoclay sample with elastic modulus of 5.26x10^{9}Pa at 1Hz to 5.38x10^{9}Pa at 10Hz at 25^{o}C, the increment in the elastic modulus was 11.4% at 1Hz and 11.9% at 10Hz respectively.

7wt% nanoclay sample showed the best tensile performance upon elevated temperature among all the compositions. The temperature of 7wt% nanoclay sample at which the elastic modulus dropped at $1x10^9$Pa increased from 43.6°C to 44.8°C at scanning frequencies at 1Hz and 10Hz respectively, while 4wt% nanoclay sample showed the lowest tensile performance, where the temperature of 4wt% nanoclay sample at which the elastic modulus dropped at $1x10^9$Pa increased only from 40.8°C to 42°C at scanning frequencies at 1Hz and 10Hz respectively, which was about 3°C lower than that of 7wt% nanoclay sample.

In general, both tensile tests and 3-point bending tests performed in DMA showed the epoxy samples with glass transition at around 40°C to 45°C. However, the increased in nanoclay content in the epoxy samples didn't make much difference on the shift of the T_g. On the other hand, the increased in the nanoclay content in the epoxy samples contributed to higher strength of the materials at room temperature and even upon elevated temperature. The increment in the elastic modulus of the 7wt% nanoclay sample when compared with pure epoxy sample was more significant in 3-point bending mode by an increase in 12% than that in tensile mode by an increase in 6% performed in DMA.

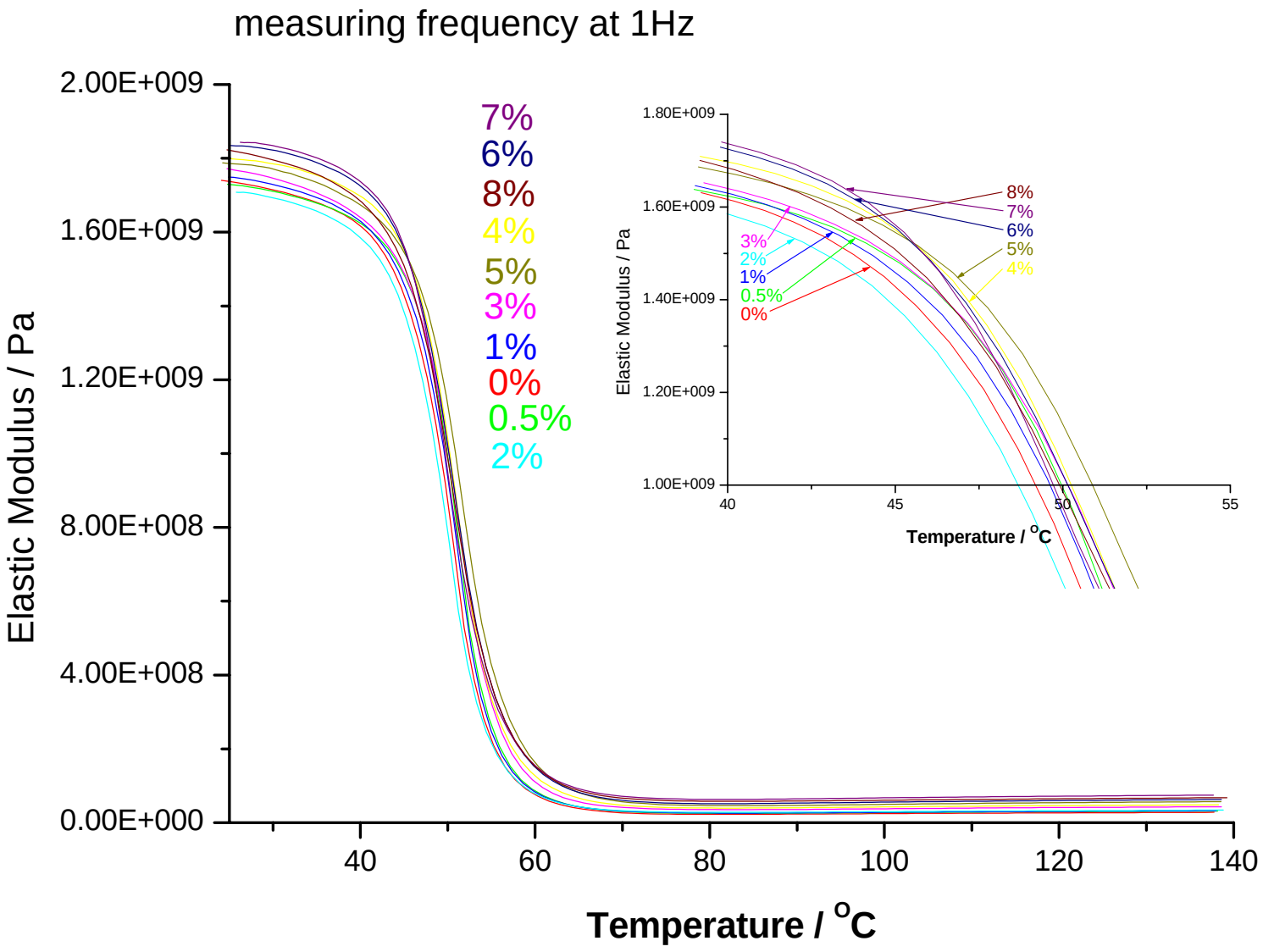

Figure 5.1 The elastic modulus of epoxy samples from 0wt% to 8wt% nanoclay as a function of temperature from 25°C to 140°C measured at 1 Hz frequency scan in DMA tensile test.

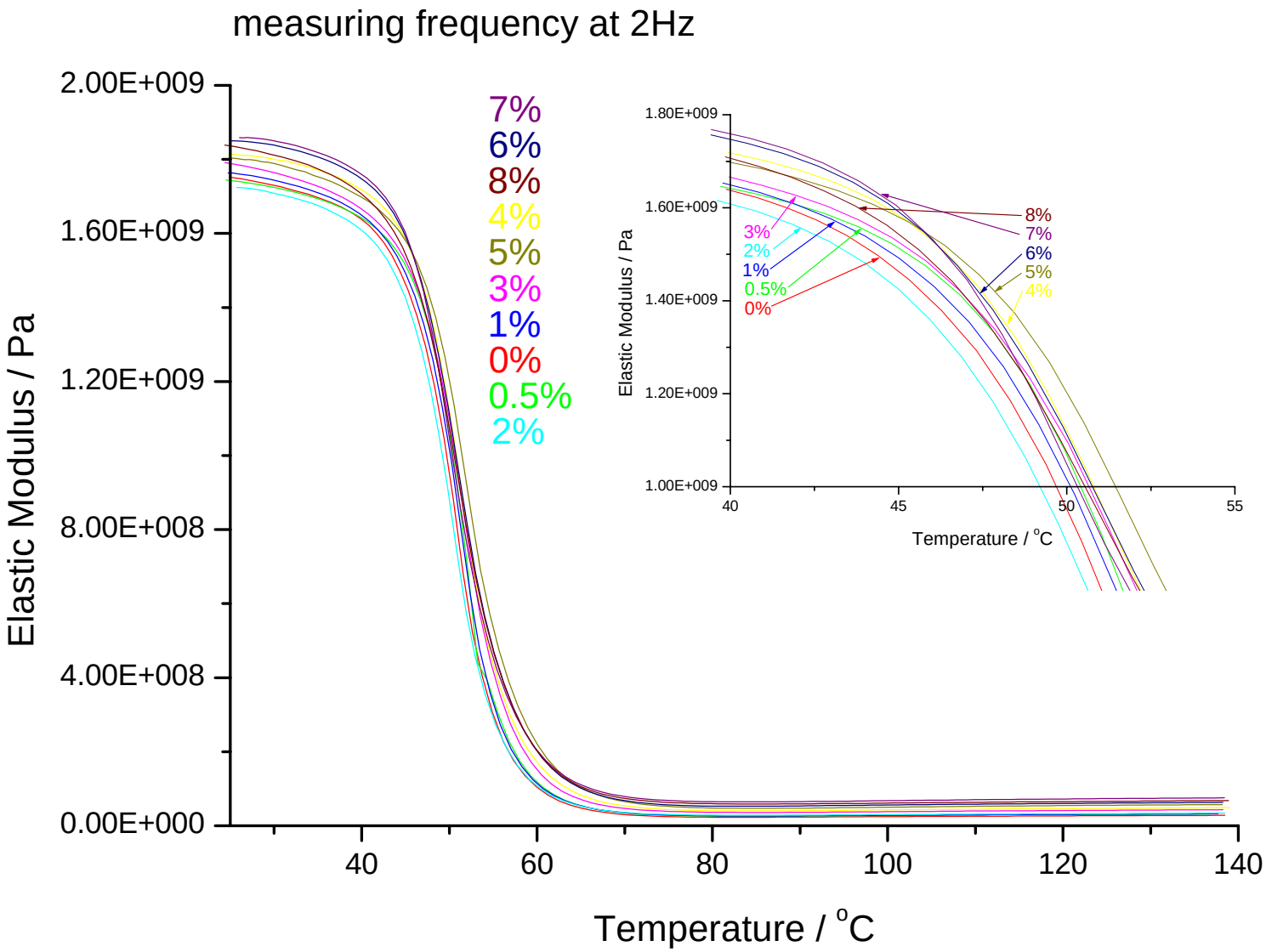

Figure 5.2 The elastic modulus of epoxy samples from 0wt% to 8wt% nanoclay as a function of temperature from 25°C to 140°C measured at 2 Hz frequency scan in DMA tensile test.

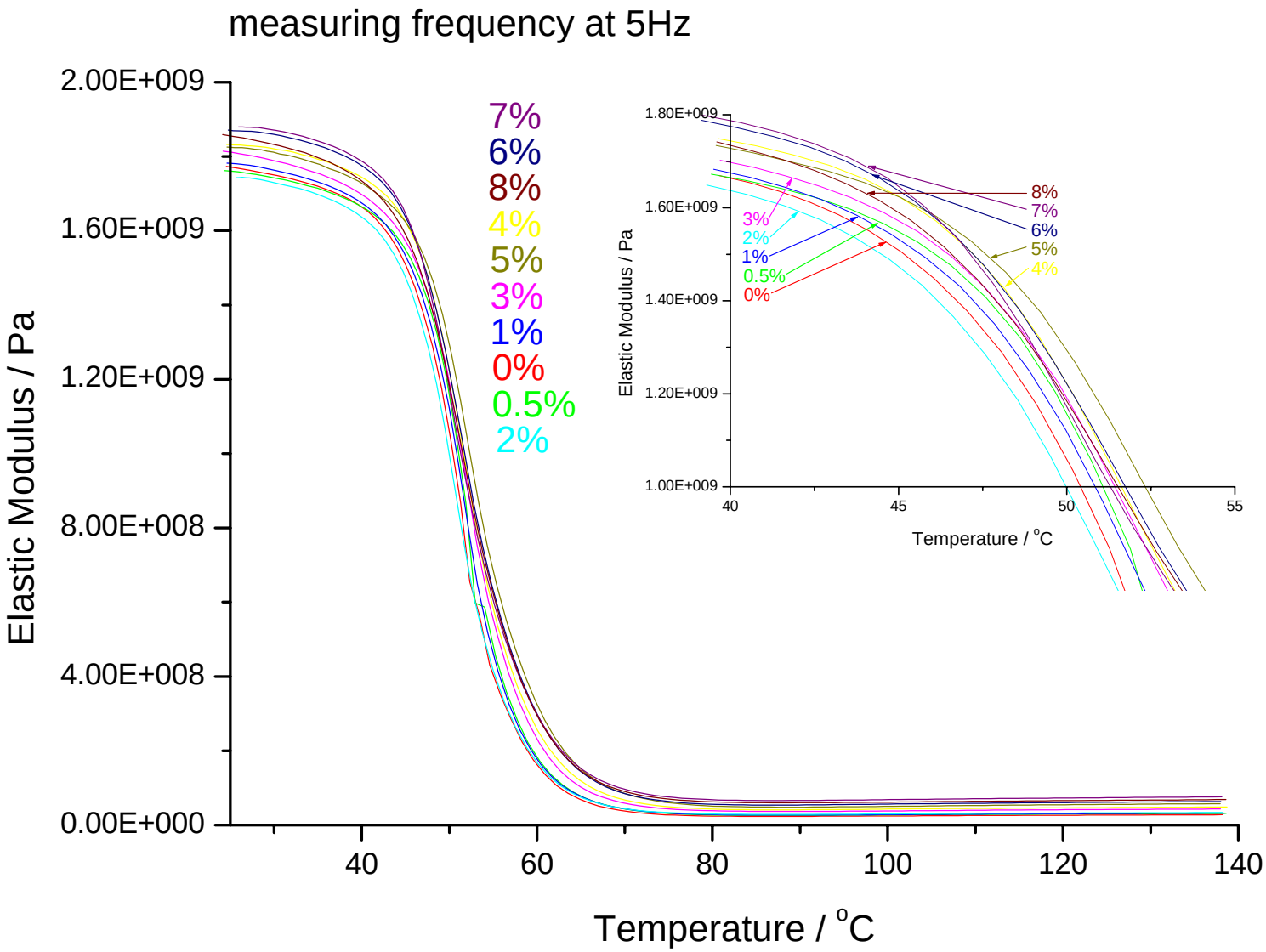

Figure 5.3 The elastic modulus of epoxy samples from 0wt% to 8wt% nanoclay as a function of temperature from 25°C to 140°C measured at 5 Hz frequency scan in DMA tensile test.

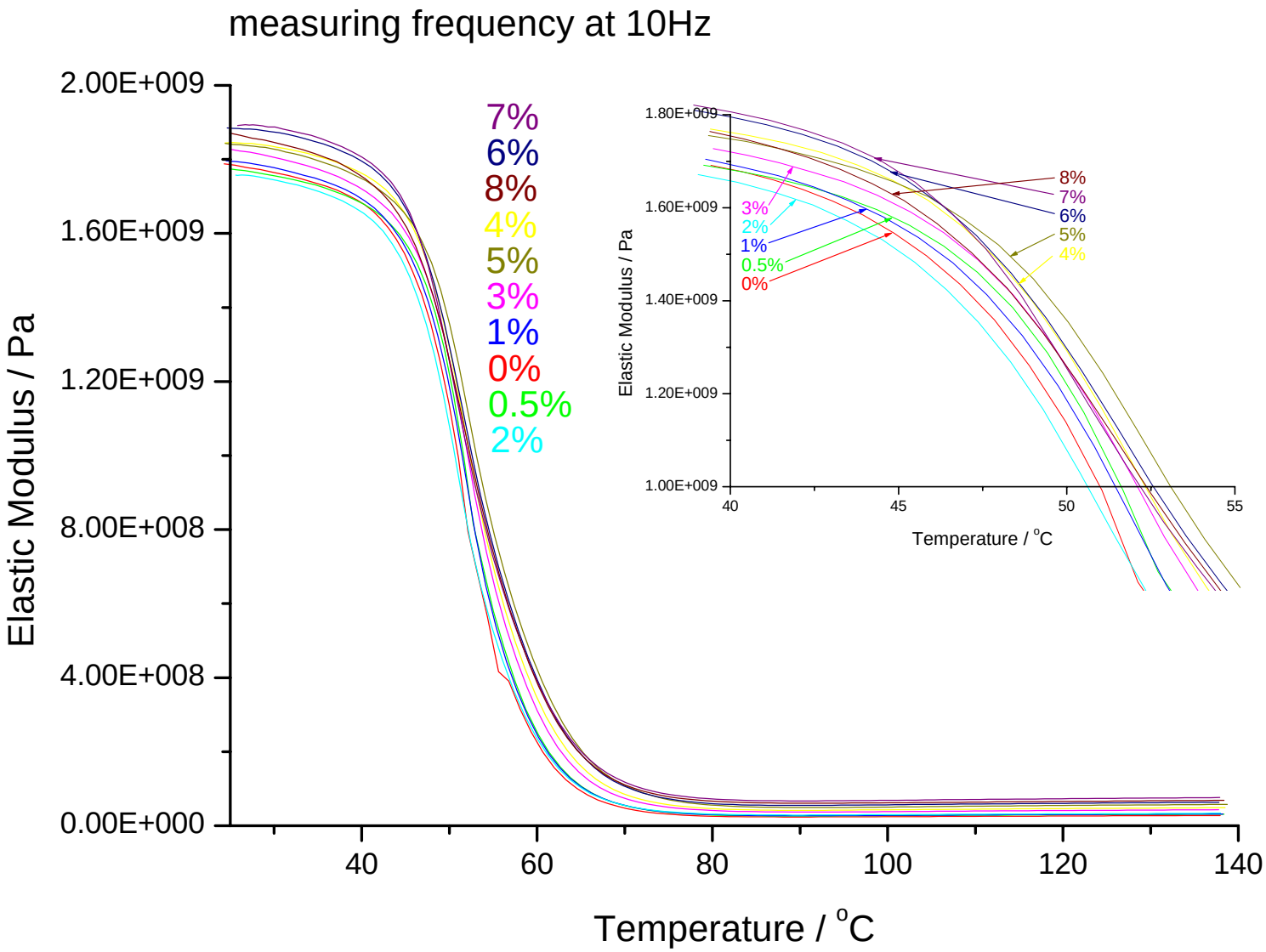

Figure 5.4 The elastic modulus of epoxy samples from 0wt% to 8wt% nanoclay as a function of temperature from 25°C to 140°C measured at 10 Hz frequency scan in DMA tensile test.

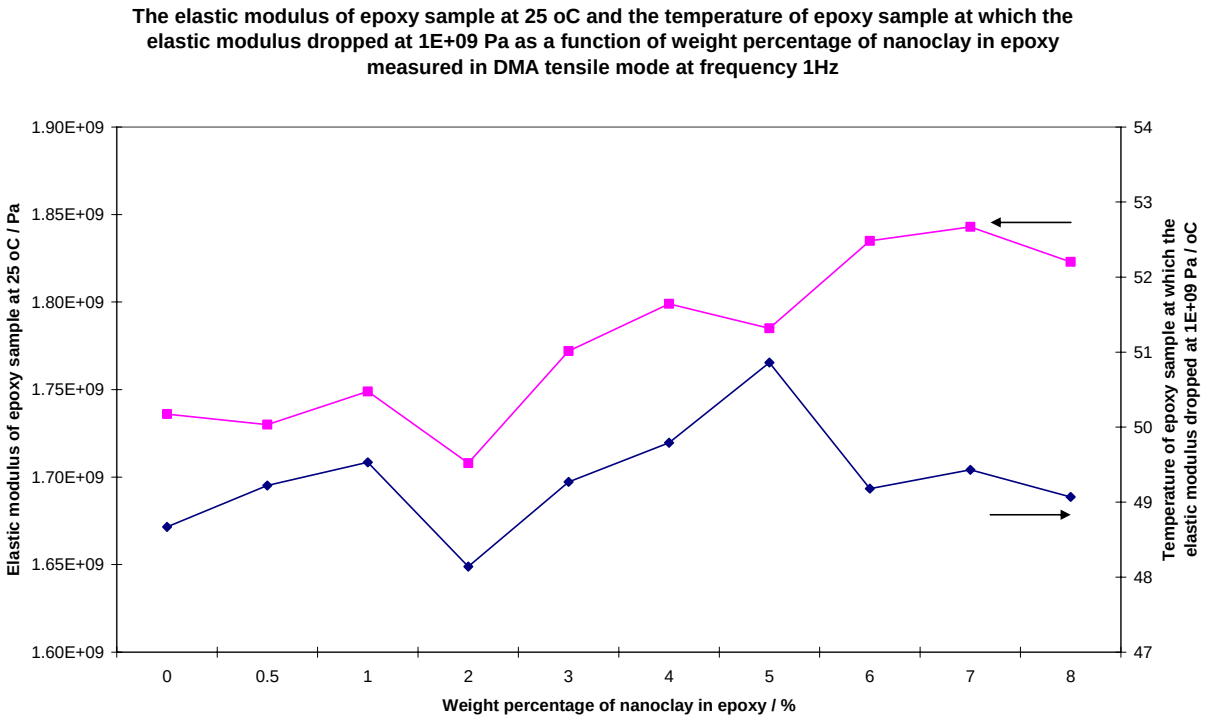

Figure 5.5 The elastic modulus of epoxy sample at 25°C and the temperature of epoxy sample at elastic modulus $1x10^9$ Pa as a function of weight percentage of nanoclay in epoxy measured in DMA tensile mode at frequency 1 Hz.

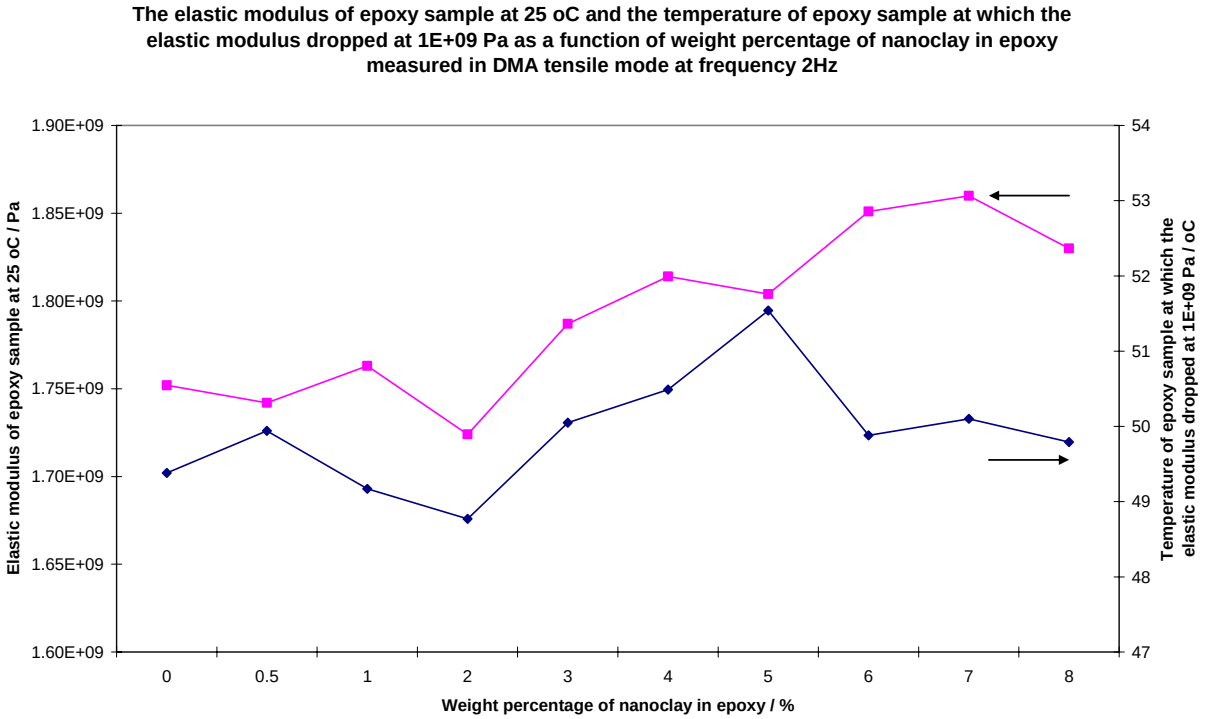

Figure 5.6 The elastic modulus of epoxy sample at 25°C and the temperature of epoxy sample at elastic modulus $1x10^9$ Pa as a function of weight percentage of nanoclay in epoxy measured in DMA tensile mode at frequency 2 Hz.

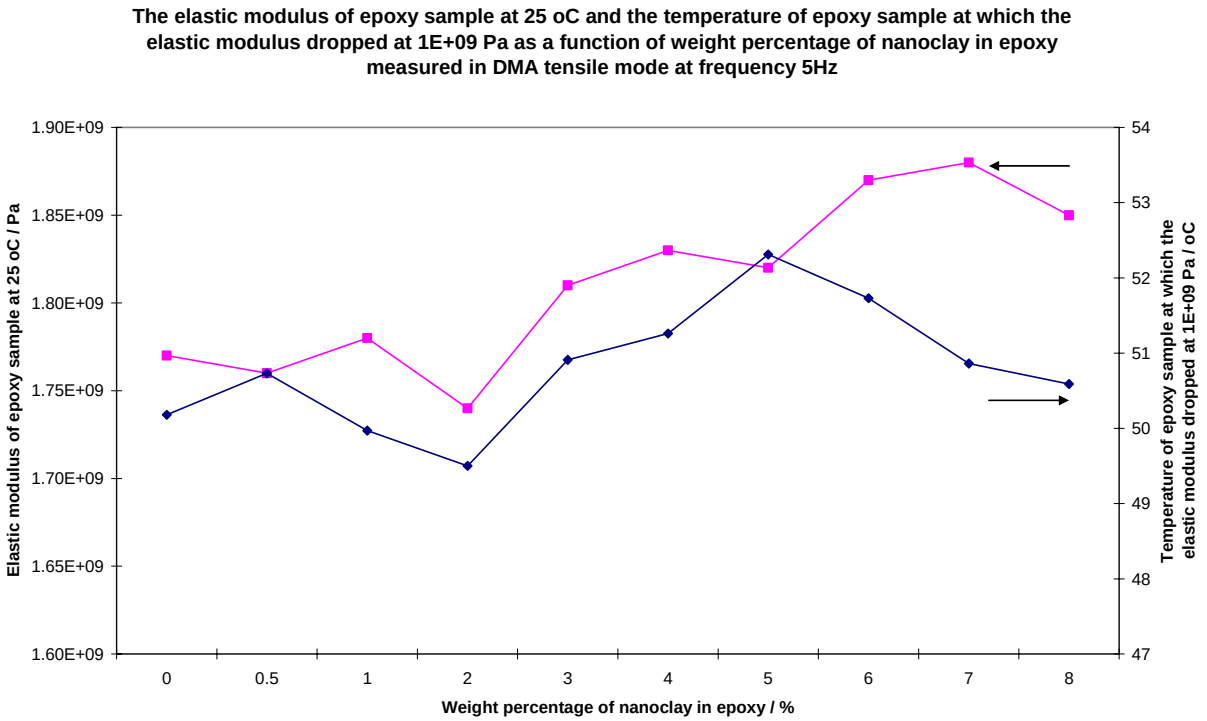

Figure 5.7 The elastic modulus of epoxy sample at 25°C and the temperature of epoxy sample at elastic modulus $1x10^9$ Pa as a function of weight percentage of nanoclay in epoxy measured in DMA tensile mode at frequency 5 Hz.

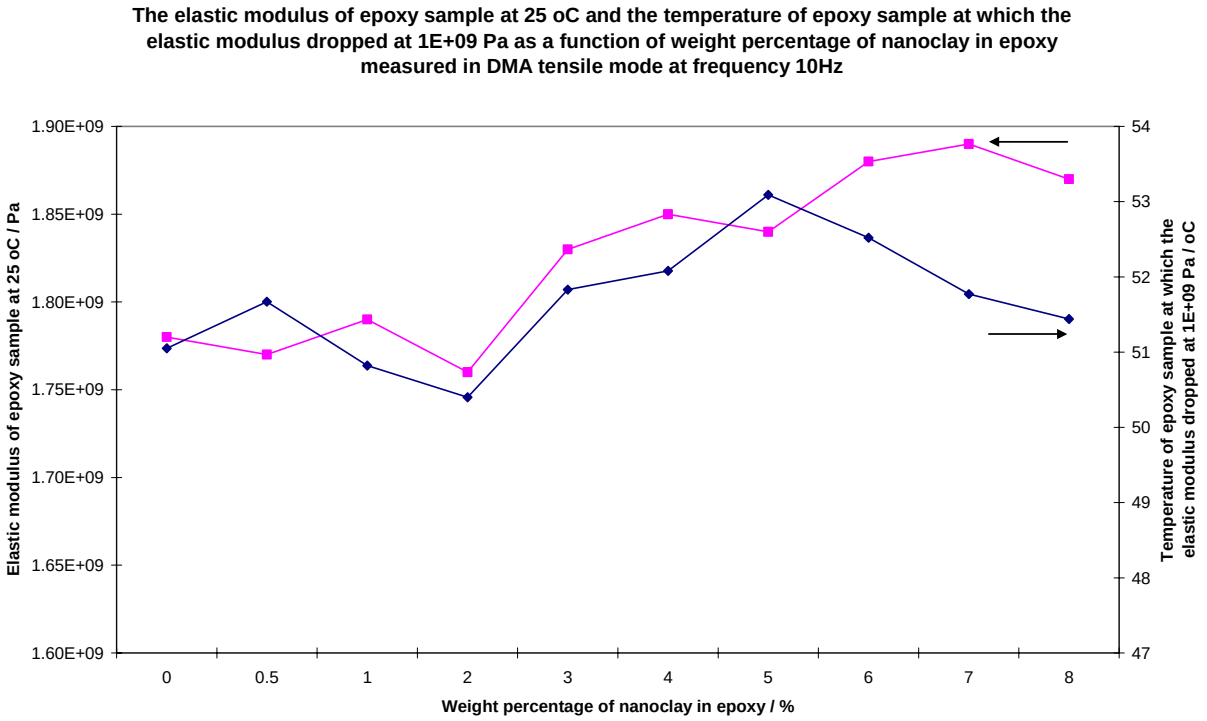

Figure 5.8 The elastic modulus of epoxy sample at 25°C and the temperature of epoxy sample at elastic modulus $1x10^9$ Pa as a function of weight percentage of nanoclay in epoxy measured in DMA tensile mode at frequency 10 Hz.

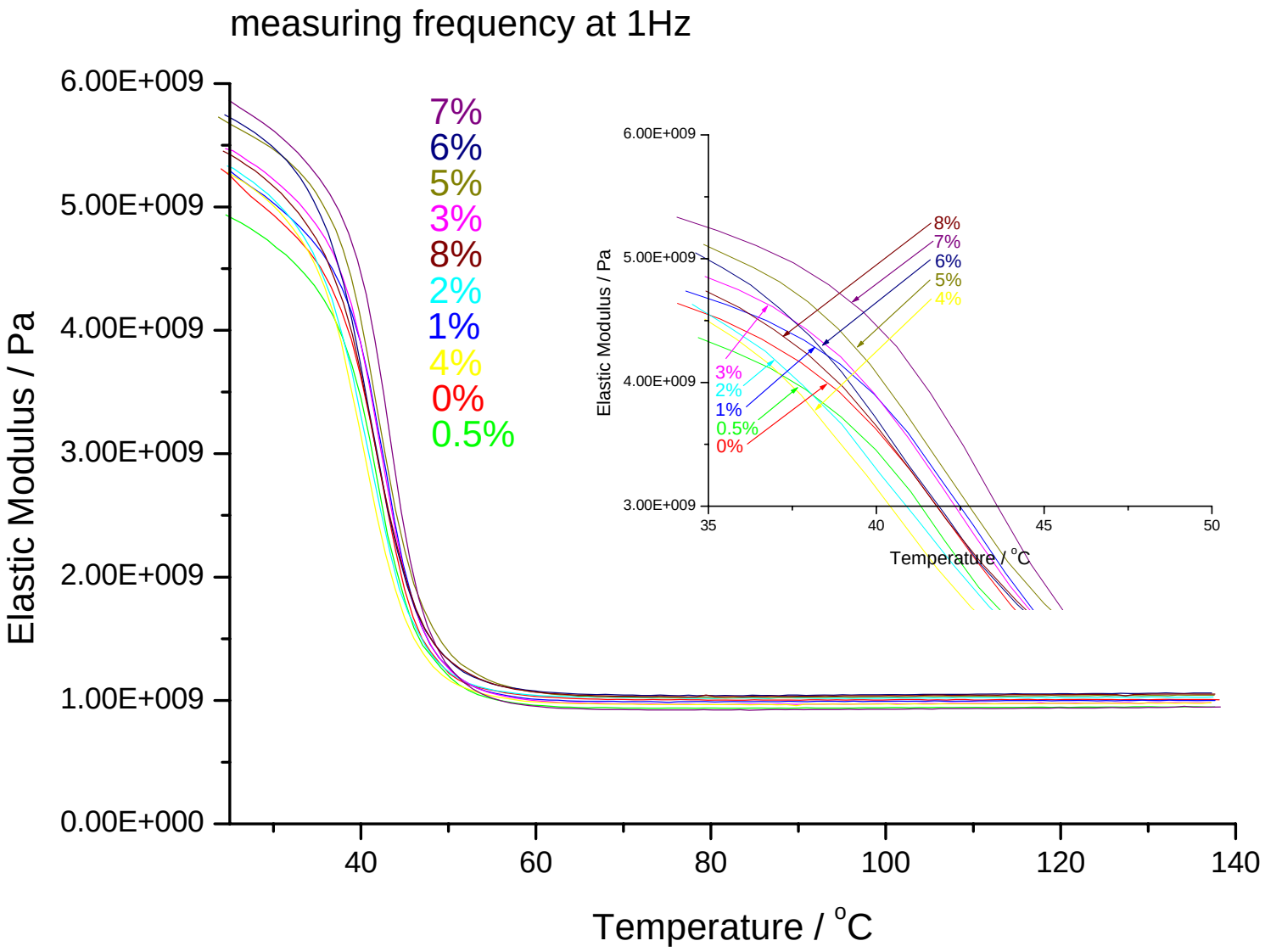

Figure 5.9 The elastic modulus of epoxy samples from 0wt% to 8wt% nanoclay as a function of temperature from 25°C to 140°C measured at 1 Hz frequency scan in DMA 3-point bending test.

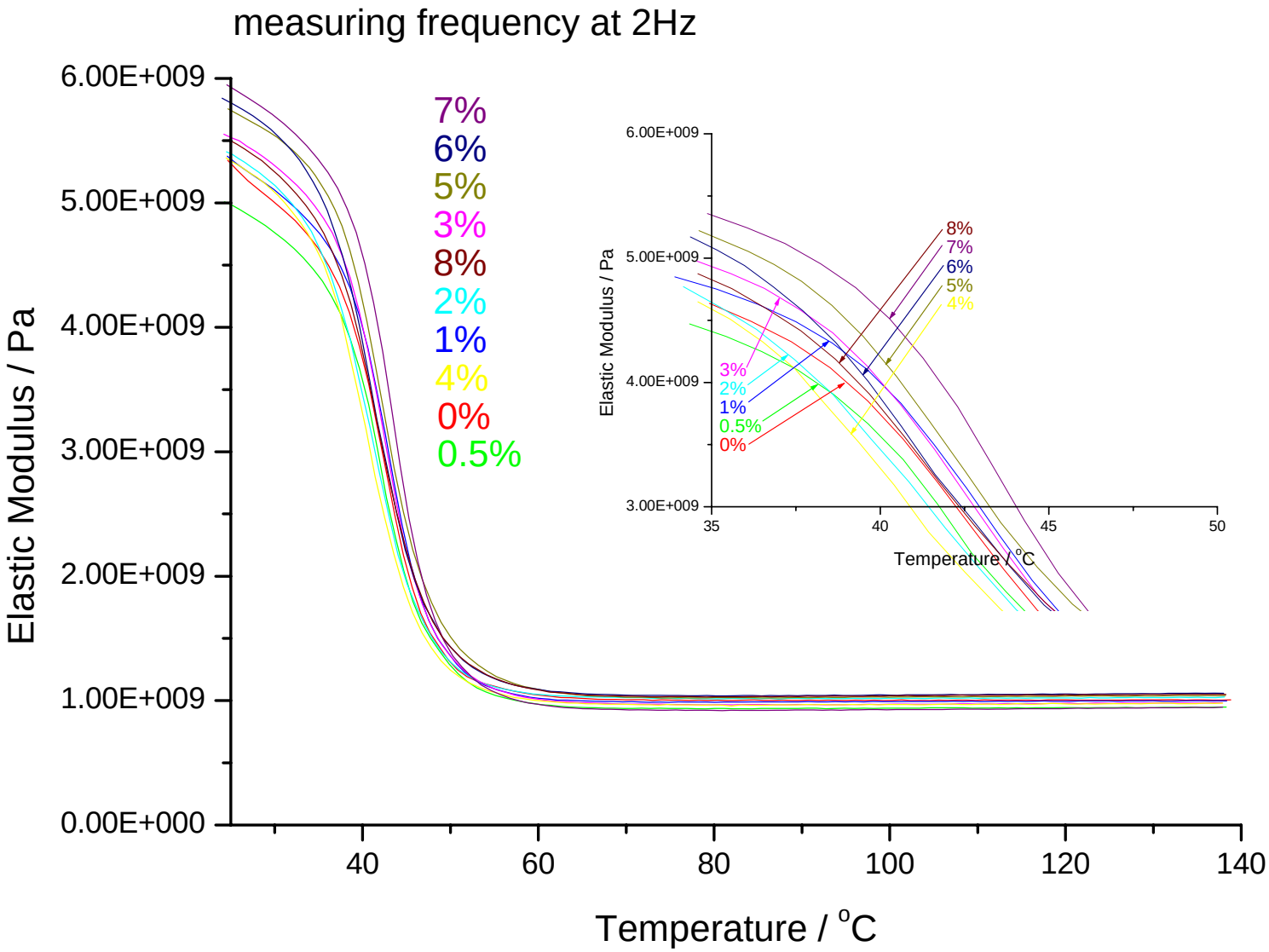

Figure 5.10 The elastic modulus of epoxy samples from 0wt% to 8wt% nanoclay as a function of temperature from 25°C to 140°C measured at 2 Hz frequency scan in DMA 3-point bending test.

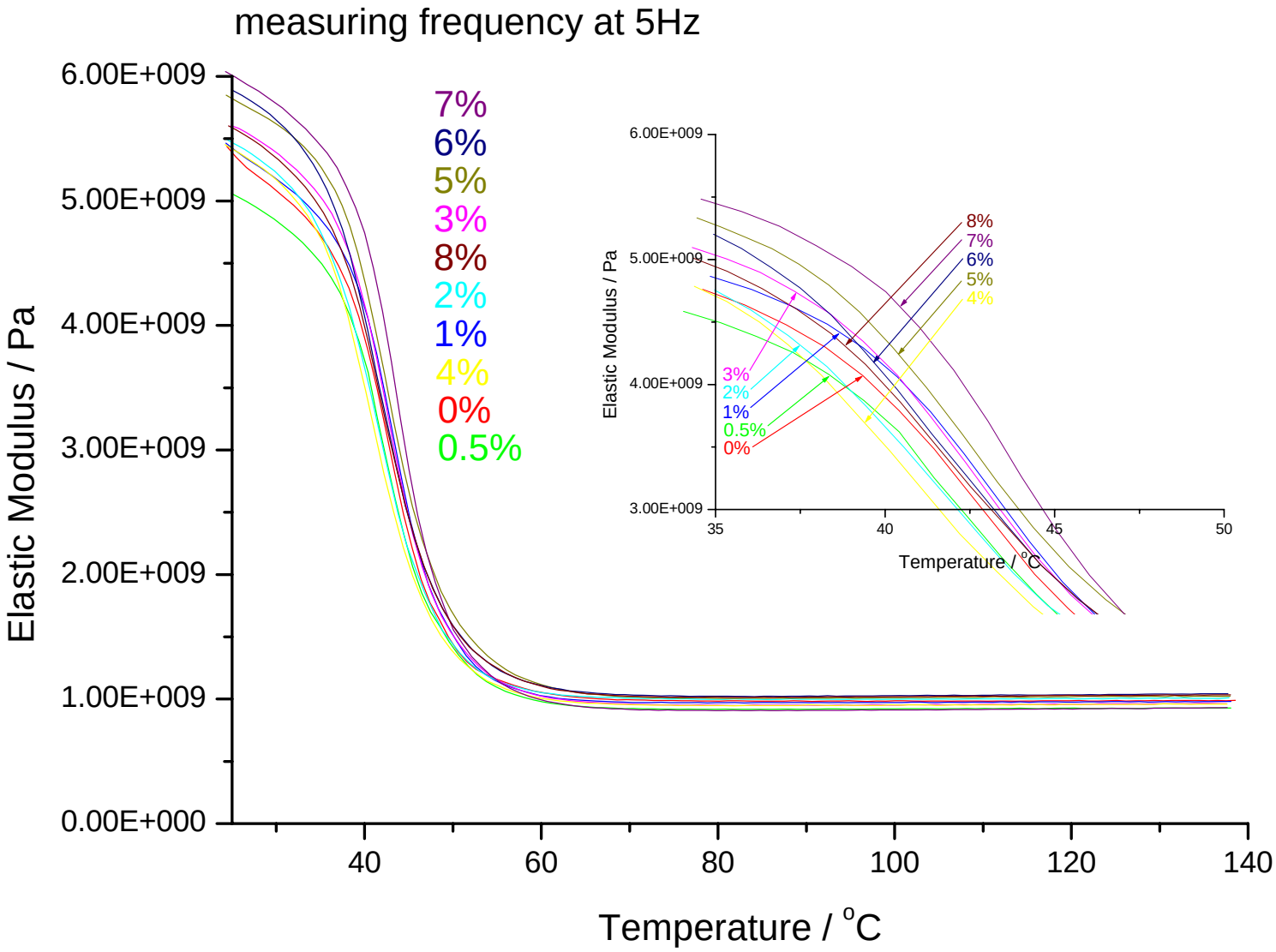

Figure 5.11 The elastic modulus of epoxy samples from 0wt% to 8wt% nanoclay as a function of temperature from 25°C to 140°C measured at 5 Hz frequency scan in DMA 3-point bending test.

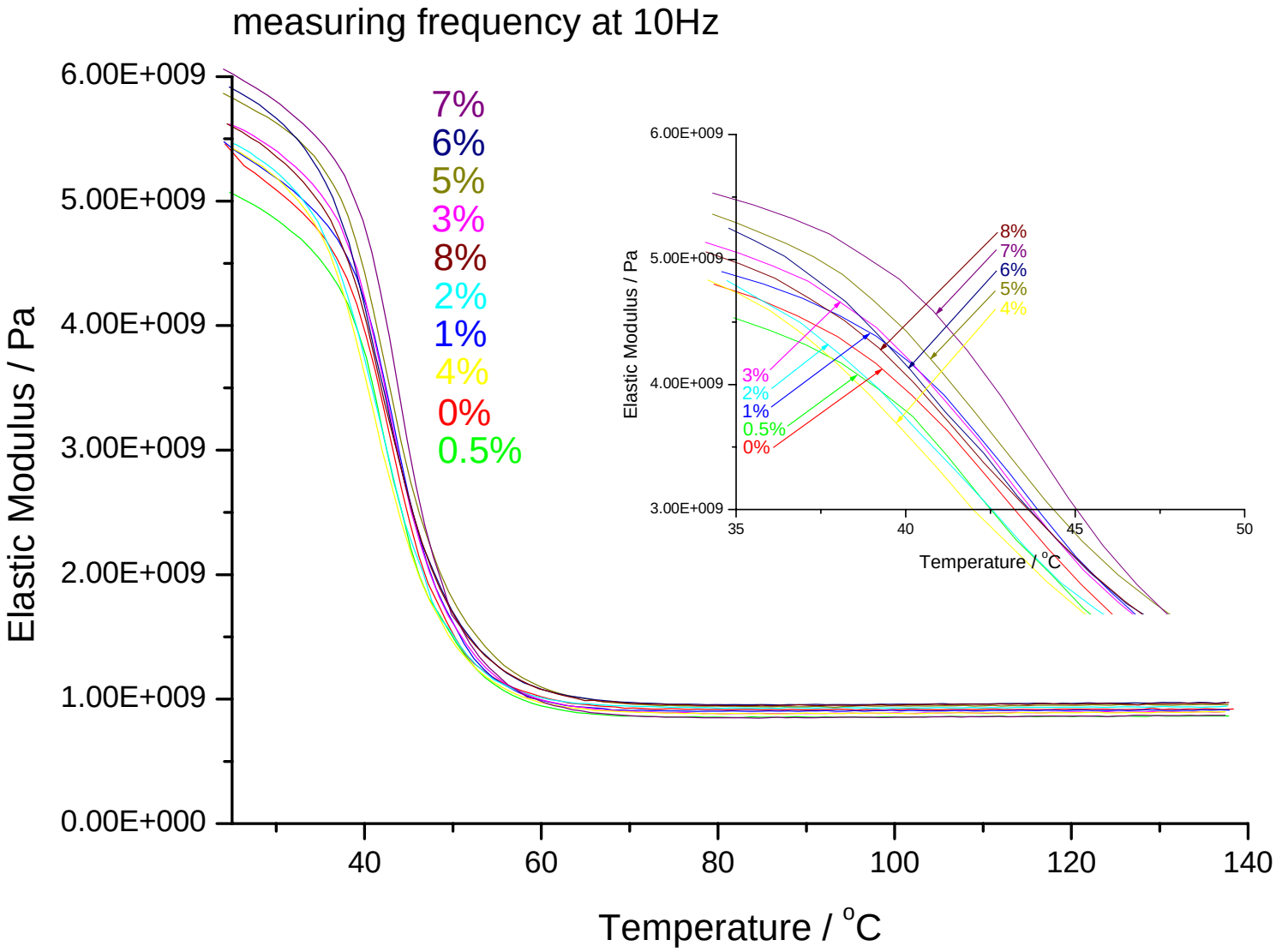

Figure 5.12 The elastic modulus of epoxy samples from 0wt% to 8wt% nanoclay as a function of temperature from 25°C to 140°C measured at 10 Hz frequency scan in DMA 3-point bending test.

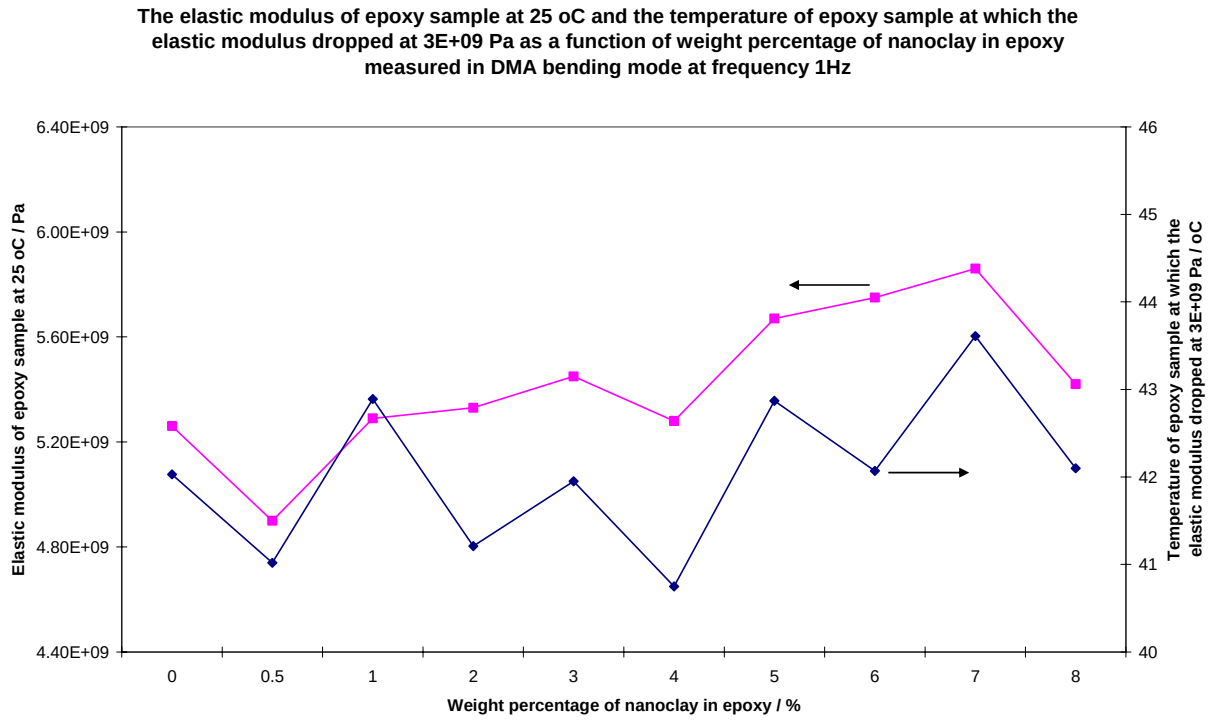

Figure 5.13 The elastic modulus of epoxy sample at 25°C and the temperature of epoxy sample at elastic modulus $3x10^9$ Pa as a function of weight percentage of nanoclay in epoxy measured in DMA bending mode at frequency 1 Hz.

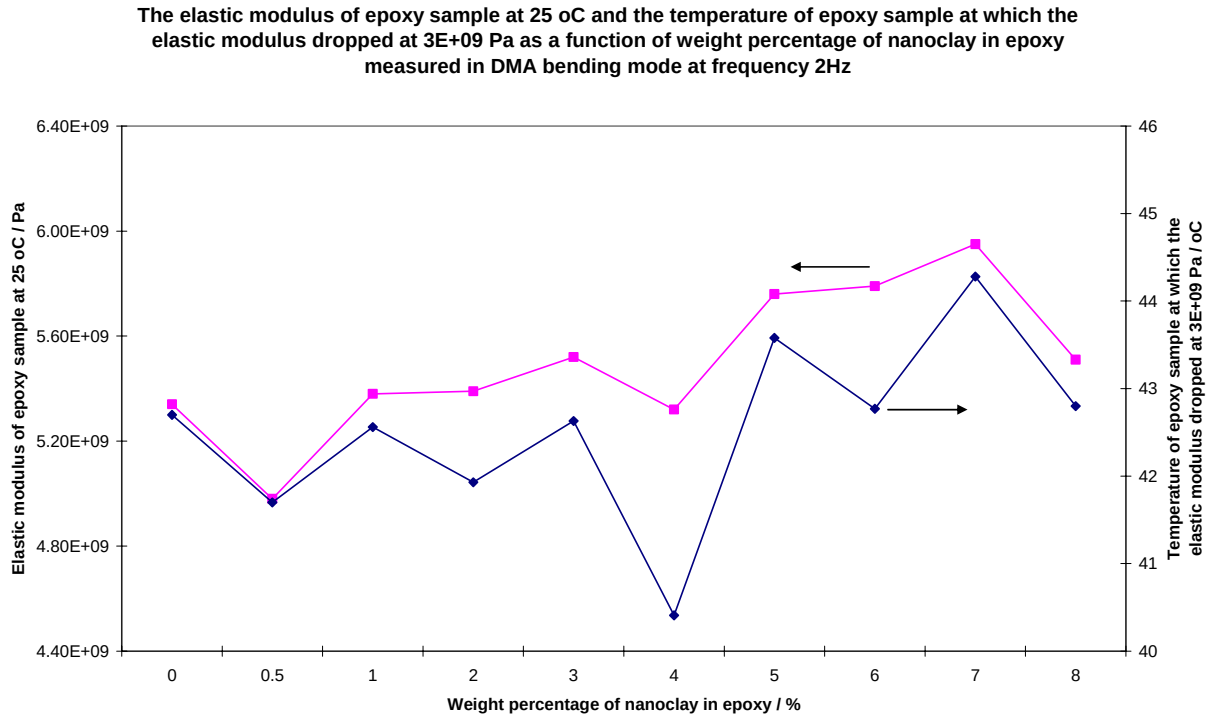

Figure 5.14 The elastic modulus of epoxy sample at 25°C and the temperature of epoxy sample at elastic modulus $3x10^9$ Pa as a function of weight percentage of nanoclay in epoxy measured in DMA bending mode at frequency 2 Hz.

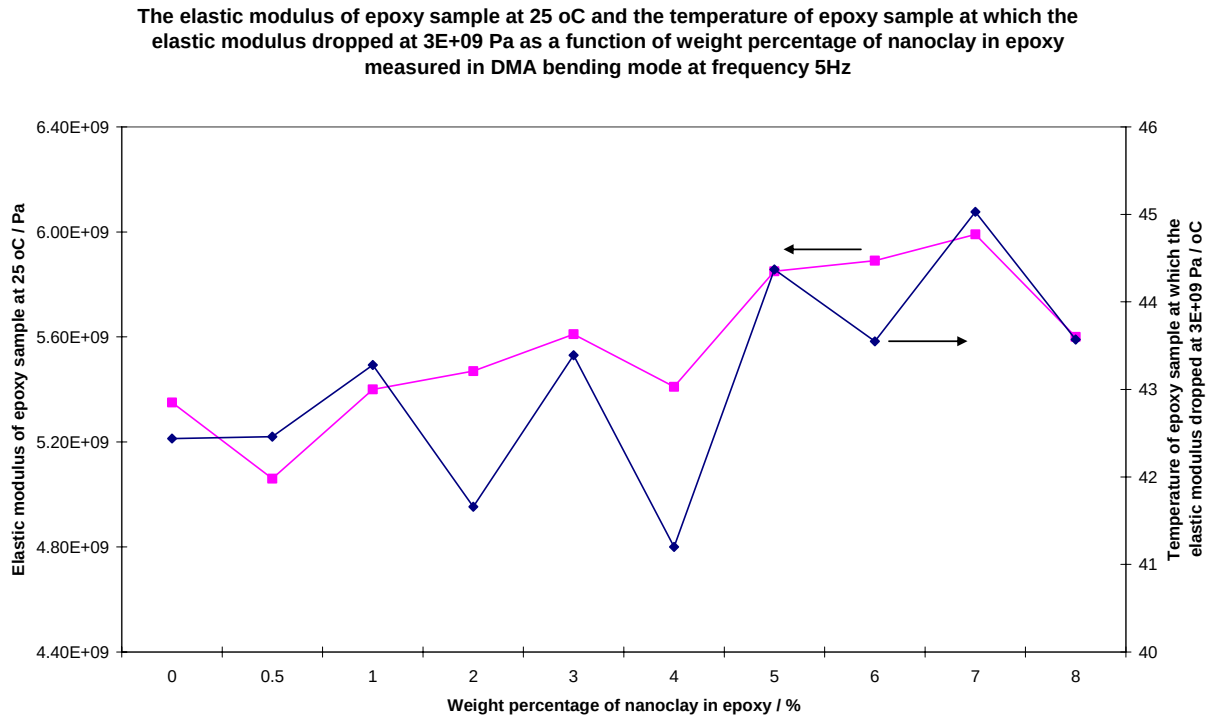

Figure 5.15 The elastic modulus of epoxy sample at 25°C and the temperature of epoxy sample at elastic modulus $3x10^9$ Pa as a function of weight percentage of nanoclay in epoxy measured in DMA bending mode at frequency 5 Hz.

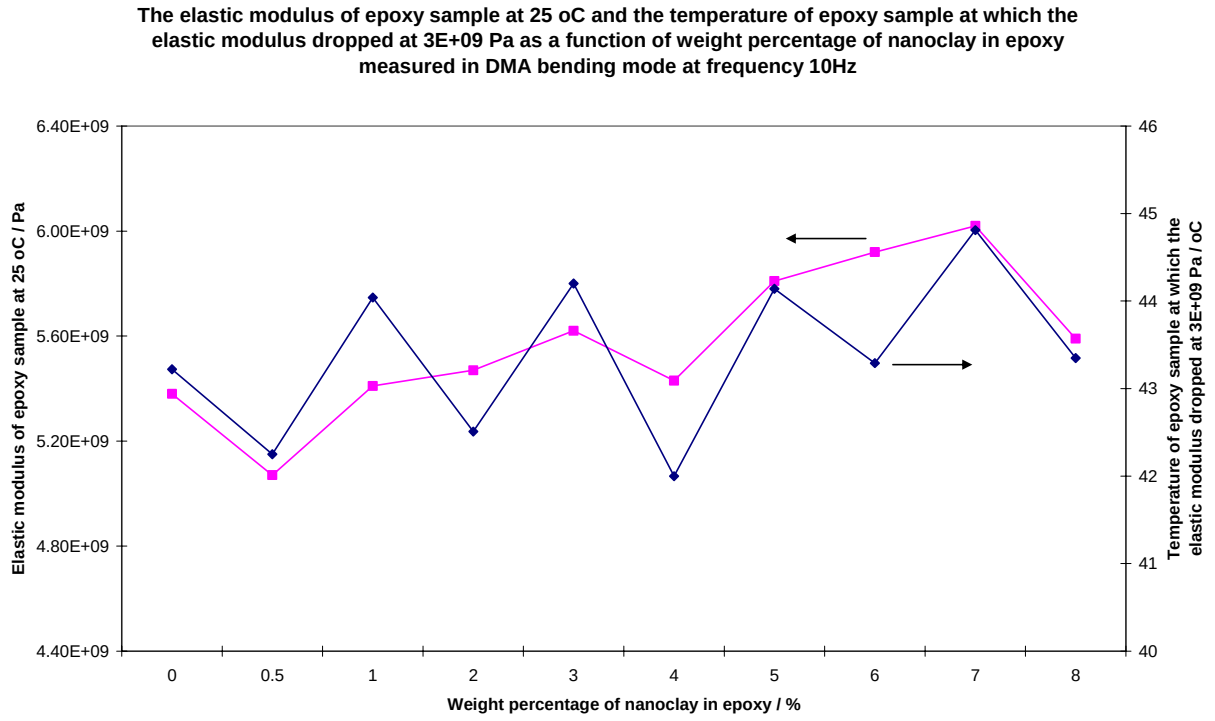

Figure 5.16 The elastic modulus of epoxy sample at 25°C and the temperature of epoxy sample at elastic modulus $3x10^9$ Pa as a function of weight percentage of nanoclay in epoxy measured in DMA bending mode at frequency 10 Hz.

5.3 Thermomechanical Analysis (TMA)

A common use of TMA is a measure of the thermal expansion of a specimen. The basis TMA principle is the change in the dimensions of a sample as a function of temperature or time, or simply to say, TMA is a very sensitive micrometer. By measuring the rate and amount of thermal expansion from CTE helps prevent the thermal mismatches between different materials that can cause failure in the final product. Different T_g values will be observed for each type of thermal testing, as they each measure a slightly different effect.

A graph of the linear coefficient of thermal expansion measured by the probe position in TMA of epoxy samples from 0wt% to 8wt% nanoclay as a function of temperature from 25^{o}C to 200^{o}C was shown in Figure 5.17. It was shown that there was a step in all 10 compositions at around 45^{o}C to 50^{o}C. This step was believed to be the glass transition as discussed in DMA session 5.2. All the 10 compositions showed about the same slope of thermal expansion with an average value of 210x10^{-6}/^{o}C. There seemed to be another change of slope above 160^{o}C in the samples, however at that temperature is beyond the normal usage of epoxy materials and no need for further investigation.

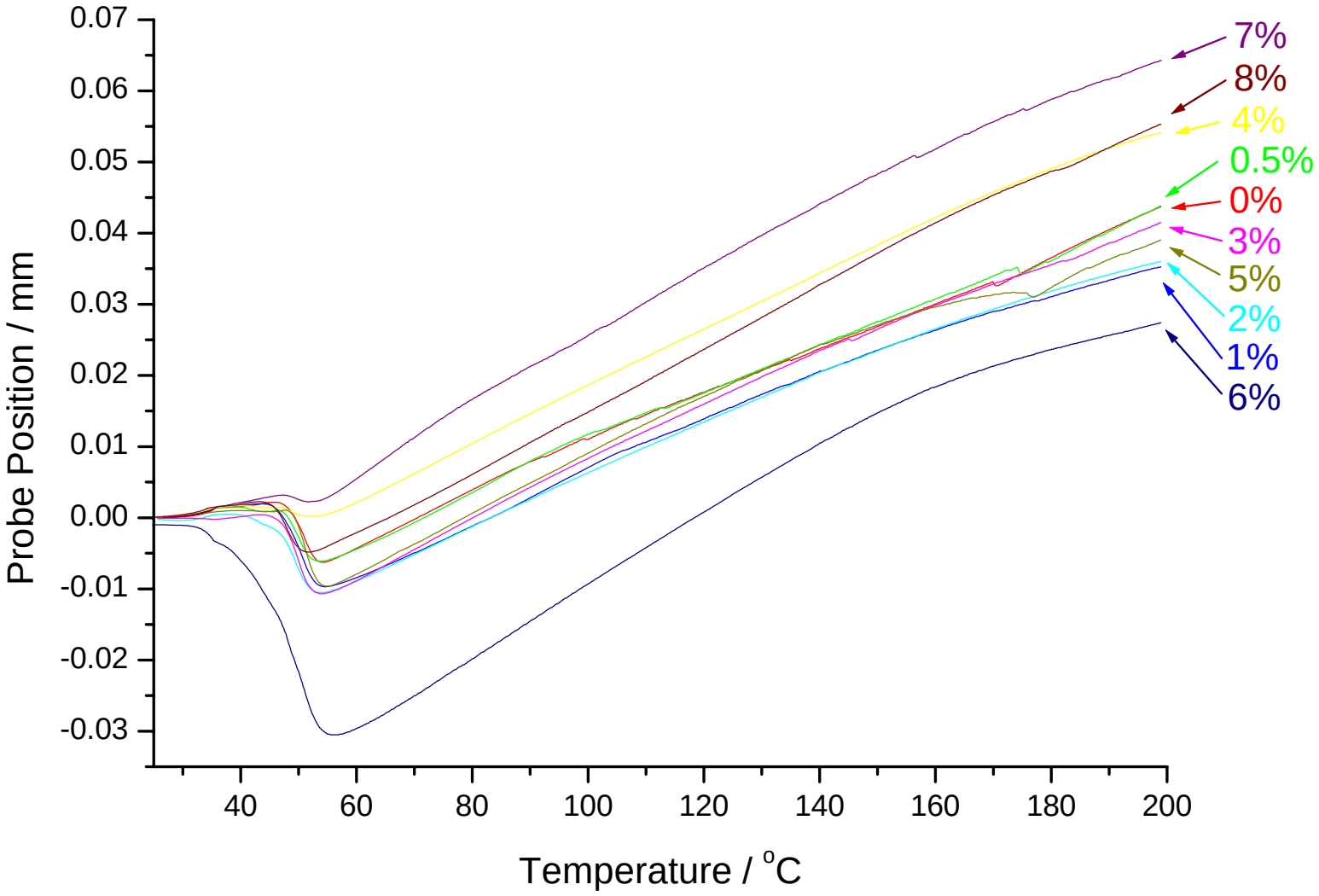

Figure 5.17 The linear coefficient of thermal expansion measured by the probe position of epoxy samples from 0wt% to 8wt% nanoclay as a function of temperature from 25°C to 200°C in TMA.

5.4 Thermogravimetric Analysis (TGA)

The basis TGA principle is a measure of the weight loss of a sample as a function of temperature or time, or simply to say, TGA is a very sensitive microbalance. By measuring the weight loss of a material as a function of temperature, the decomposition temperature or by how much weight the material will remain at a definite temperature can be obtained.

A graph of the percentage weight loss in TGA of epoxy samples from 0wt% to 2wt% nanoclay as a function of temperature from 25^{o}C to 600^{o}C was shown in Figure 5.18. Due to the difficulties in the clean-up process after each analysis run down, the TGA measurement was stopped at after 2wt% nanoclay epoxy sample, as samples with higher nanoclay content believed to behave the same results as those from 0wt% to 2wt% nanoclay samples.

From the graph, the epoxy samples seemed to be burnt out at about 450^{o}C. From the magnified figure at 200^{o}C to 300^{o}C weight loss region at the top right hand corner in Figure 5.18, samples had their first 10% weight loss at about 285^{o}C. All the 4 compositions behaved the same weight loss manner, as the introduction of nanoclay content inside the epoxy samples didn't change much of the decomposition rate.

In general, when combining with the DMA, TMA and TGA results together, the introduction of nanoclay content inside the epoxy samples seemed do not make much change in the thermal properties such as the T_g, CTE and decomposition temperature. The results were consistent with what V. G. Gregoriou found in polymer nanocomposites prepared by melt-mixing syndiotactic polypropylene (sPP) with a quaternary modified montmorillonite [47]. They found from DMA that the presence of the nanoclay resulted in a slight improvement of the mechanical properties of sPP, while via DSC, a small increase in the glass transition temperature of sPP was found, which implied that restriction in the movement of the polymeric chains took

place due to the presence of the nanoclay. Moreover, S. G. Lei also found the glass transition temperature and the melting temperature didn't change much on polypropylene nanocomposites prepared with different types of clay by melt processing using a Brabender plasticorder [48].

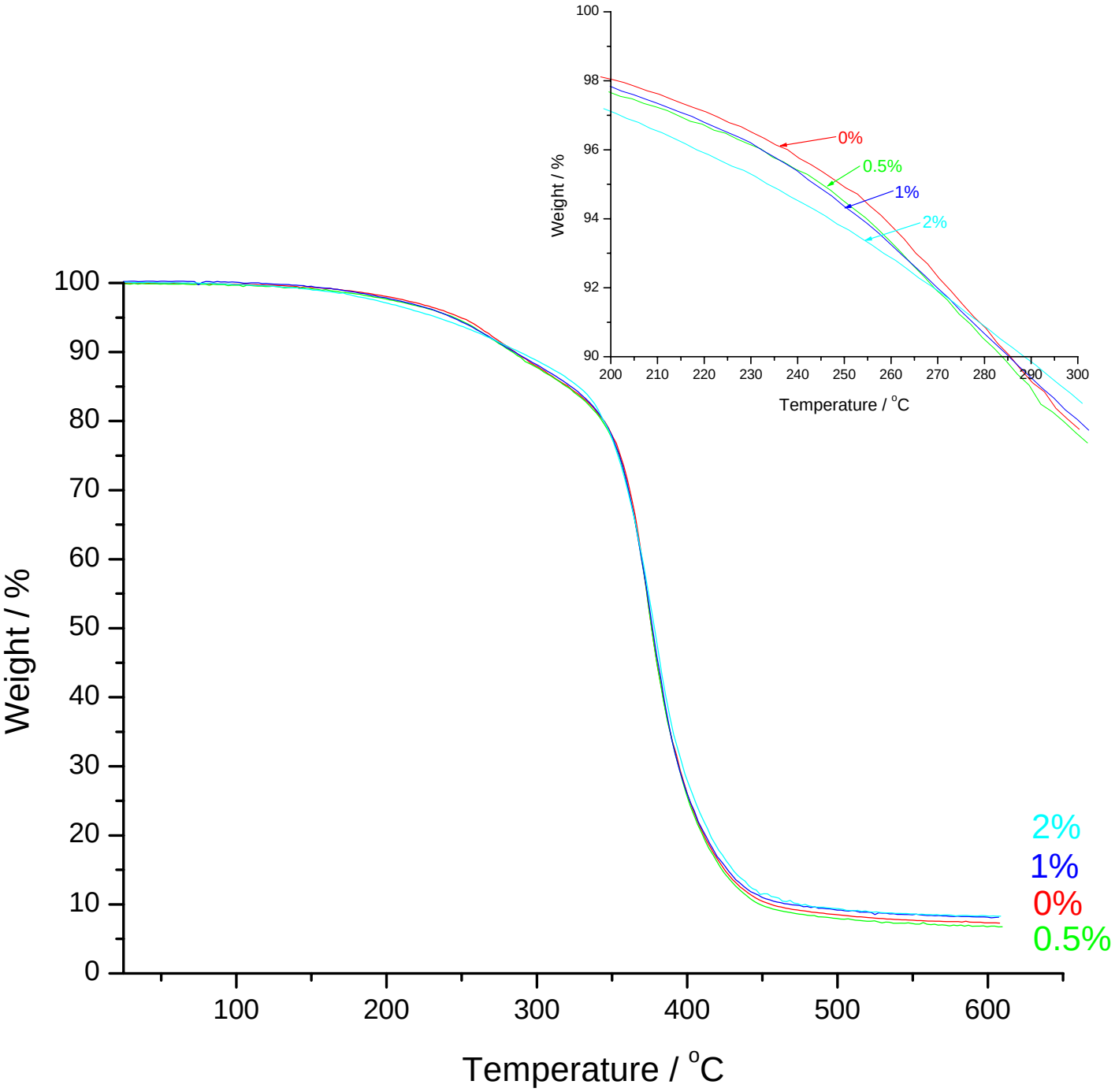

Figure 5.18 The decomposition temperature measured by the weight loss of epoxy samples from 0wt% to 2wt% nanoclay as a function of temperature from 25°C to 600°C in TGA.

Chapter 6

Microstructural Analysis

6.1 Introduction

From the results of mechanical and thermal analyses, the concrete parameters such as ultimate tensile strength, elongation at break, flexural strength, Vickers' hardness value, transition temperature, linear coefficient of thermal expansion & decomposition temperature etc. can be obtained. These are the primary data or the facial information revealing the physical properties of the materials. However, what cause for such material behaviors are still unknown. Then, microstructural analysis should be applied to investigate the causes. In this Chapter 6, X-Ray Diffraction (XRD) and Scanning Electron Microscope (SEM) will be employed to study the microstructural behaviors of the nanoclay-epoxy samples in order to reveal the cause for such physical behaviors of the materials.

6.2 X-Ray Diffractometry (XRD)

X-ray diffraction (XRD) can disclose information about the crystal structure of a material. When a beam of X-rays having a single wavelength as the same order of magnitude as the atomic spacing of a material, which strikes on certain crystallographic planes at specific angles of that material, and satisfy Bragg's law $2d_{hkl}\sin\theta = \lambda$, diffractions occurred. The angle θ is half

the angle between the diffracted beam and the original beam direction, λ is the wavelength of the X-rays beam, and d_{hkl} is the interplanar spacing between the planes that causes constructive reinforcement of the beam. Therefore, a collection of the diffracted beams at distinguish peak positions will give a characteristic diffraction pattern of a crystalline material. However, for amorphous materials such as epoxy or other polymers, no peak or several broad peaks will be observed in an X-ray diffractograph, because the amorphous materials have no definite crystal structure.

The broad peak at 2θ about 20^o in all the XRD scans in Figure 6.1 was due to the amorphous phase of epoxy, as epoxy is a cross-linked polymer, which has no definite crystal structure. From the XRD scans of nanoclay and the epoxy samples from 0wt% to 8wt% nanoclay as shown in Figure 6.1, the nanoclay main diffraction peak (0 0 1) at 2θ about 7^o became significant above 1wt% nanoclay content in the epoxy samples, while samples below 1wt% nanoclay content, the nanoclay main diffraction peak vanished, but it won't have enough evident to claim the nanoclay was completely exfoliated inside the epoxy matrix, the diffraction peak may be too little to be detected by XRD.

It was found that as the nanoclay content in the epoxy samples increased, the height of the main diffraction peak (0 0 1) of nanoclay in the epoxy samples also increased, and the increase was varied linearly with the nanoclay content from 1wt% to 8wt%, showing that there was no great loss of nanoclay content in this casting method of samples in any specific weight percentage. All the compositions can reflect their exact weight contents in a certain extent.

On the other hand, the peak positions of nanoclay diffraction peaks in all the epoxy samples remained unchanged as if they were the pure nanoclay diffraction peaks. This indicated

that this kind of nanoclay (Garamite 1958) acted like a nanodispenser all over the whole epoxy matrix as there was no peak shifting, therefore, no expansion of gallery in the nanoclay structure.

The other explanations may be given by P. B. Messersmith et al. that the choice of curing agent was critical in determining the delamination and the optical clarity [28]. They found that many epoxy curing agents studies showed little or no increase in layer separation, especially all bifunctional primary and secondary amine curing agents used were found to have this effect and resulted in opaque composites, while composites with the delamination of nanoclay were transparent. One possibility might be the strong bridging behavior of the bifunctional amine molecules with the epoxy resin within the silicate layers, which hindered further expansion of the layers' galleries. Another possibility might be the polar N-H groups in the primary and secondary amines that were too polar to cause reaggregation of the exfoliated silicate layers.

Moreover, J. Morawiec et al. used low density polyethylene (LDPE) as a polymer matrix and employed melt mixing method to produce nanocomposites containing organo-modified montmorillonite nanoclay (MMT-ODA) and maleic anhydride grafted low density polyethylene as a compatibilizer [49]. They found there was only a change in peak height with no significant peak shift in XRD, no significant change in melting point characterized by DSC, no significant change in decomposition temperature characterized by TGA in N_2 atmosphere, and not much improvement in tensile properties of the nanocomposites when compared with pure LDPE.

Furthermore, M. A. Osman et al. studied the influence of the organic monolayer structure on the exfoliation of organo-montmorillonite (OM) and the tensile properties of the high density polyethylene (HDPE) composites [50]. They found from wide angle XRD that the trioctadecyl ammonium ions treated nanoclay and its respective 2.8 vol% HDPE composites had the same peak positions but with different peak heights, showing that there was no peak shifting even

though the organo-modified clay was claimed exfoliated in polymer chains. However, the composites showed an increase in elastic modulus and yield stress but a decrease in yield strain and stress at break.

Similarly in this research work, as the nanoclay Garamite 1958 recommended by Southern Clay Products for application in epoxy system, whether or not this kind of nanoclay was organically surface modified, there was no peak shifting found from XRD among the composites introduced with Garamite 1958, no expansion of gallery in the nanoclay structure was found, therefore, the nanoclay may be only intercalated or evenly distributed all over the epoxy matrix as tactoid. However, from the mechanical properties points of view in Chapter 4, it was found that the ultimate tensile strength had been increased by 5% with 4-6wt% nanoclay content, the flexural strength was increased by 4.3% with 6wt% nanoclay content, and the Vickers' hardness value was increased by 15% with 5wt% nanoclay content. Those enhancements in the mechanical properties were due to the present of nanoclay inside the epoxy matrix, which hindered the movement of the polymer chains in order to strengthen the epoxy matrix. On the other hand, the extension at ultimate tensile strength and the elongation at break of the epoxy samples as a function of weight percentage of nanoclay decreased, therefore the epoxy samples with higher nanoclay content became brittle.

From the thermal properties points of view in Chapter 5, it was found that the elastic modulus, the glass transition temperature and the tensile performance upon elevated temperature increased with the nanoclay content in the epoxy samples. As glass transition is associated with the gradual polymer chains movement. The increase in the elastic modulus and the glass transition temperature of the epoxy samples was a result of the difficulty in the movement of the polymer chains caused by the presence of nanoclay.

In general, even though there was no peak shift in XRD, the addition of that kind of nanoclay inside the epoxy matrix enhanced both the mechanical and thermal properties of the composites in a certain extent, however 2-fold or 3-fold increment was never obtained. Then, how comes the enhancement in mechanical and thermal properties of the composites if there is no evident of exfoliation of nanoclay displayed from XRD results?

The enhancement in the mechanical and thermal properties of the composites may come from the adhesion between the epoxy polymer chains and the nanoclay surface, that is the bonding between the matrix and the fillers. If the bonding is strong enough, the load can be transferred elastically from the relatively soft matrix to the fillers. For organo-modified nanoclay, it is the organic part of the organo-nanoclay to transfer the load, if the organo-nanoclay is fully and highly exfoliated, the distance between each clay layer increase. Now the situation is each clay layer need to deal with the load, not several layers combined together as in intercalated form or in tactoid form, then do a single clay layer stronger or several layers combined together stronger? Moreover, in exfoliated state, the galleries of the nanoclay are expanded by the polymer chains and the organo-modifiers, then do the bonding between the polymer chains and the organo-modifiers still capable of transferring the load and at the same time act as pillars to expand the clay layers' galleries? Since most of the time is devoted to the distribution of nanoclay to give an exfoliated state in polymer matrix, is it worth to pursue an exfoliated state in spite of the tedious and complicated preparation method? The bonding between the polymer chains and the organo-modifiers play an important role in enhancing the mechanical and thermal properties of the nanocomposites besides obtaining an exfoliated state in a nanocomposite.

Therefore, the kind of organo-modifiers used to treat the nanoclay, the degree of organicity of the nanoclay modified by the organo-modifier, the polarity and the wettability of

the polymer chains to compatible with the organo-modified nanoclay, the modulus of the nanoclay, the aspect ratio of the nanoclay, the geometry of the nanoclay, the orientation of nanoclay dispersed in a polymer matrix and the level of exofoliation of nanoclay inside a polymer matrix were all the characteristics and important parameters to determine the effectiveness of nanoclay reinforced polymer composites.

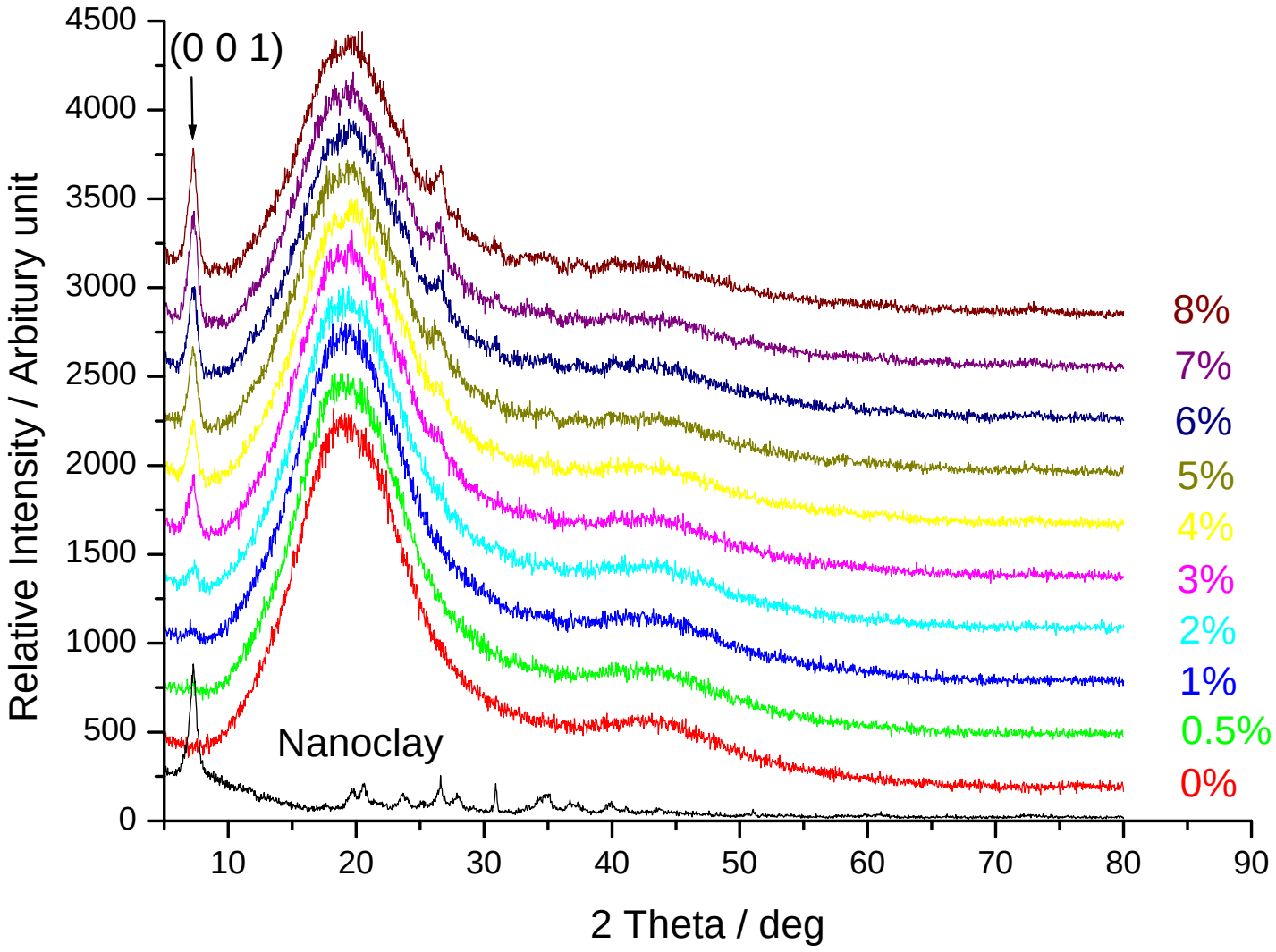

Figure 6.1 XRD scans of nanoclay and epoxy samples from 0wt% to 8wt% nanoclay, scanned from 5^{o} to 80^{o} in 2-θ scan.

6.3 Scanning Electron Microscopy (SEM)

Scanning Electron Microscope is becoming a common, popular and necessary piece of instrument to be equipped in materials science studies. Unlike tradition optical microscope limited by the nature of light (a very narrow spectrum of electro-magnetic wave in the range of $4x10^{-7} – 7x10^{-7}$m in wavelength), the object to be observed in micron size, magnitude in $1x10^{-6}$m, will be heavily affected by the optical aberrations or a limited level of depth of field. With the invention of SEM and the continuing improvement in the technique, these problems are overcome. SEM can provide a wide depth of field and investigate sample even in sub-micron interval, but the sample to be investigated should better be conductive.

The working principle of SEM is another level of discussion with tradition optical microscope. It can be said that SEM image is not a real picture, but a computer generated photo. SEM uses a high energy electron beam at 20kV to kick off the secondary electrons on the surface of the sample to be observed, then an electron detector is employed to detect the secondary electrons being kicked off by the scan of the electron beam on the sample surface, and represented the quantites of electrons detected in terms of pixels (dark or bright spots) at the same synchronizing speed of the scan of the electron beam in the monitor. Therefore, the SEM image is black and white, no color, unlike the colorful picture observed from the optical microscope, because the source of "light" is different.

From the SEM images of the nanoclay as illustrated in Figure 6.2 magnified in 20,000X & Figure 6.3 magnified in 50,000X, the nanoclay was shown as nano-ribbon with about several microns in length and about 100 nm in width or 10 nm in thickness, therefore the aspect ratio of this nano-ribbon may reach at 500. Elemental analysis of the nanoclay was determined by energy dispersive X-ray spectrometry (EDX) within the SEM and identified that nanoclay contained

Silicon and Magnesium only, no other minerals. Referring to Chapter 1 on the nomenclature of the species on Smectite clay, this nanoclay Garamite 1958 was identified as Hectorite, which is classified as Magnesium Silicate and has strip morphology.

It was not hard to imagine when this kind of nano-ribbon was evenly distributed across the matrix, it would easily inter-lock and entangle with the polymer chains in the matrix. For this special morphology of the nanoclay, it is now called the nanoclay as nano-ribbon or strip silicate.

On the other hand, based on the XRD results that there was no peak shifting, no expansion of gallery in the nanoclay structure, therefore, whether the effect of the strong bridging behavior of amine molecules with the epoxy resin within the silicate layers or the effect of the inter-locking mechanism of the nano-ribbon entangling with the polymer chains in the matrix, or both the effects which hindered the expansion of the layers' galleries were still unknown.

The SEM images of the epoxy samples from 0wt% to 8wt% nanoclay all magnified in 500X were shown in Figure 6.4 – Figure 6.13 respectively for comparison. The SEM image of pure epoxy sample as shown in Figure 6.4 that the cleavage surface was clear-cut and mirror-plane without bubbles or holes. The SEM images of 0.5wt% - 2wt% nanoclay epoxy samples as shown in Figures 6.5 – 6.7 respectively were completely different from that of the pure epoxy sample, the cleavage surfaces were very rough and fractured with small pieces. The SEM images of 3wt% - 6wt% nanoclay epoxy samples as shown in Figures 6.8 – 6.11 were a bit not as rough as those in 0.5wt% - 2wt% nanoclay content, in fact, they fractured with even smaller pieces. The SEM images of 7wt% & 8wt% nanoclay epoxy samples as shown in Figures 6.12 & 6.13 were as rough as those in 3wt% - 6wt% nanoclay content, but they fractured with crack lines. 8wt% nanoclay epoxy sample even had big holes, those big holes were originated from mixing

the hardener with the resin-nanoclay mixture. At 8wt% nanoclay content, the viscosity of resin-nanoclay mixture was high enough to trap any bubbles inside when mixing with hardener. Once the sample was cured, the bubbles trapped inside the sample would form holes.

The SEM images of the epoxy samples from 0wt% to 8wt% nanoclay all magnified in 2000X were shown in Figure 6.14 – Figure 6.23 respectively. At higher magnification, the SEM image of pure epoxy sample as shown in Figure 6.14 even looked like a plane mirror. In general, the SEM images of 0.5wt% - 8wt% nanoclay epoxy samples as shown in Figures 6.15 – 6.23 had a trend that the cleavage surface broken with smaller and rougher fracture pieces. For 0.5wt% - 8wt% nanoclay epoxy samples, the fracture edges were stress whitened. When compared with the plane mirror-like cleavage surface of pure epoxy sample, the stress whitened edges must be due to the shear stress failure caused by the debonding or dis-entanglement between the epoxy polymer chains and the nano-ribbon surfaces. By observing the size of the stress whitened edges, as the nanoclay content increased, the stress whitened edges were smaller and closely packed together. That may provide an indirect evident that the nano-ribbons were evenly distributed and tried to connect each other inside the epoxy matrix as the nanoclay content increased. Those stress whitened edges were the evident to prove the load was transferred by shear stress in the interface between the epoxy polymers chains and the nano-ribbon surfaces.

The SEM images of the epoxy samples from 0wt% to 8wt% nanoclay all magnified in 20,000X were shown in Figure 6.24 – Figure 6.33 respectively. At even higher magnification, the SEM image of pure epoxy sample as shown in Figure 6.24 did have some small dark lines. For 0.5wt% - 2wt% nanoclay epoxy samples, the SEM images as shown in Figures 6.25 – 6.27 looked like big pieces of rocks with sharp stress whitened edges. For 3wt% - 8wt% nanoclay epoxy samples, the SEM images as shown in Figures 6.28 – 6.33 illustrated a trend that fracture

edges were rougher, irregular in shape and broken down into tiny pieces with stress whitened sharp edges, a lot of white spots or white lines, which believed to be the nanoclay (the nano-ribbon), were found coming out from the fracture surfaces. Clearly, the stress was concentrated at the interfaces between the epoxy polymer chains and the nano-ribbon surfaces.

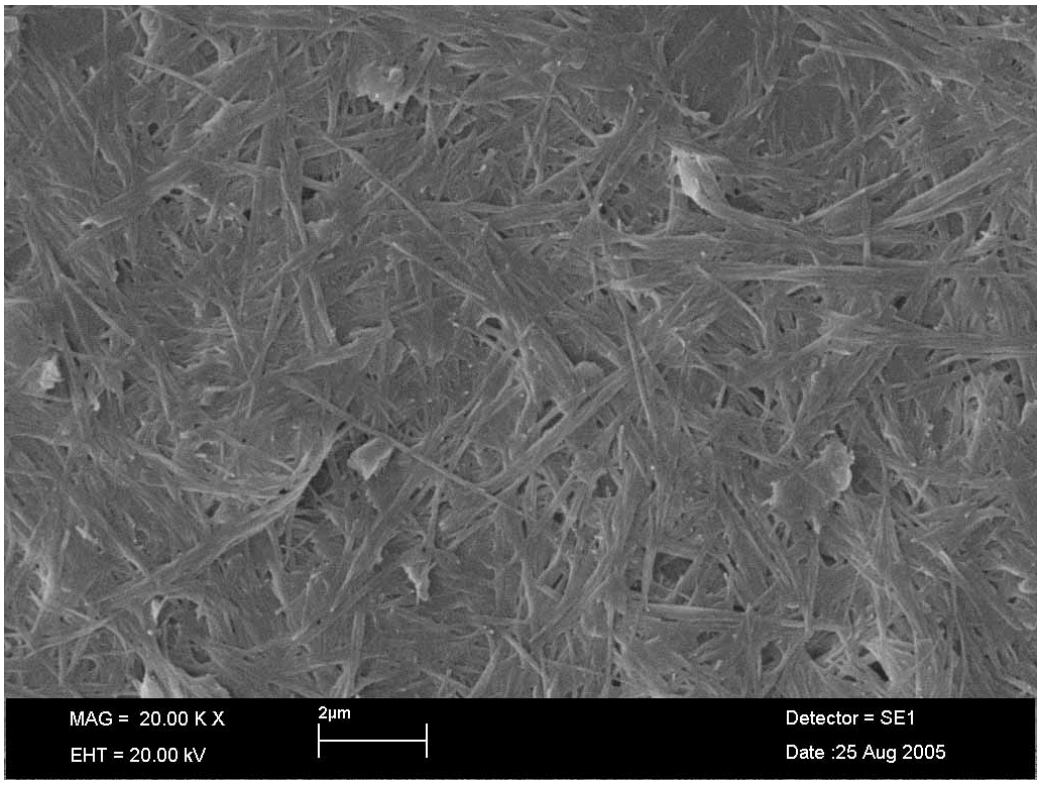

Figure 6.2 The SEM image of nanoclay magnified in 20,000X.

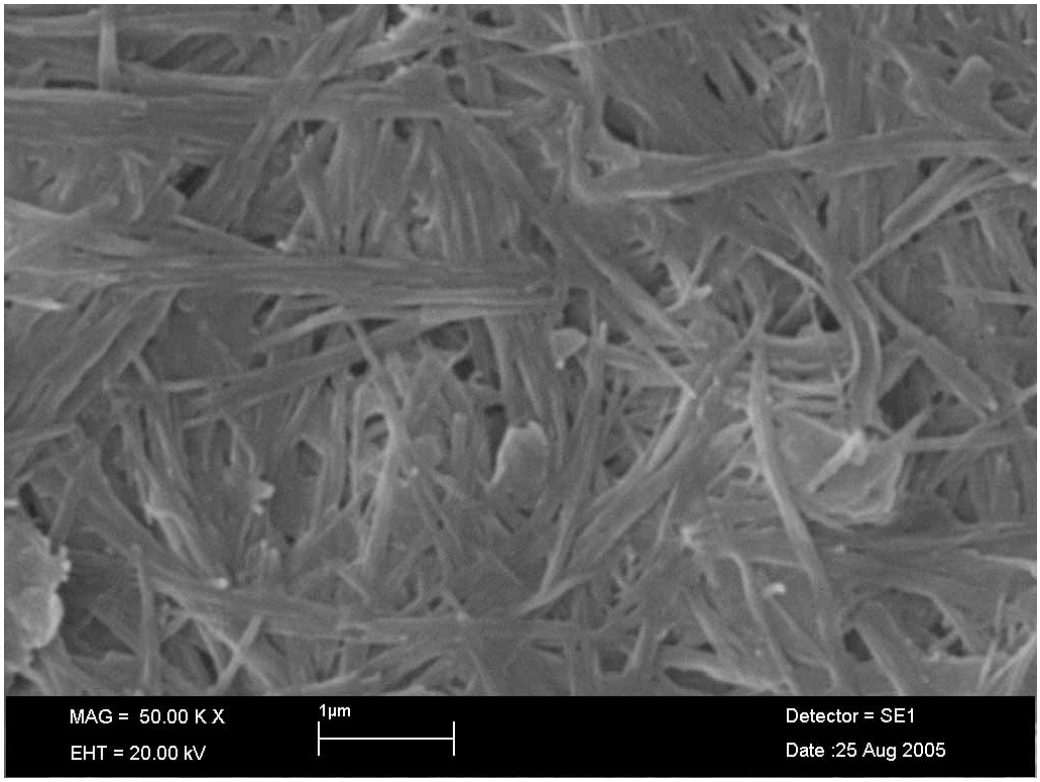

Figure 6.3 The SEM image of nanoclay magnified in 50,000X.

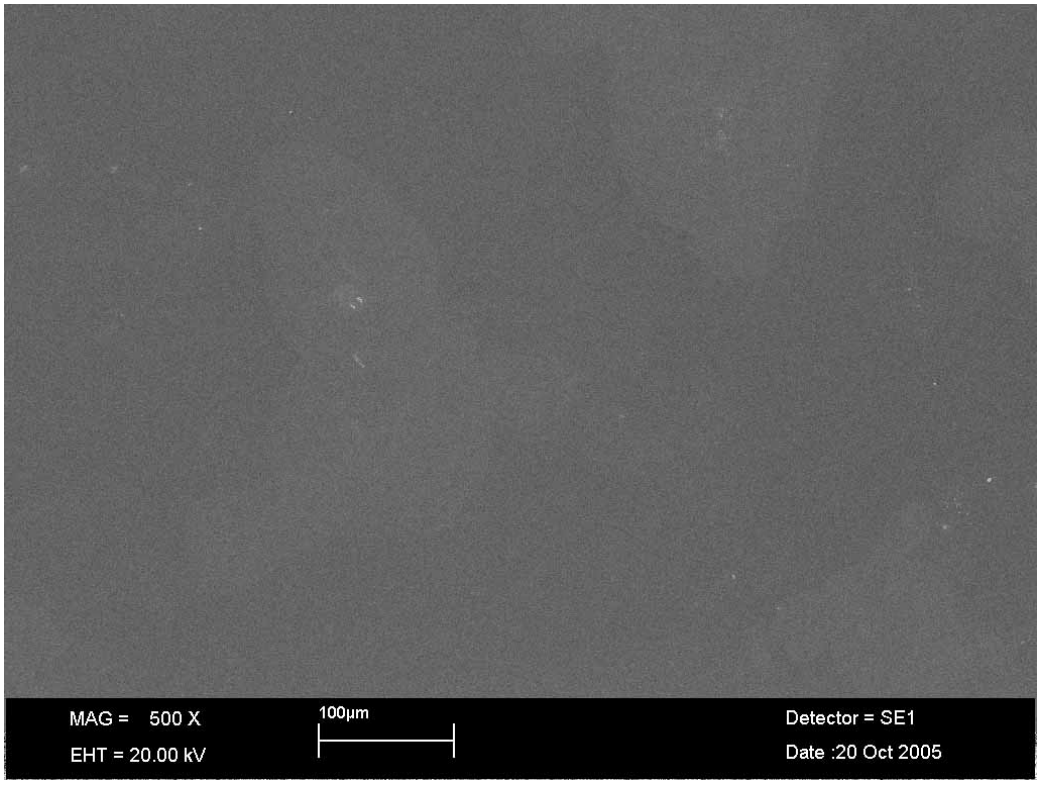

Figure 6.4 The SEM image of pure epoxy sample (0wt% nanoclay) magnified in 500X.

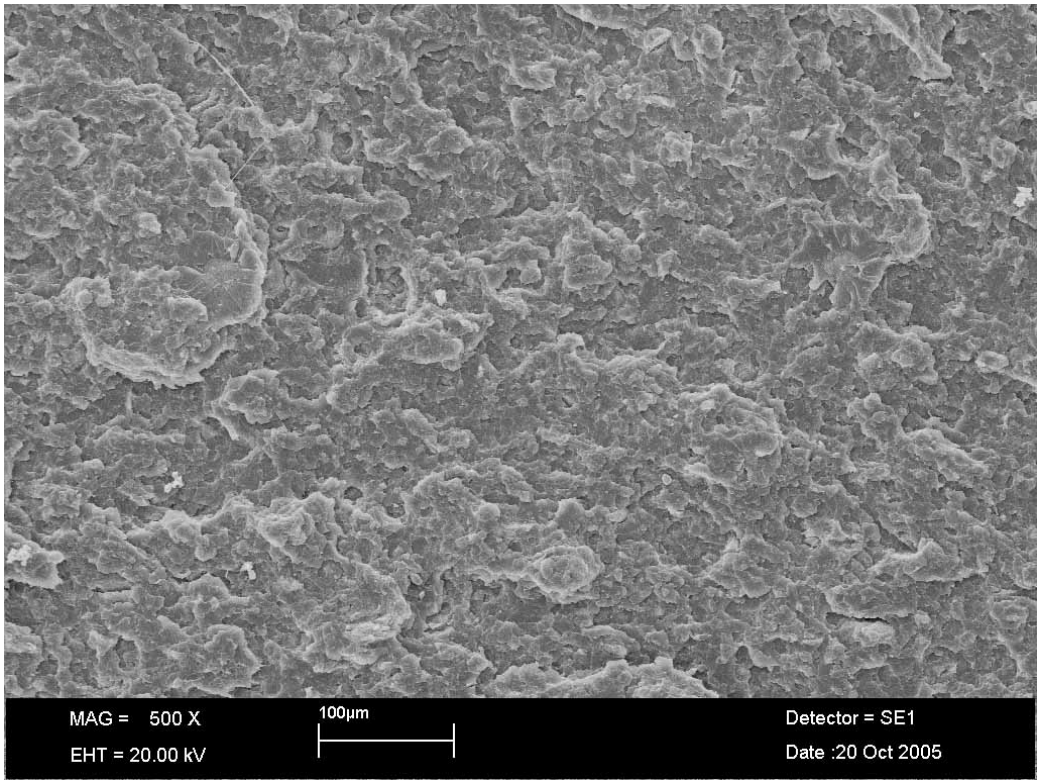

Figure 6.5 The SEM image of 0.5wt% nanoclay epoxy sample magnified in 500X.

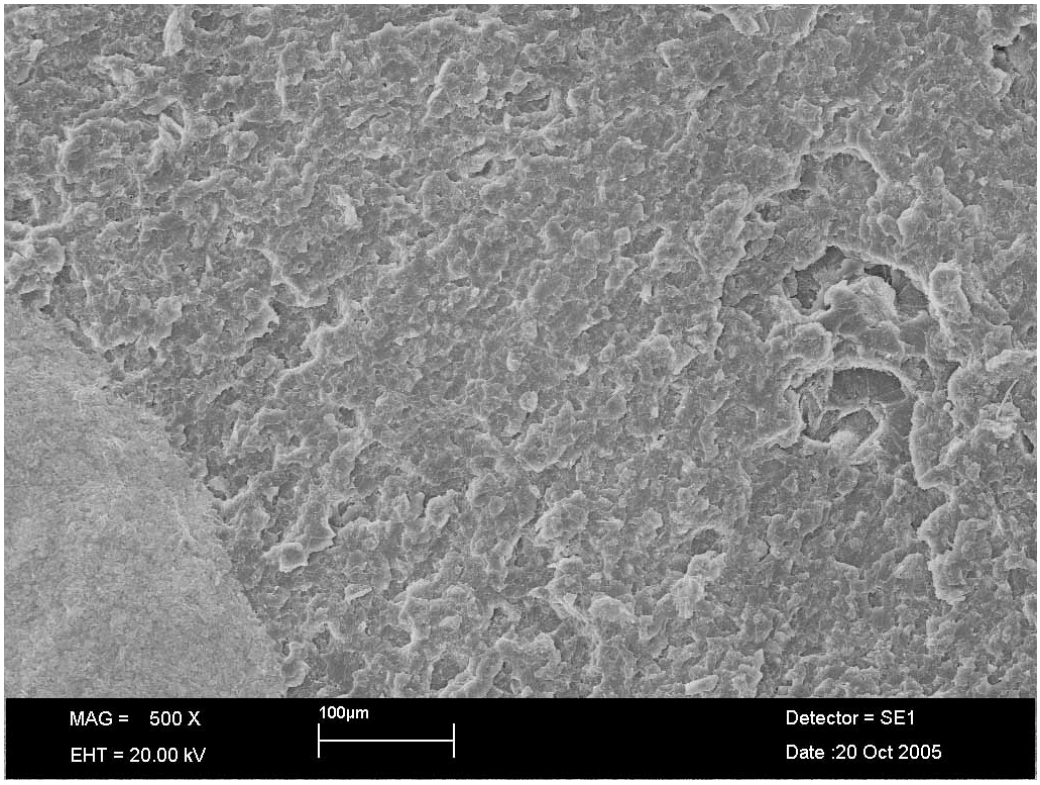

Figure 6.6 The SEM image of 1wt% nanoclay epoxy sample magnified in 500X.

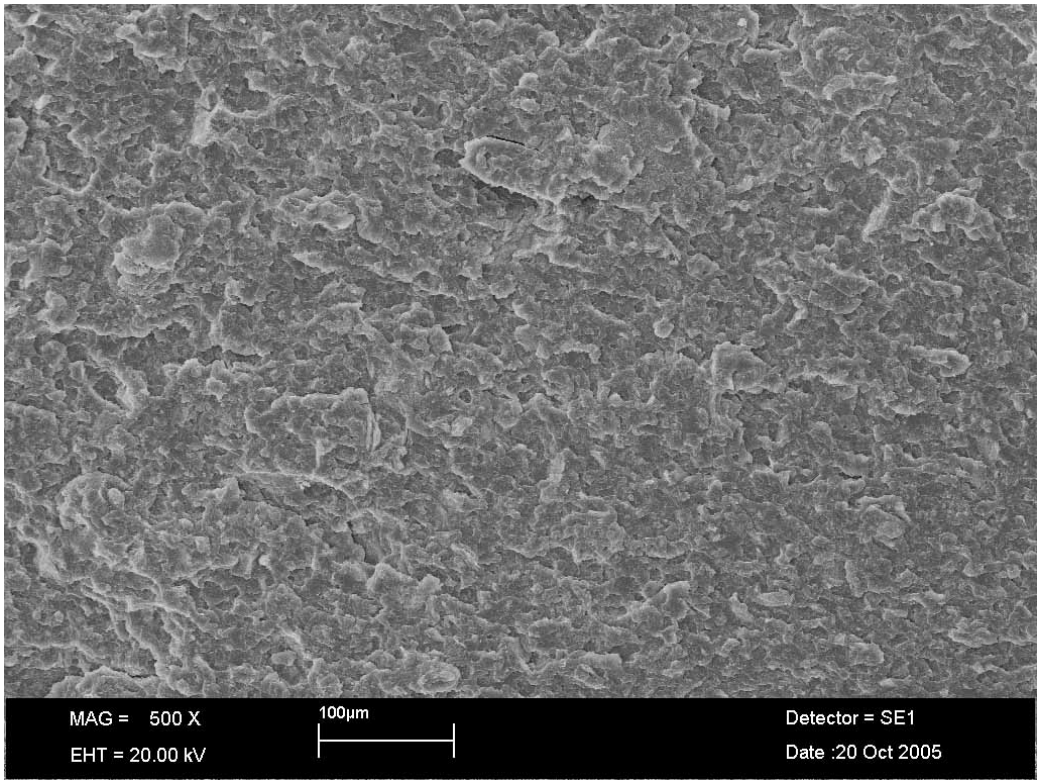

Figure 6.7 The SEM image of 2wt% nanoclay epoxy sample magnified in 500X.

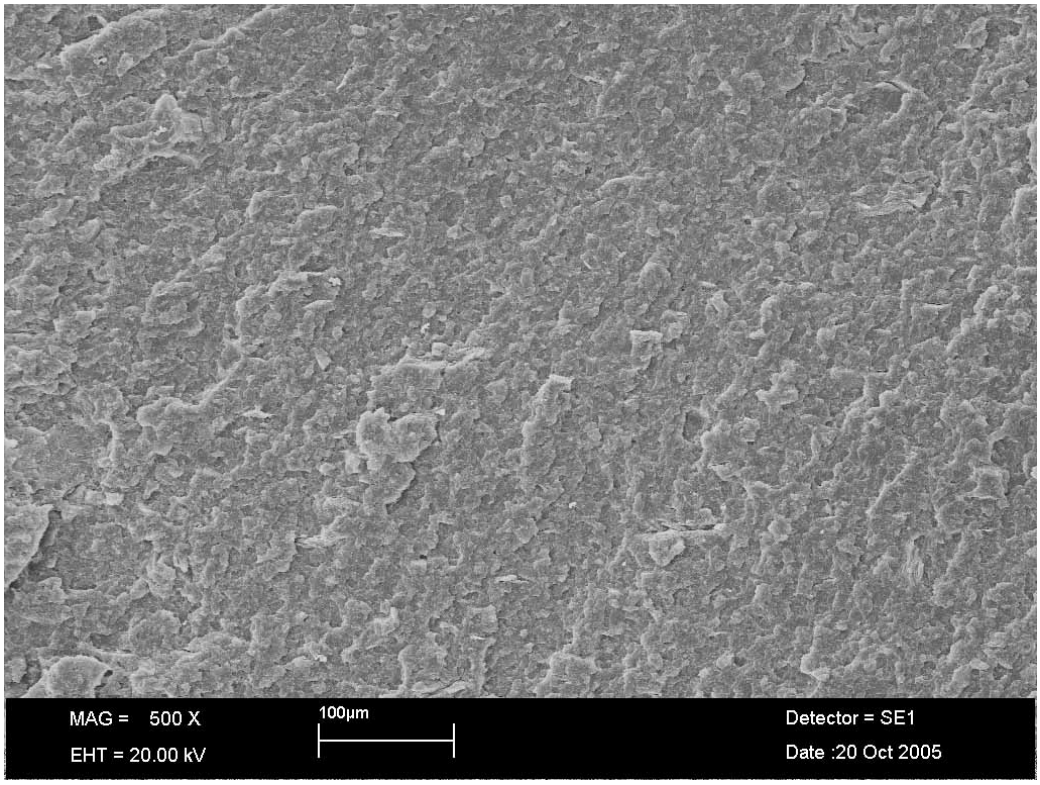

Figure 6.8 The SEM image of 3wt% nanoclay epoxy sample magnified in 500X.

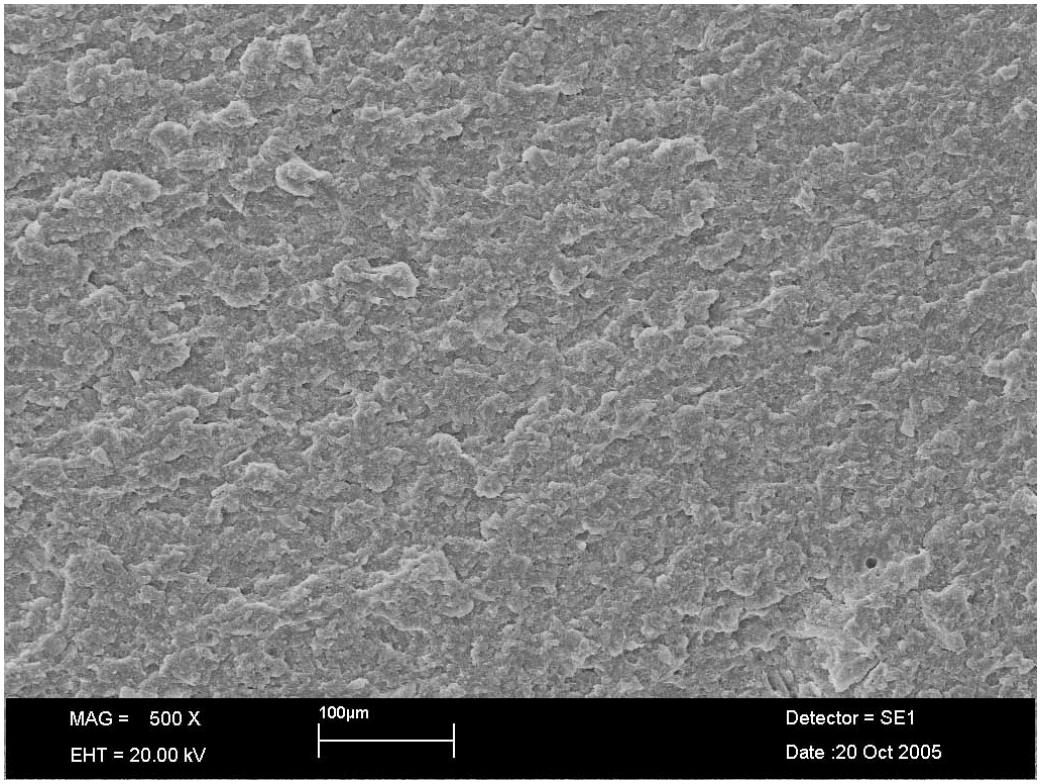

Figure 6.9 The SEM image of 4wt% nanoclay epoxy sample magnified in 500X.

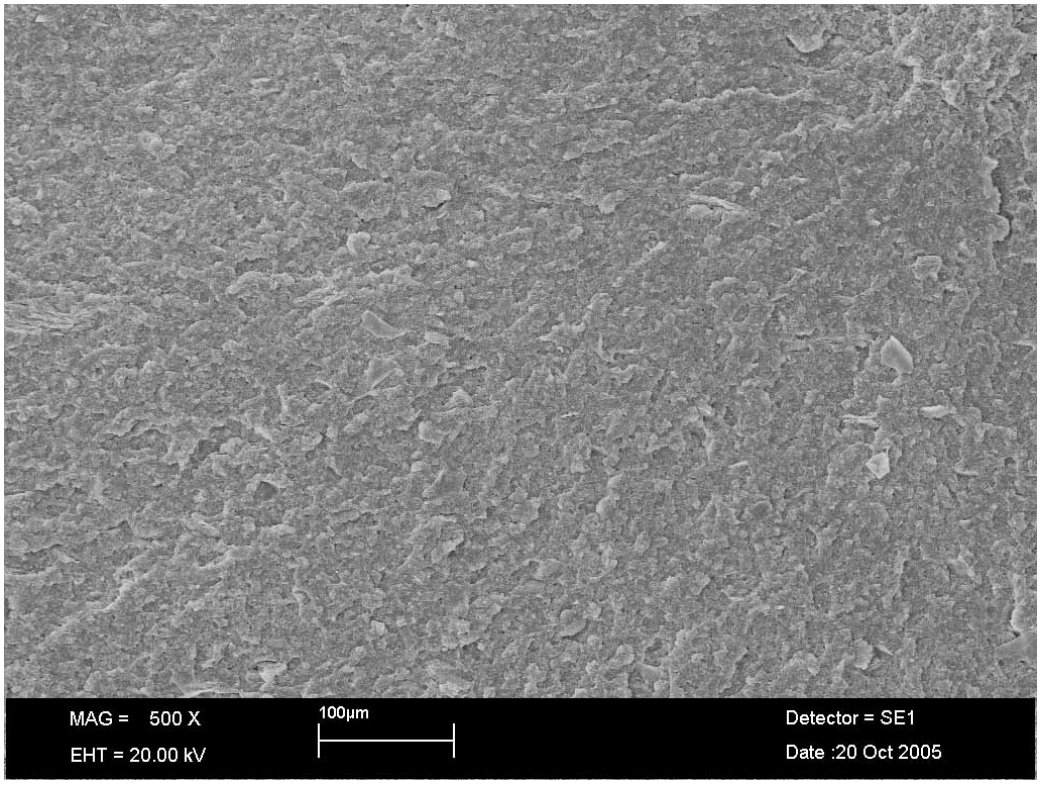

Figure 6.10 The SEM image of 5wt% nanoclay epoxy sample magnified in 500X.

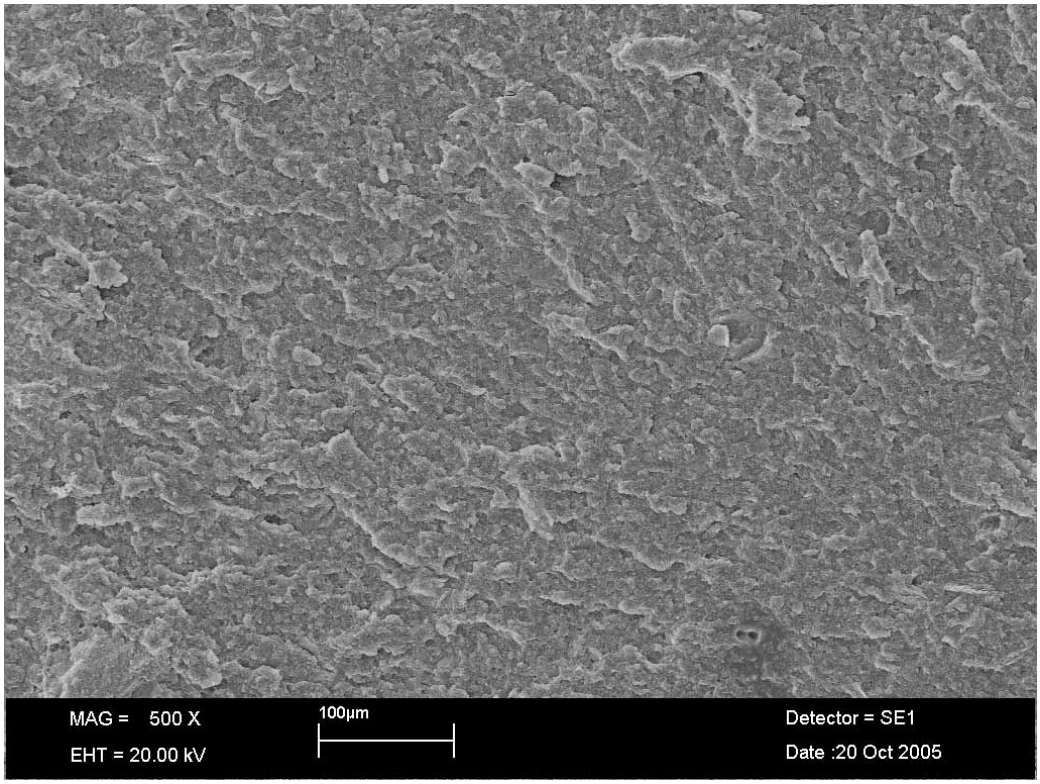

Figure 6.11 The SEM image of 6wt% nanoclay -epoxy sample magnified in 500X.

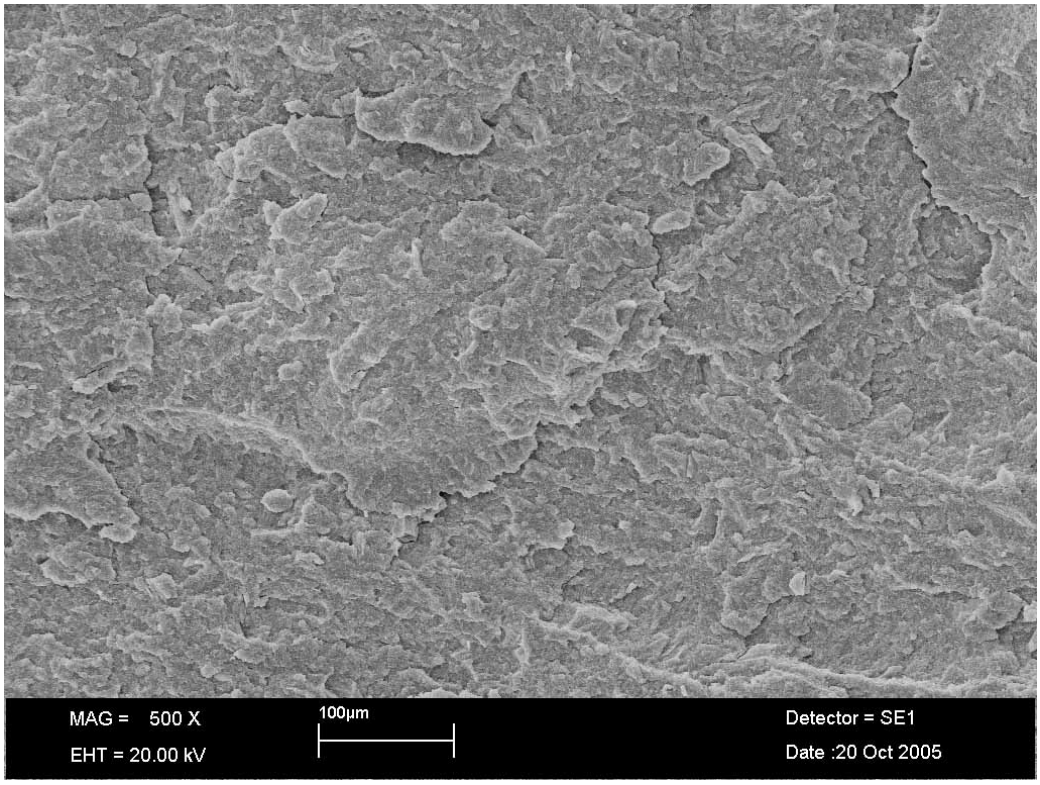

Figure 6.12 The SEM image of 7wt% nanoclay epoxy sample magnified in 500X.

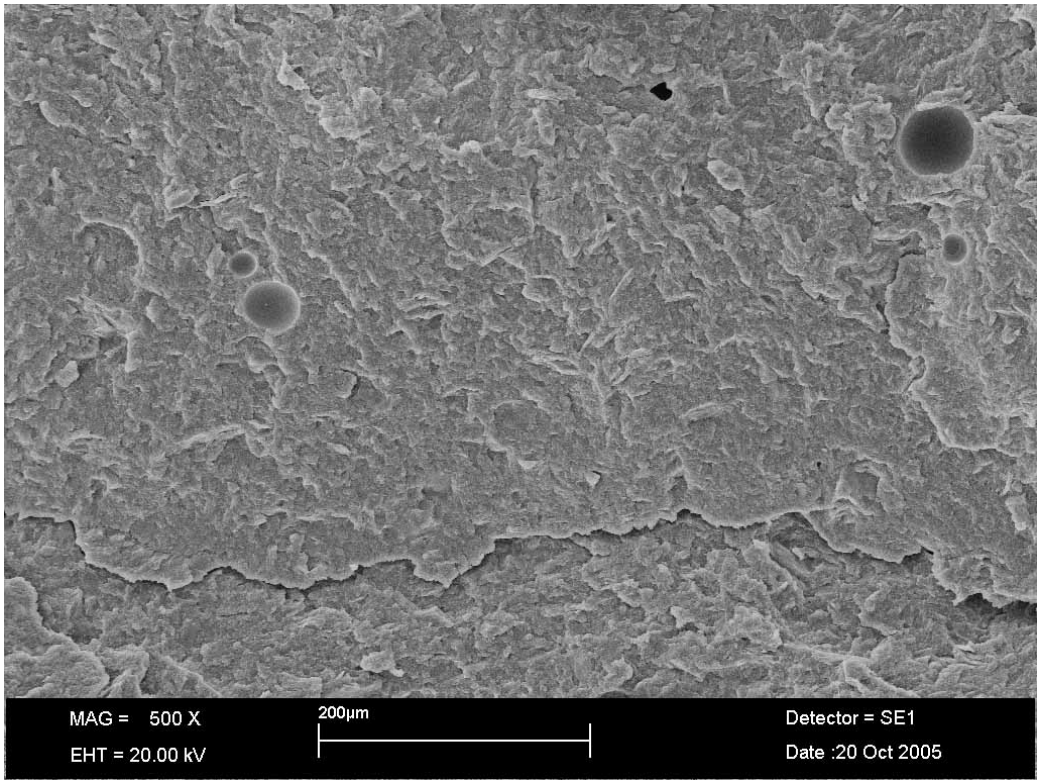

Figure 6.13 The SEM image of 8wt% nanoclay epoxy sample magnified in 500X.

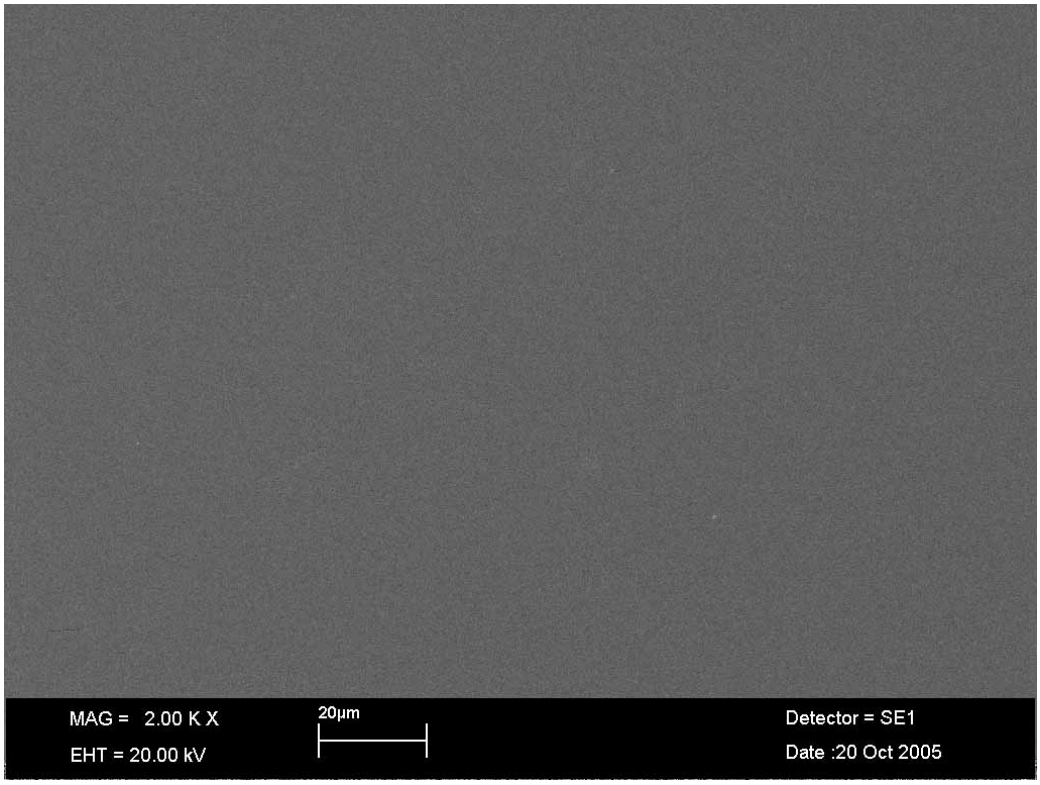

Figure 6.14 The SEM image of pure epoxy sample (0wt% nanoclay) magnified in 2,000X.

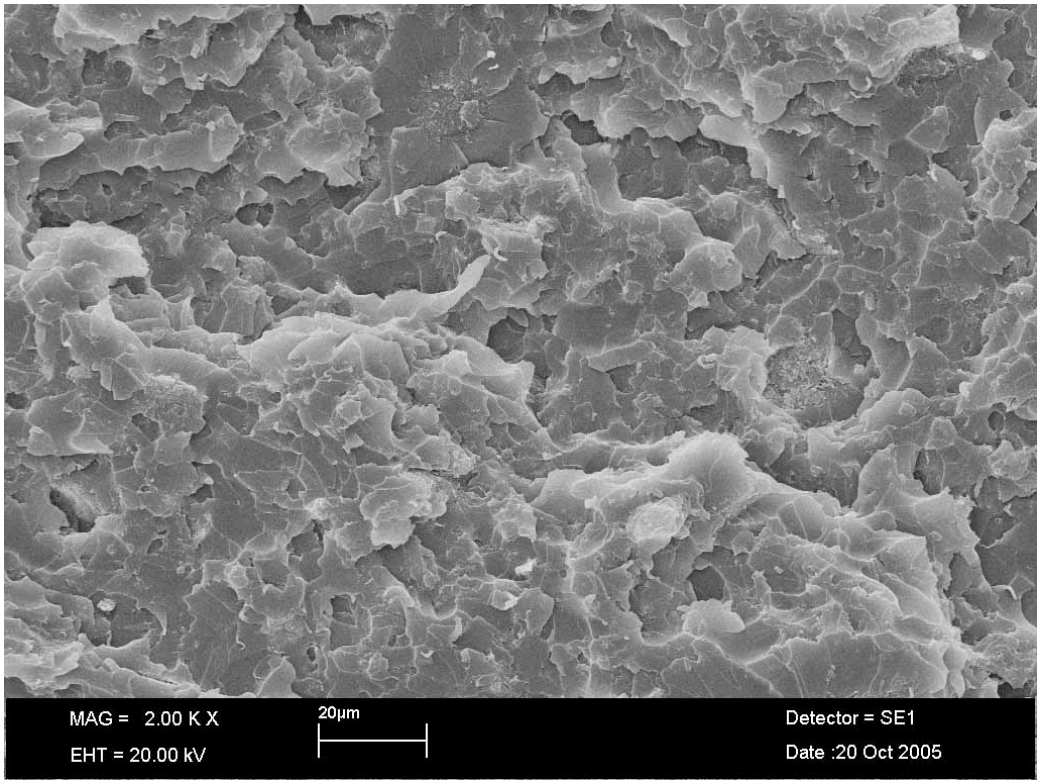

Figure 6.15 The SEM image of 0.5wt% nanoclay epoxy sample magnified in 2,000X.

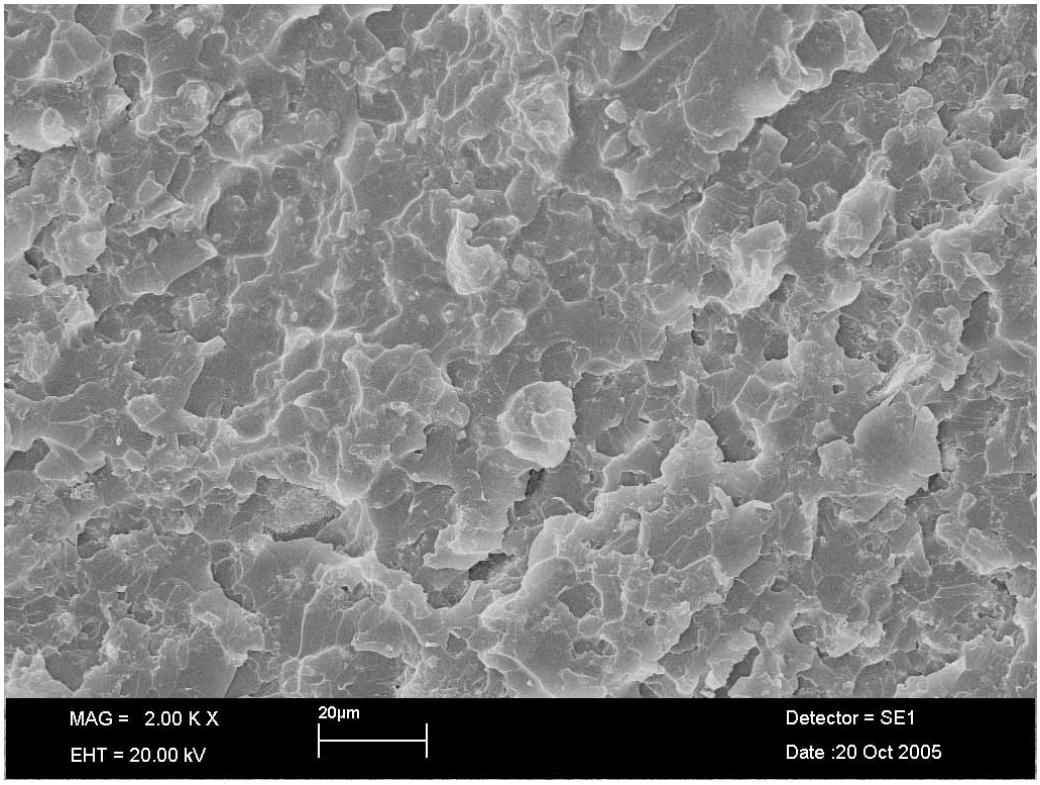

Figure 6.16 The SEM image of 1wt% nanoclay epoxy sample magnified in 2,000X.

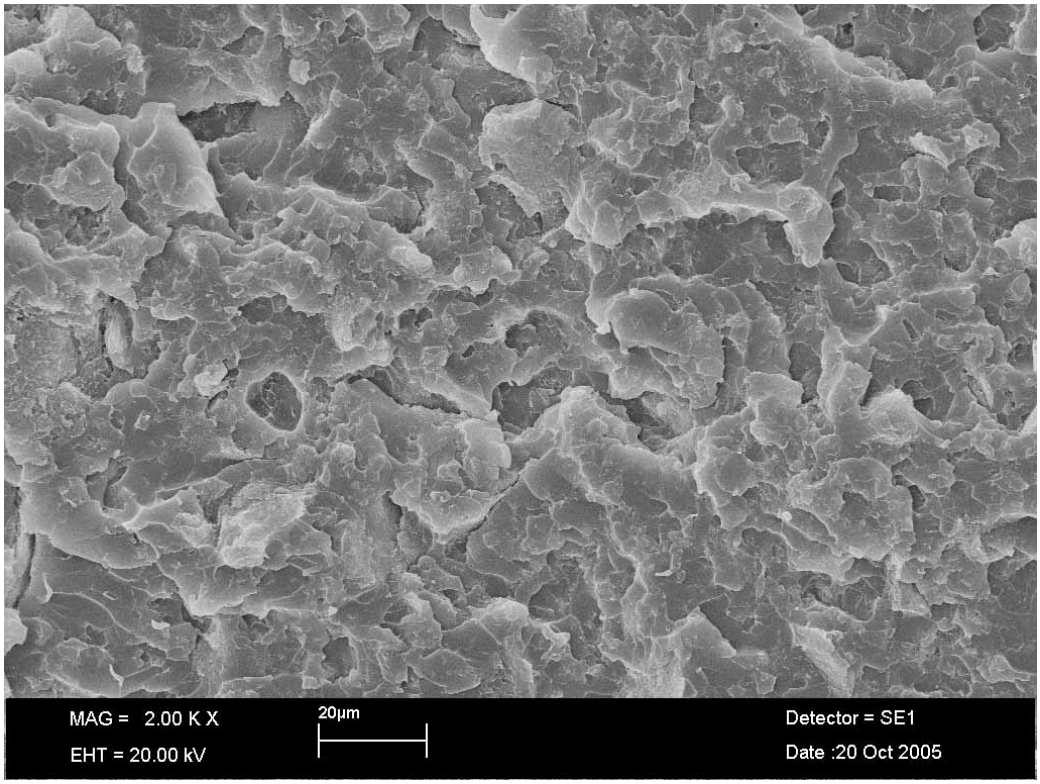

Figure 6.17 The SEM image of 2wt% nanoclay epoxy sample magnified in 2,000X.

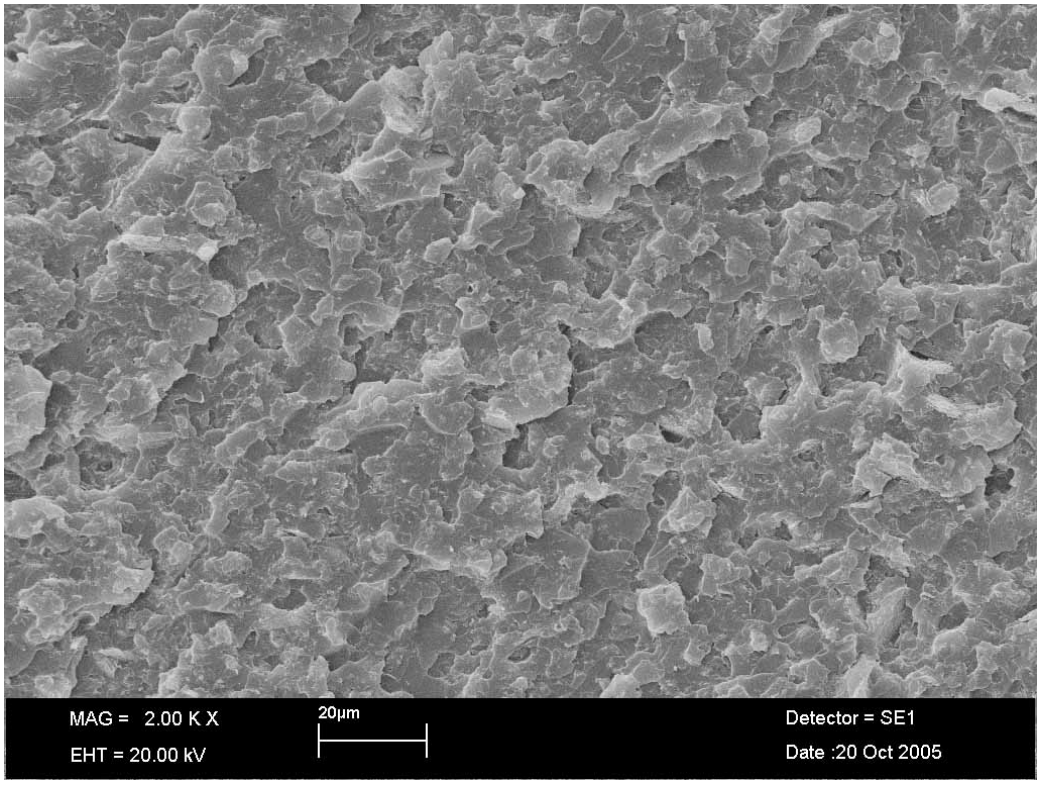

Figure 6.18 The SEM image of 3wt% nanoclay epoxy sample magnified in 2,000X.

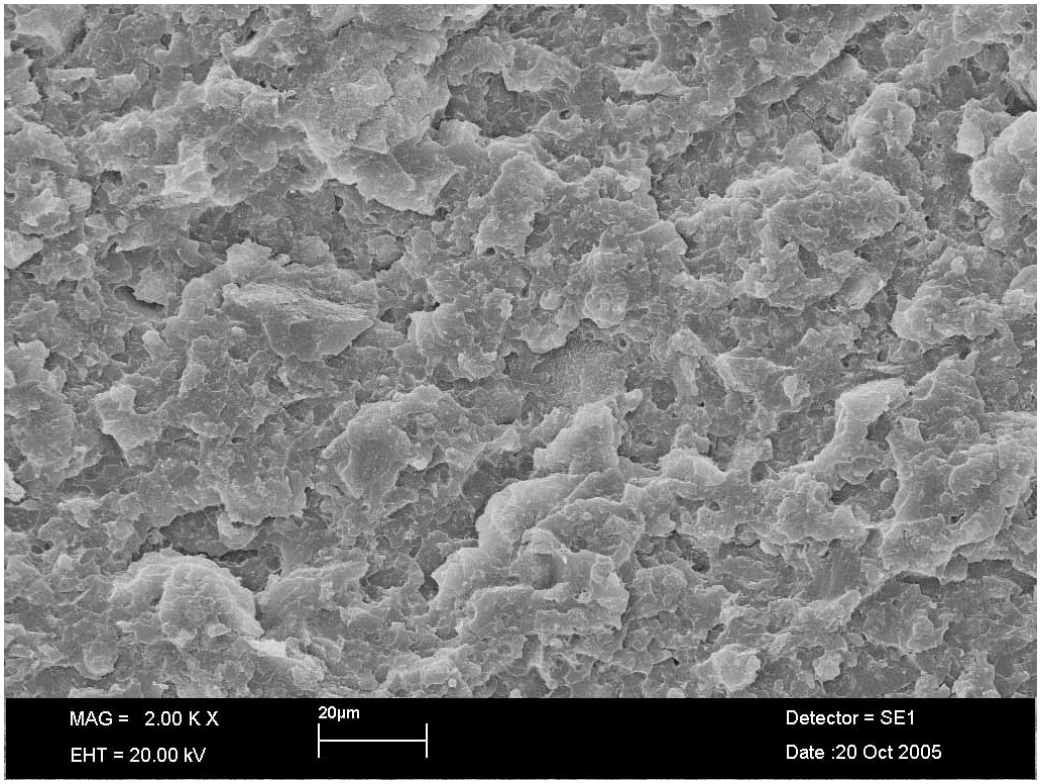

Figure 6.19 The SEM image of 4wt% nanoclay epoxy sample magnified in 2,000X.

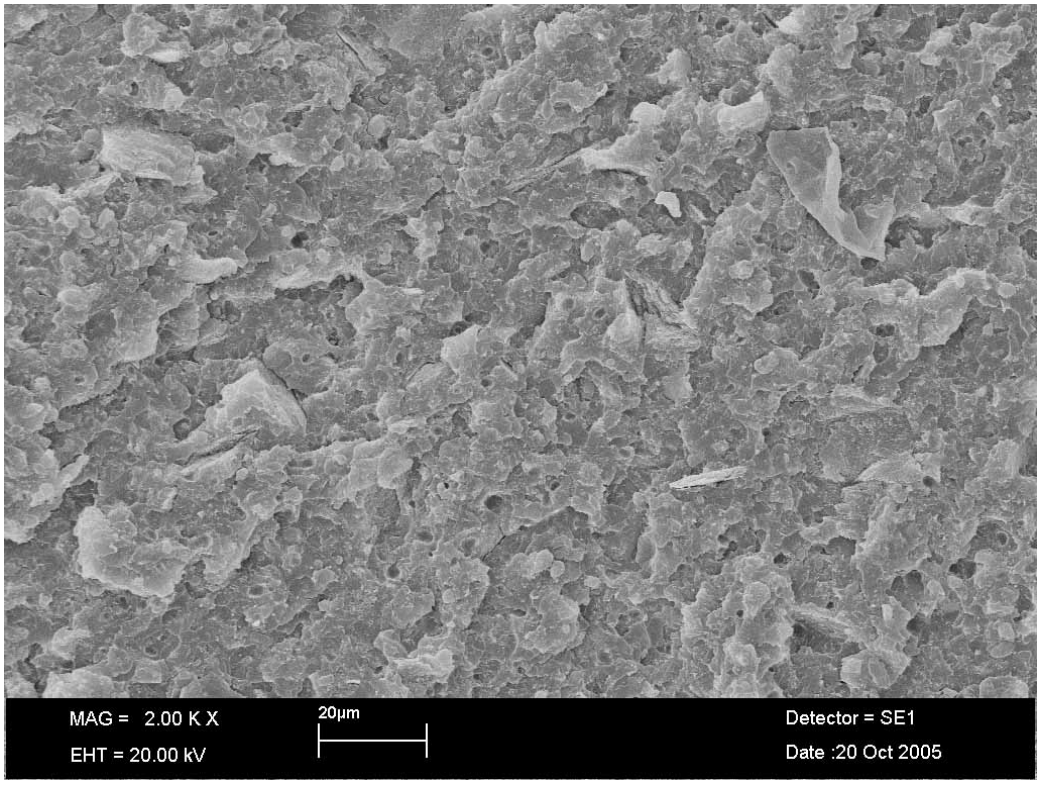

Figure 6.20 The SEM image of 5wt% nanoclay epoxy sample magnified in 2,000X.

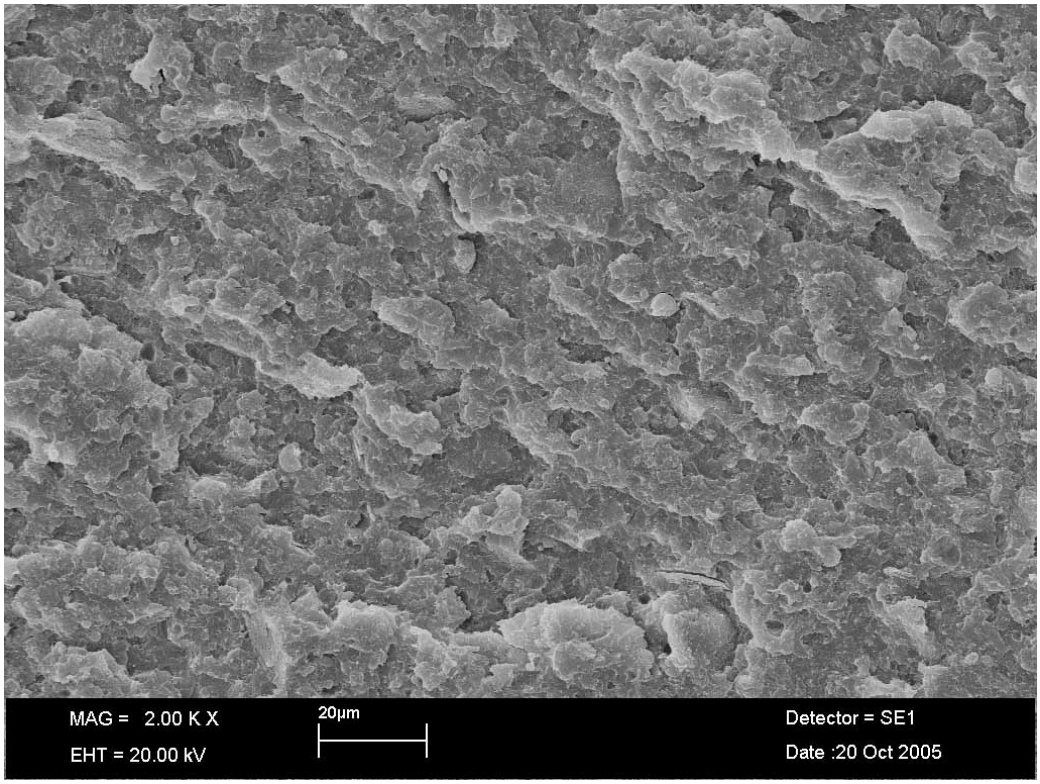

Figure 6.21 The SEM image of 6wt% nanoclay epoxy sample magnified in 2,000X.

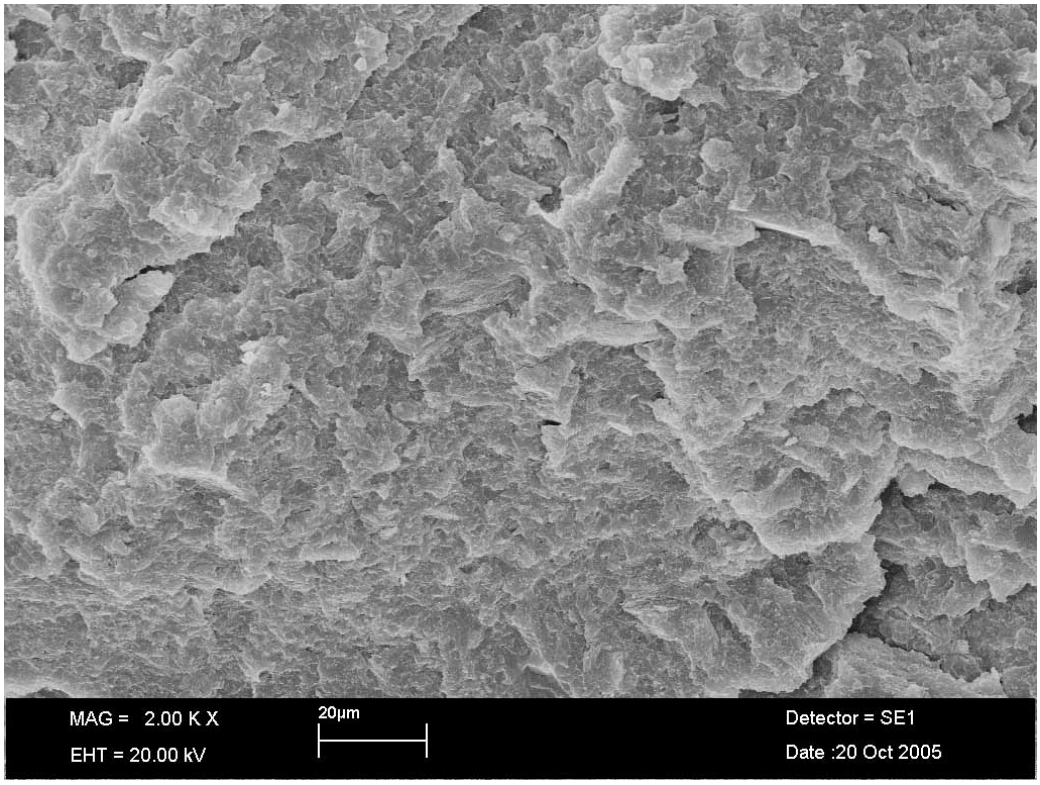

Figure 6.22 The SEM image of 7wt% nanoclay epoxy sample magnified in 2,000X.

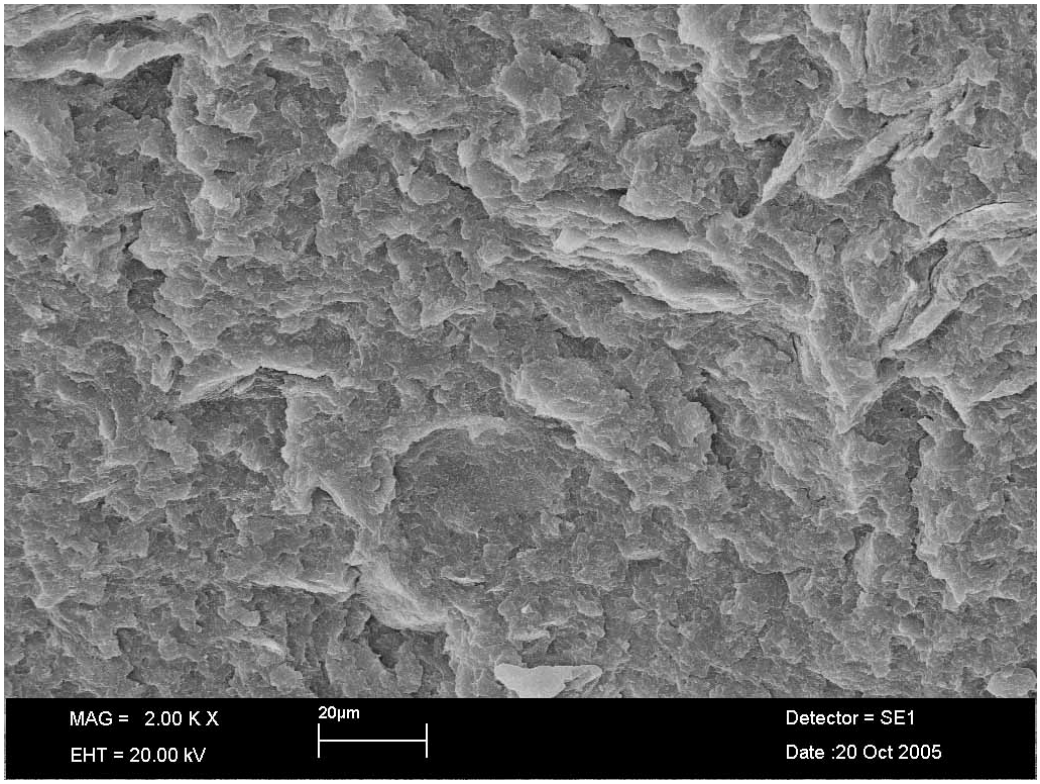

Figure 6.23 The SEM image of 8wt% nanoclay epoxy sample magnified in 2,000X.

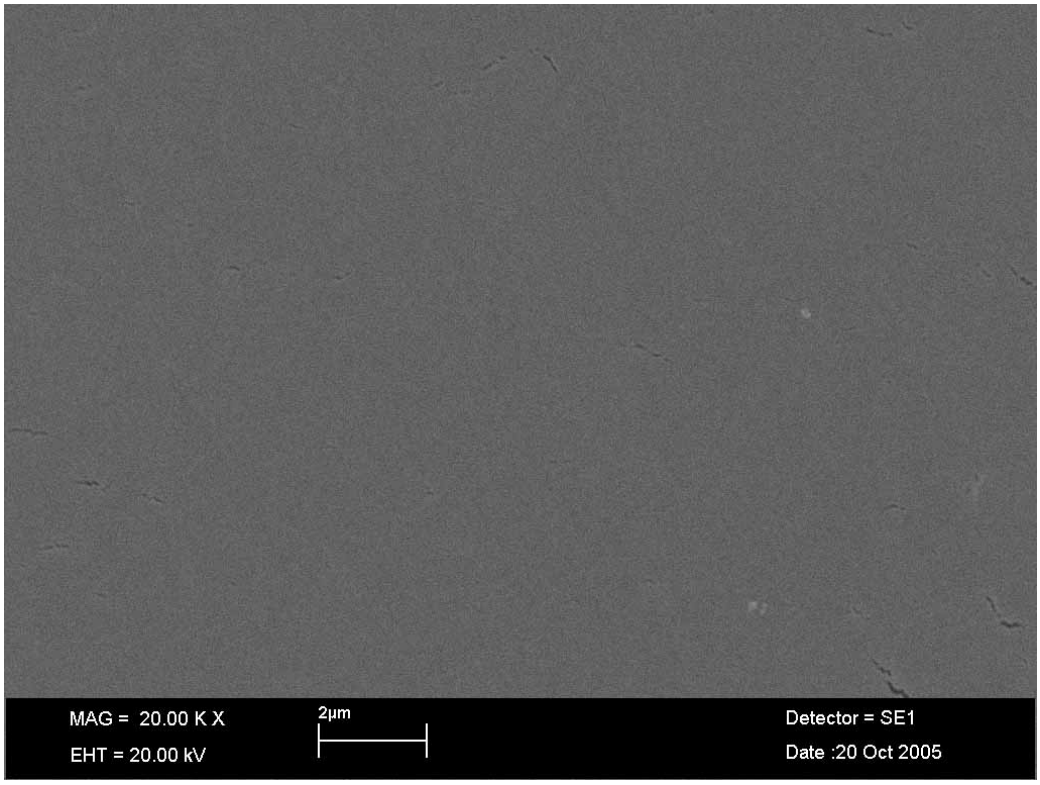

Figure 6.24 The SEM image of pure epoxy sample (0wt% nanoclay) magnified in 20,000X.

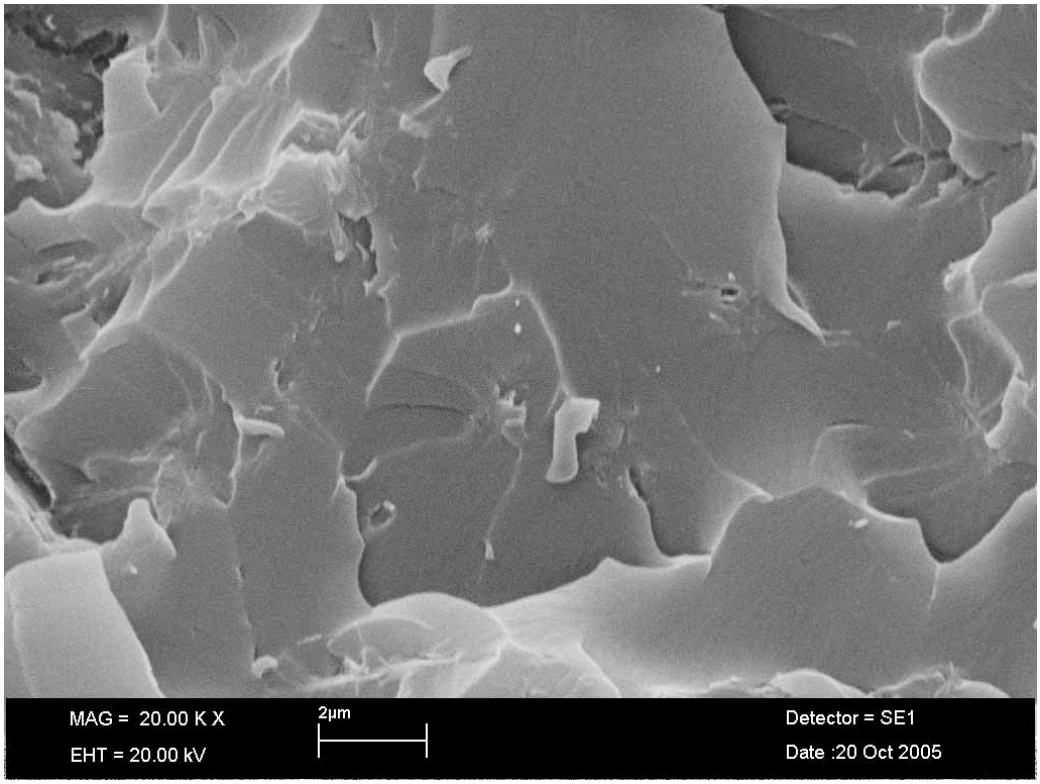

Figure 6.25 The SEM image of 0.5wt% nanoclay epoxy sample magnified in 20,000X.

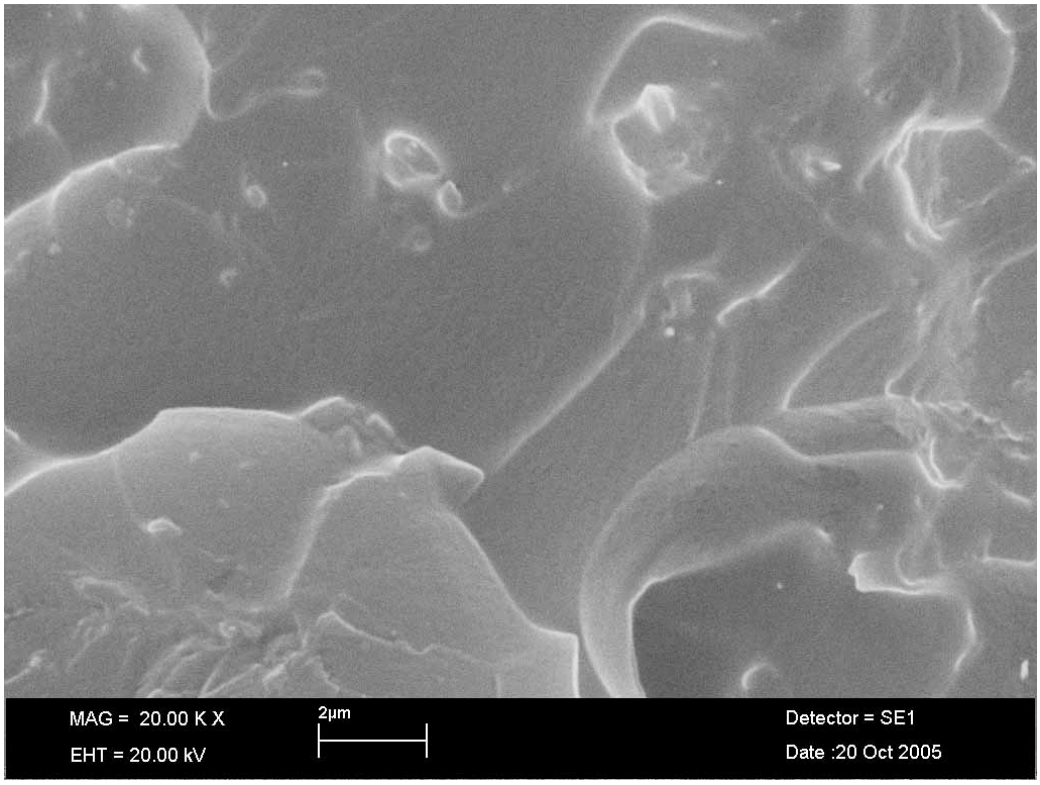

Figure 6.26 The SEM image of 1wt% nanoclay epoxy sample magnified in 20,000X.

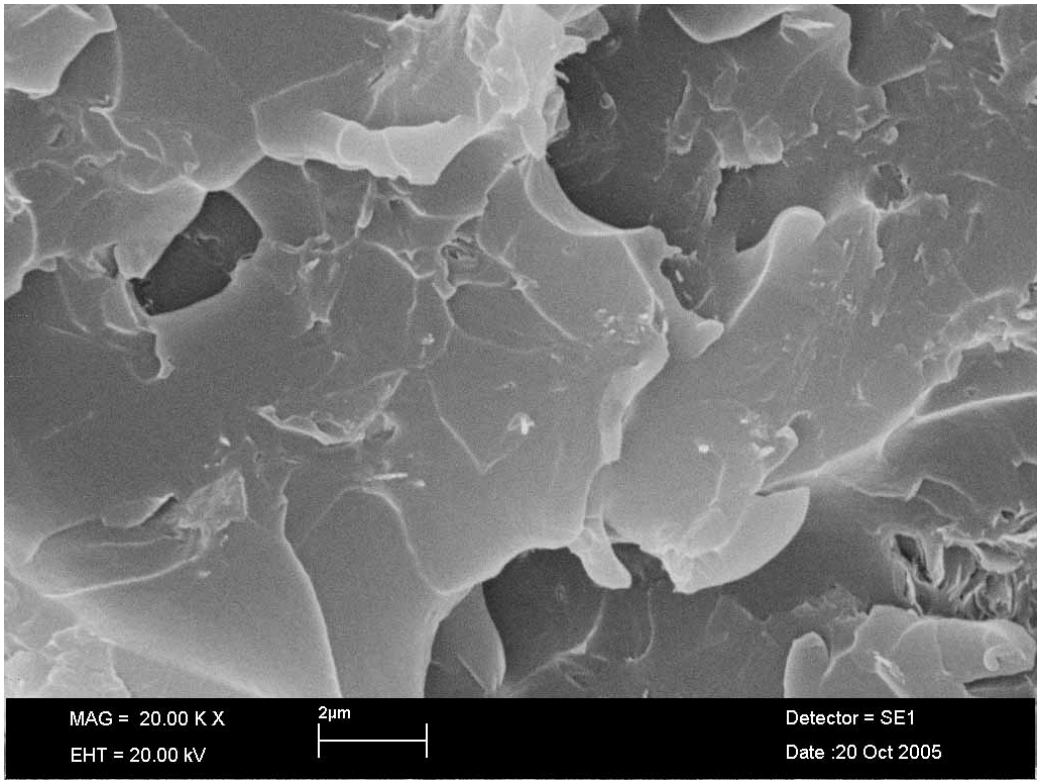

Figure 6.27 The SEM image of 2wt% nanoclay epoxy sample magnified in 20,000X.

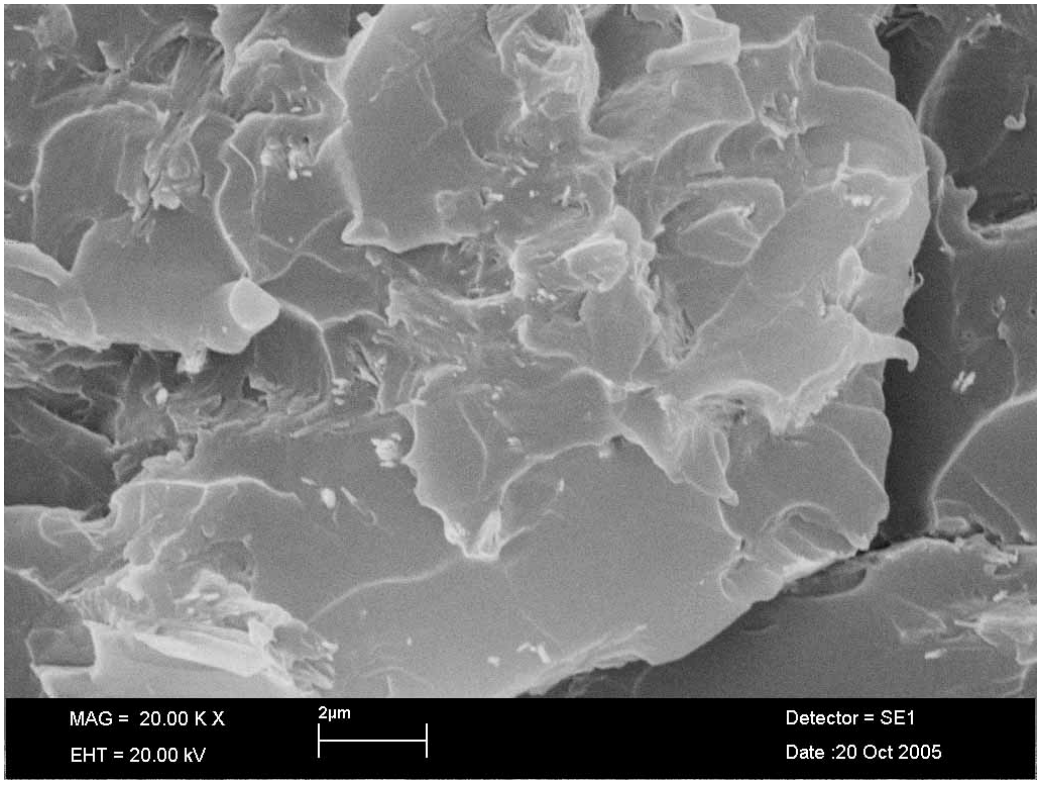

Figure 6.28 The SEM image of 3wt% nanoclay epoxy sample magnified in 20,000X.

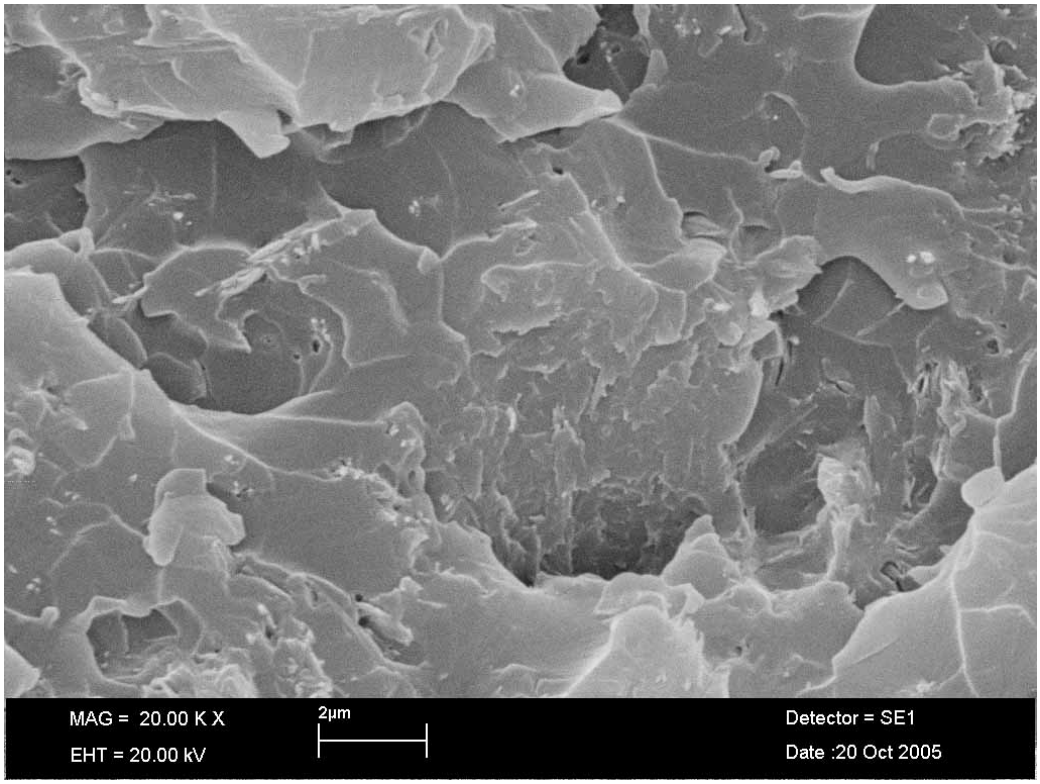

Figure 6.29 The SEM image of 4wt% nanoclay epoxy sample magnified in 20,000X.

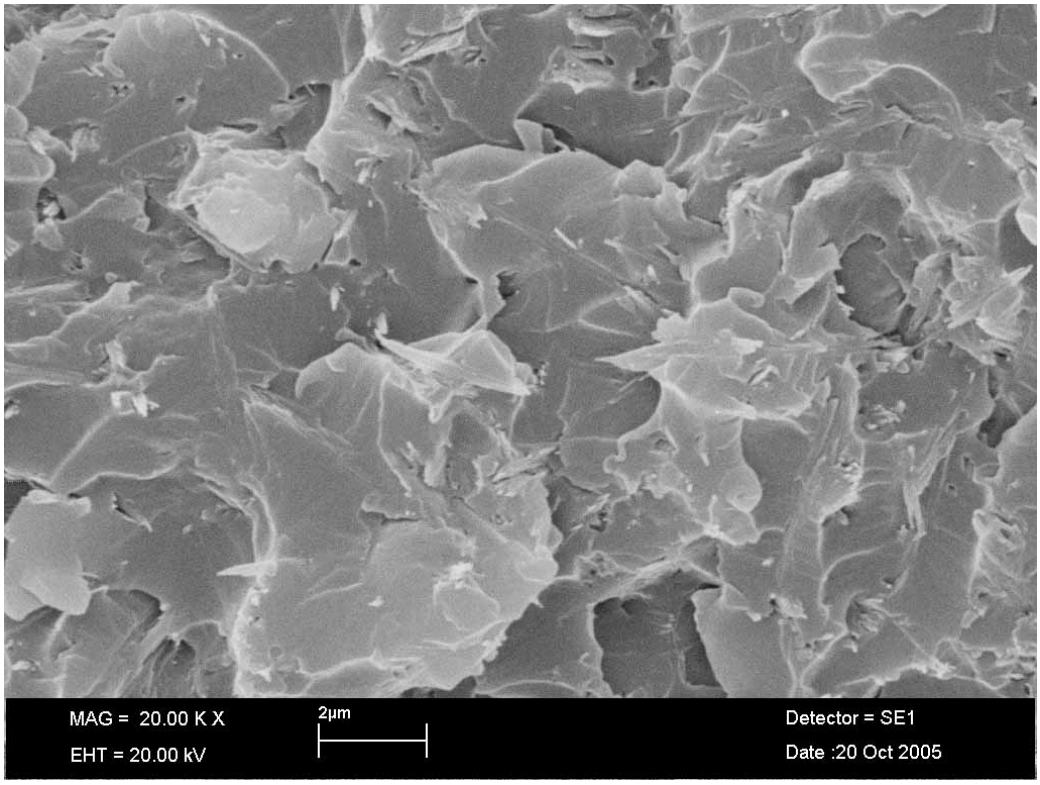

Figure 6.30 The SEM image of 5wt% nanoclay epoxy sample magnified in 20,000X.

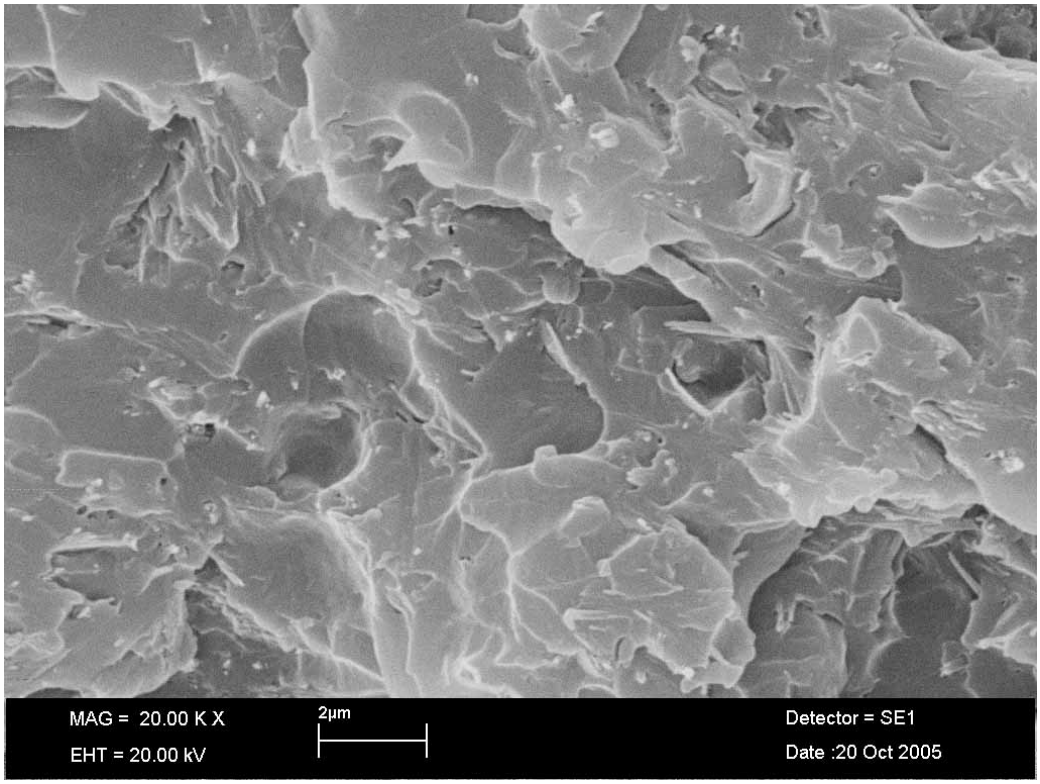

Figure 6.31 The SEM image of 6wt% nanoclay epoxy sample magnified in 20,000X.

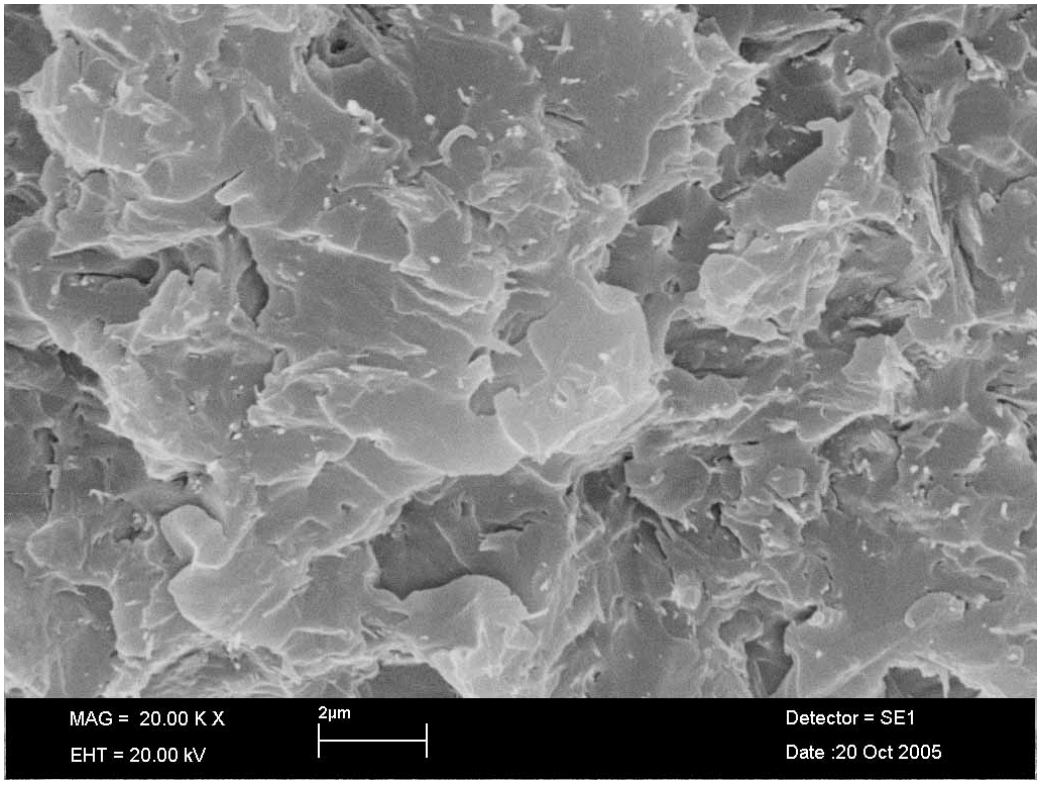

Figure 6.32 The SEM image of 7wt% nanoclay epoxy sample magnified in 20,000X.

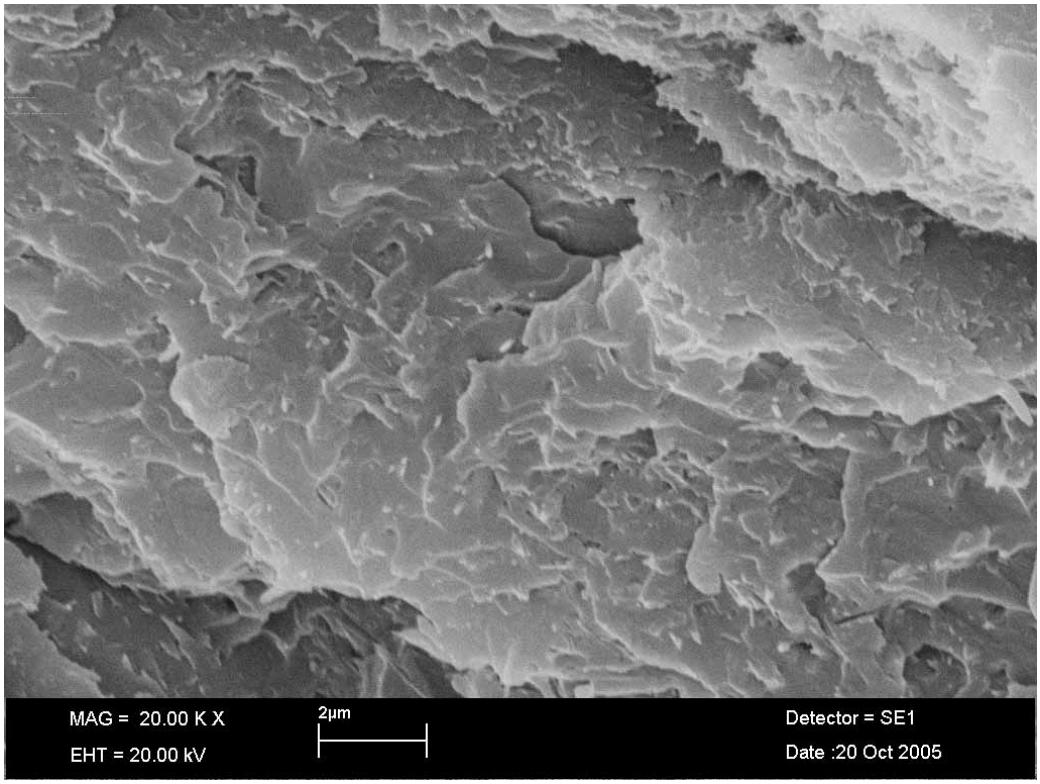

Figure 6.33 The SEM image of 8wt% nanoclay epoxy sample magnified in 20,000X.

Chapter 7

Discussions, Conclusions and Future Work

7.1 Discussions

As a quick review from the experimental results of the nanoclay-epoxy samples in Chapters 4, 5 & 6 that the introduction of nanoclay inside the epoxy matrix contributes to higher tensile strength, flexural strength and Vickers' hardness. But the ductility decreased with the nanoclay content inside the epoxy samples. On the other hand, from the XRD results, it was shown that there was no interaction between the nanoclay and the epoxy matrix as there was no peak shift in the nanoclay diffraction peak. Moreover, it was further verified in DMA, TMA and TGA results that there was no significant change of glass transition, thermal expansion and decomposition temperature in the nanoclay-epoxy samples when compared with that of pure epoxy. Therefore, it was confident to say that nanoclay was just evenly distributed in the epoxy matrix. Finally, it was found from the SEM images that there was a trend as the nanoclay content in the epoxy samples increased, the fracture surfaces were rougher, irregular in shape and broken down into tiny pieces with stress whitened sharp edges, a lot of white spots or white lines, which believed to be the nanoclay, were found coming out from that fracture surfaces. Moreover, from the SEM image of the nanoclay, it was found that it looked like a nano-ribbon, therefore, it was obvious to imagine when this kind of nano-ribbon was evenly distributed across the matrix, it

would easily inter-lock and entangle with the polymer chains in the epoxy matrix. In general, a model is deduced from all the experimental results, which is called a “net” model.

7.2 NET model

Nanoclay, which is about several microns in length and about 100 nm in width, can provide a huge surface area once it is evenly distributed. When this kind of nano-ribbon is spread inside the epoxy matrix, it acts like the grid line of a net. Or let’s say in another situation, the nano-ribbon acts like the platelet in our blood stream. When there is a wound on the hand and blood is bleeding, the platelets will continuously coming, forming a net to block the wound. In analogue to the nanoclay, this grid line or platelet is the nano-ribbon. When the nanoclay content inside the epoxy samples increases, as if the number of grid lines of the net increase or the platelets are agglomerating to form a net, then sieve holes of the net become smaller and smaller. This model is consistent with the SEM results that as the nanoclay content in the epoxy samples increased, the fracture surfaces were rougher, irregular in shape and broken down into tiny pieces with stress whitened sharp edges.

A simulation sketch of this net model applied in the nanoclay-epoxy samples is shown in Figures 7.1 & 7.2. In Figure 7.1, when a pure epoxy sample is under tension, it will elongate and contract as ordinary ductile material. At breaking strength, the sample fractures with a clear-cut and mirror-like plane surface as found out in the SEM images in Figures 6.4, 6.14 & 6.24.

In Figure 7.2, the distribution of low nanoclay content in an epoxy sample is sketched at the upper left position. The net model needs not be a square net, it may be a rectangular net, triangular net, circular net etc, as long as the nano-ribbon is evenly distributed inside the matrix. For simplicity reason, a square net model is used for explanation. As stated before, the

characteristic geometry of nano-ribbon will easily inter-lock and entangle with the polymer chains in the epoxy matrix, and epoxy has a cross-linked structure, the high aspect ratio of nano-ribbon will follow the polymer chains and will be directed by the polymer cross-linked structure into a kind of regular square pattern. When this low nanoclay content epoxy sample is under tension, it will elongate and contract as the pure epoxy sample does, but due to the square net inside the sample, the elongation and contraction cannot be as great as in pure epoxy sample. The deformation is pinned by the vertical and horizontal alignments of the nano-ribbon, as if the nanoclay strengthens both the vertical and horizontal directions.

When the tensile force generally increases, the nano-ribbon tends to align with the vertical tensile force, or the square pattern nano-ribbon in return directs the cross-linked polymer chains of epoxy to the vertical tensile force. Now, it looks like a bundle of polymer chains are being pulled rather than of a whole cross-linked structure. However, due to the rigidity in the horizontal direction pinned by the nano-ribbon, the sample cannot contract the same amount as in the pure epoxy sample under the same tensile force. Therefore, an imaginary force is stressed on the horizontal direction. If however, there is a small hole or crack in the horizontal direction, the horizontal force will follow the crack propagating direction and tear down the sample easily, like a sword to cut through the waist of the sample. That's why the ductility will decrease when nanoclay is introduced inside the epoxy matrix. As discussed in Chapter 6, the enhanced in tensile strength of the nanoclay-epoxy sample was due to the bonding or entanglement between the epoxy polymer chains and the nano-ribbon surfaces. Therefore, the shear failure of these regular pattern interfaces, the fracture surface will be rough with sharp edges.

On the other hand, the distribution of high nanoclay content in an epoxy sample is sketched at the lower left position in Figure 7.2. In this case, the increase in the amount of nano-

ribbon will be directed by the polymer cross-linked structure even into a more closely packed regular square pattern. Hence, when the high nanoclay content epoxy sample is under tension, it won't elongate and contract as much as in the low nanoclay content epoxy sample, due to the close packed pattern of the nano-ribbon net inside the matrix.

When the tensile force generally increases, the more closely packed square nano-ribbon pattern will direct the cross-linked polymer chains of epoxy to align with the vertical tensile force. Now, it really looks like a bundle of polymer chains is being pulled rather than of a cross-linked structure. And at the same time, a larger horizontal imaginary force is stressed up on both sides of the sample. As explained in Chapter 3, for a higher nanoclay content epoxy sample, due to its high viscosity, bubbles will easily be trapped inside the sample during curing. This horizontal force will easily tear down the sample, that's why the ductility will decrease drastically in epoxy samples with high nanoclay content and the failure is catastrophic. Moreover, the fracture surface is rougher and in even smaller pieces with sharp edges because of the debonding or dis-entanglement between the increased interfaces of the epoxy polymer chains and the nano-ribbon surfaces. Furthermore, the simulation pictures presented here are only in 2 dimensions. The true situation is in 3 dimensions, that's why the fracture surface was as rough and tiny as in the SEM images in higher nanoclay content samples like 7wt% or 8wt% nanoclay.

When generalizing this net model to the explanation for all the experimental results, the addition of this kind of "nano-ribbon" into the epoxy matrix, the nano-ribbon will interlock, entangle and follow the cross-linked polymer chains of epoxy to be directed to align in a regular pattern in a 3 dimensional network. Since, the nanoclay has no interaction with the epoxy, as it is just a net in the matrix, so there is no peak shifting in XRD, no significant glass transition difference found in DMA, not much difference in thermal expansion found in TMA, not much

change in decomposition temperature in TGA among all the nanoclay-epoxy samples. But the nanoclay did make the sample stiffer at elevated temperature as shown in the increased in the elastic modulus in DMA, because the net strengthen the nanoclay-epoxy samples to become more rigid, so they will show higher tensile, bending strength and Vickers' hardness value. But the rigidity of the net caused the decreased in the ductility and the shear failure of these regular pattern interfaces lead to the rough fracture surfaces with sharp stress whitened edges in the SEM results.

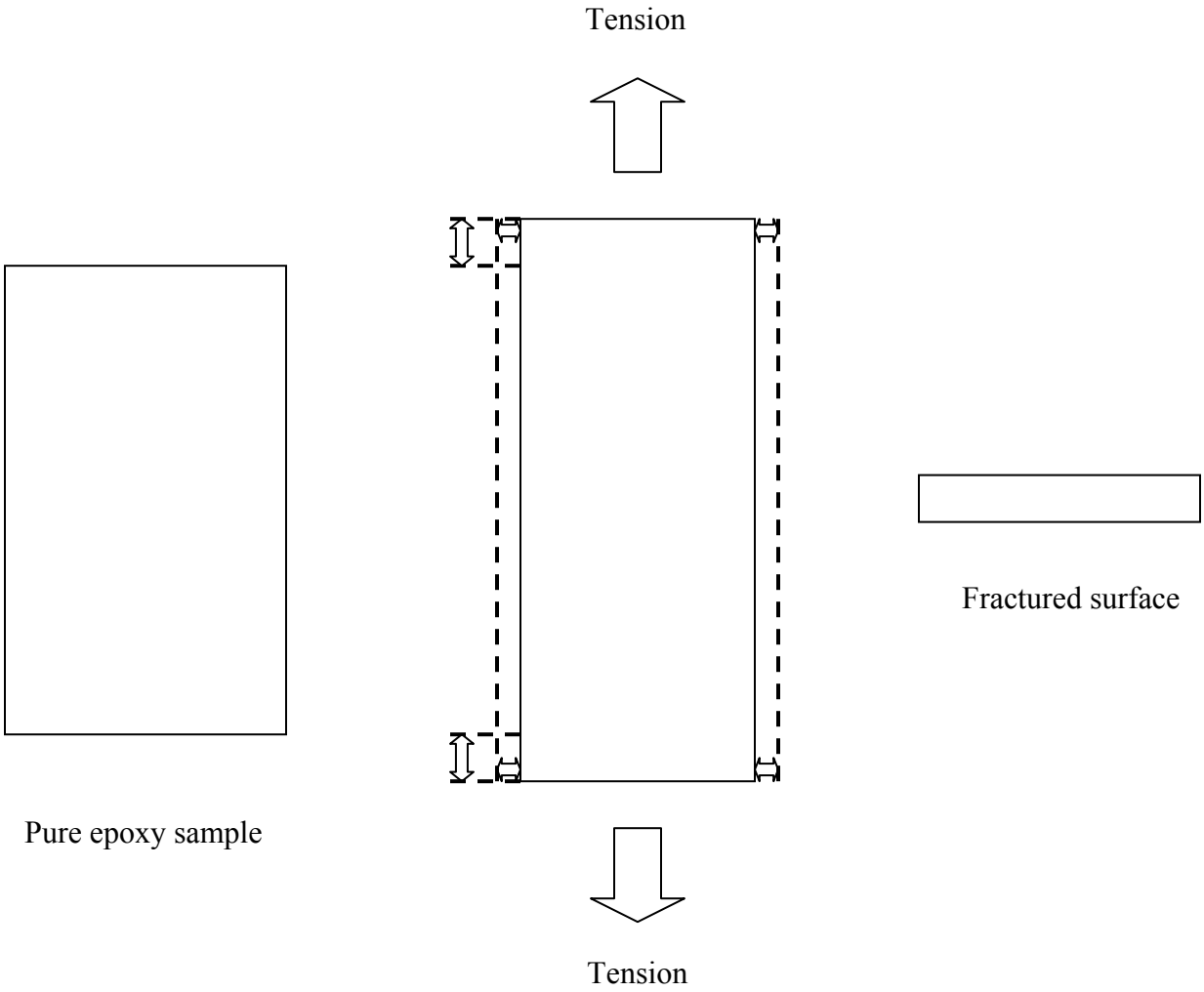

Figure 7.1 A schematic sketch of a pure epoxy sample (left). When under tension (middle), it will elongate and contract. At breaking strength, the fracture surface is clear-cut and mirror-plane (right).

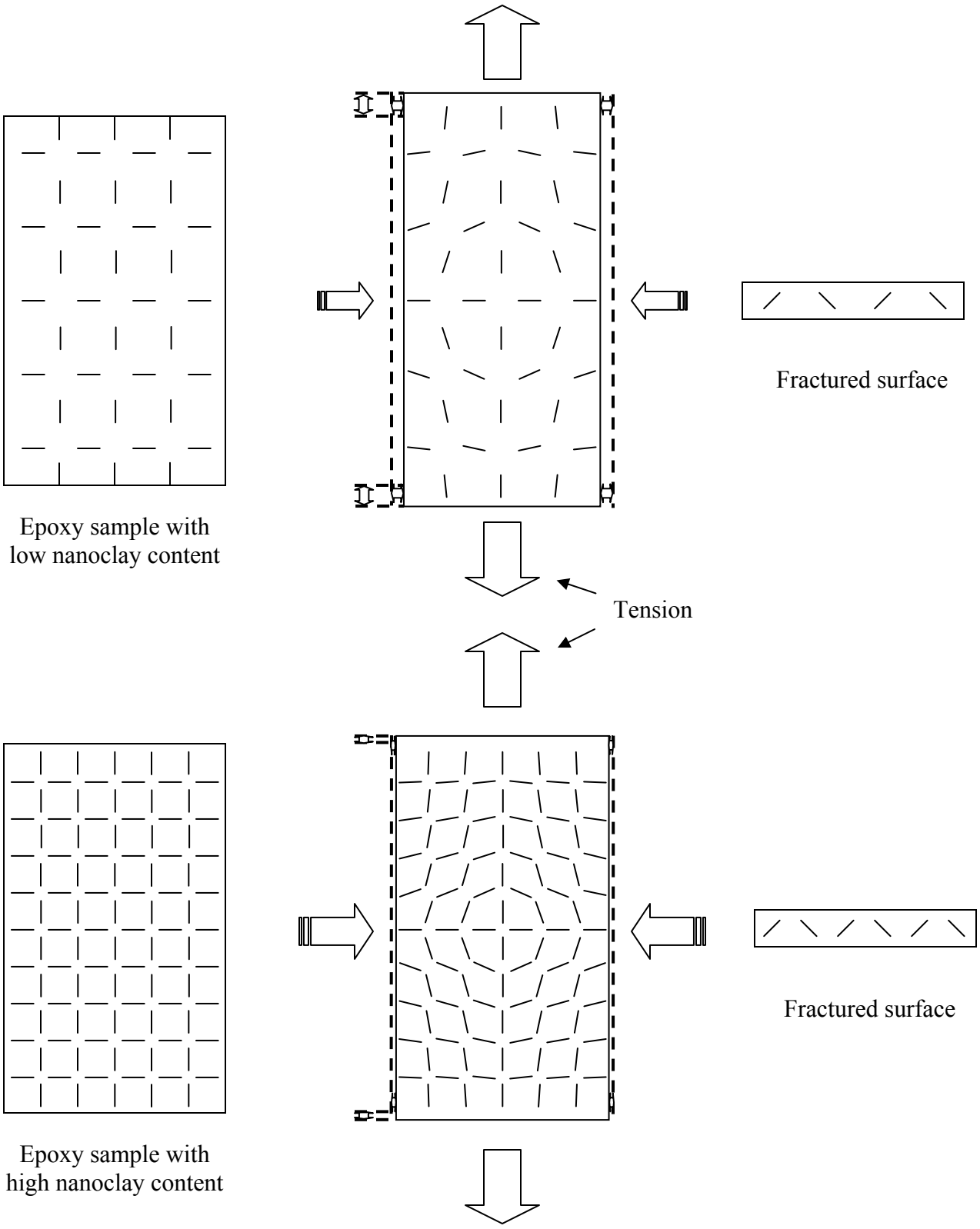

Figure 7.2 A simulation sketch of a low nanoclay content (upper left) and high nanoclay content (lower left) epoxy samples, when under tension (middle), the imagine nanoclay behaviors inside the samples, and the appearance of the fracture surfaces at breaking strength (right).

7.3 Mathematical prediction

In Chapter 4, session 4.2, a graph of the ultimate tensile strength of samples as a function of weight percentage of nanoclay in epoxy from 0wt% to 8wt% was shown in Figure 4.2, so the relationship between the ultimate tensile strength as a function of weight percentage of nanoclay content is going to be investigated. According to T. D. Fornes et al., they demonstrated the clay/nylon-6 nanocomposites have a higher efficiency in improving the Young's modulus than the glass fiber reinforced nylon-6 composites in the filler loading up to 10 wt% [10]. However, the silicates nanocomposites can't compete with the traditional fiber reinforced composites in the high filler range. There is an effectiveness limit in the nanaclay weight percentage in polymer matrix composites. Moreover, in real situation, according to this research finding, this limit in the weight percentage may be even lower than 10wt% nanoclay content.

Therefore, in this session, the experimental data points of the ultimate tensile strength of samples as a function of weight percentage of nanoclay in epoxy was compared with the conventional composites using composite theory by Halpin - Tsai equation, $\frac{E}{E_m} = \frac{1 + \zeta\eta\phi_f}{1 - \eta\phi_f}$ where E and E_m represent the Young's modulus of the composite and matrix, respectively, ζ is a shape parameter dependent upon filler geometry and loading direction, ϕ_f is the volume fraction of filler, and η is given by $\eta = \frac{E_f/E_m - 1}{E_f/E_m + \zeta}$ where E_f represents the Young's modulus of the filler. Furthermore, the Halpin - Tsai equations retain the same form for discontinuous cylindrical fibers and lamellar shape reinforcements, such as ribbons or rectangular platelets. However, when calculating elastic moduli E_{11} and E_{22} in the case of ribbons or rectangular platelets, ζ is equal to (ℓ/t), where ℓ is the length and t is the thickness of the dispersed phase. In this research finding, the aspect ratio of length to thickness difference is very high, about 500, for simplicity reason, ζ is assumed to approach infinity. When $\zeta \rightarrow \infty$ the theory reduces to the rule

of mixtures (upper bound) $E = \phi_f E_f + (1 - \phi_f) E_m$ The modulus of nanoclay is assumed to be 100 MPa, which is far smaller than the quoted 178 GPa in the paper [10], the volume fraction of the filler in the equation is assumed to be weight percentage of the filler in order to compatible with the experimental data. A graph of the ultimate tensile strength of samples compared with Halpin-Tsai equation as a function of weight percentage of nanoclay in epoxy from 0wt% to 8wt% is shown in Figure 7.3. A trend line in the 4th order of equation is drawn to simulate the tendency of the ultimate tensile strength as a function of nanoclay content by Microsoft Excel.

It is shown in the Halpin - Tsai upper bound equation that a straight line for the ultimate tensile strength as a function of weight percentage of nanoclay content is obtained, rather than a trend line with a gradual drop in the ultimate tensile strength starts at 5wt% nanoclay content.

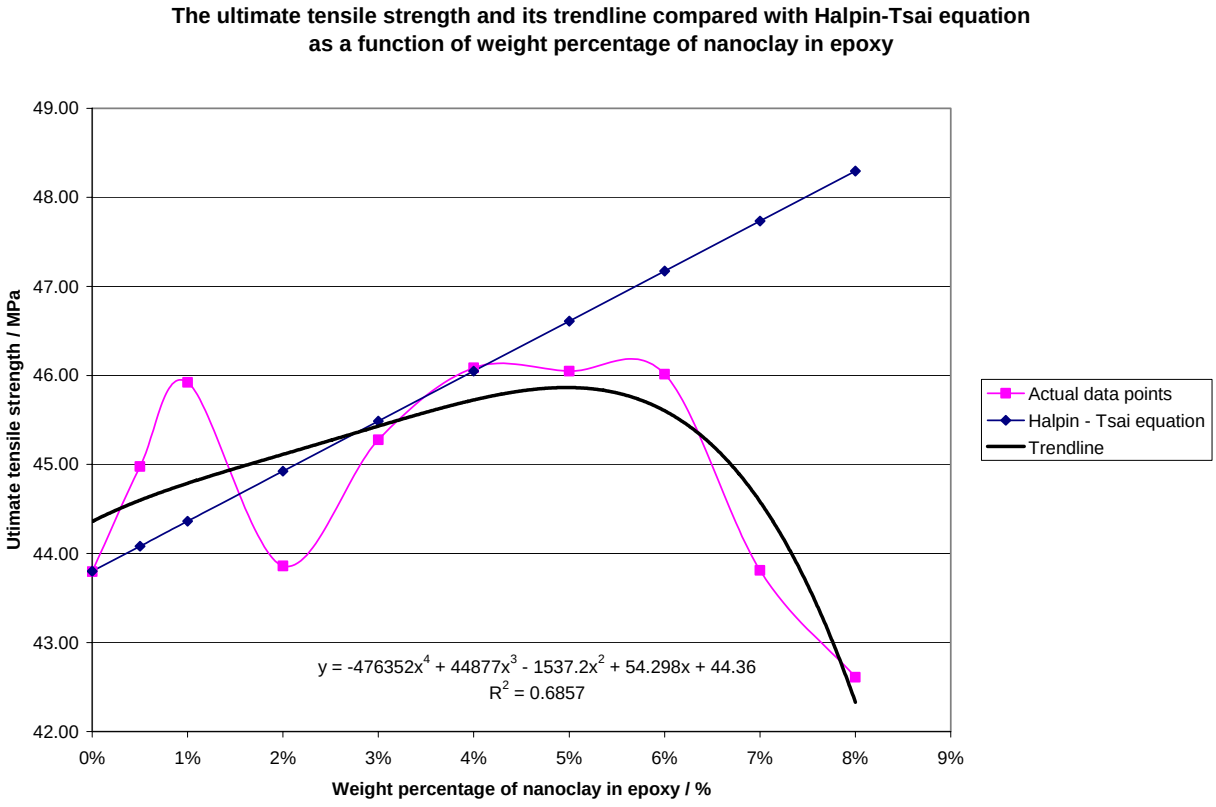

Figure 7.3 The ultimate tensile strength of samples and its trendline compared with Halpin-Tsai equation (upper bound) as a function of weight percentage of nanoclay in epoxy from 0wt% to 8wt%.

There is a difference between the composite theory and the experimental data once the nanoclay content increase. This discrepancy may be due to the porosity inside the sample as discussed in Chapter 4 & 6, where in the theory there is a perfect wetting between the matrix and the filler, but in reality, it is not. Moreover, the composite theory assumes unidirectional alignment of filler, while in this research, the nanoclay formed a uniform net structure strengthen in both directions. Furthermore, the uneven distribution in aspect ratio of the nanoclay and the level of exofoliation of nanoclay inside a polymer matrix are also the factors for the discrepancy between the theory and the experimental results. A graph of different order of equation of the trend lines for the ultimate tensile strength of samples compared with Halpin-Tsai equation as a function of weight percentage of nanoclay in epoxy from 0wt% to 25wt% is shown in Figure 7.3.

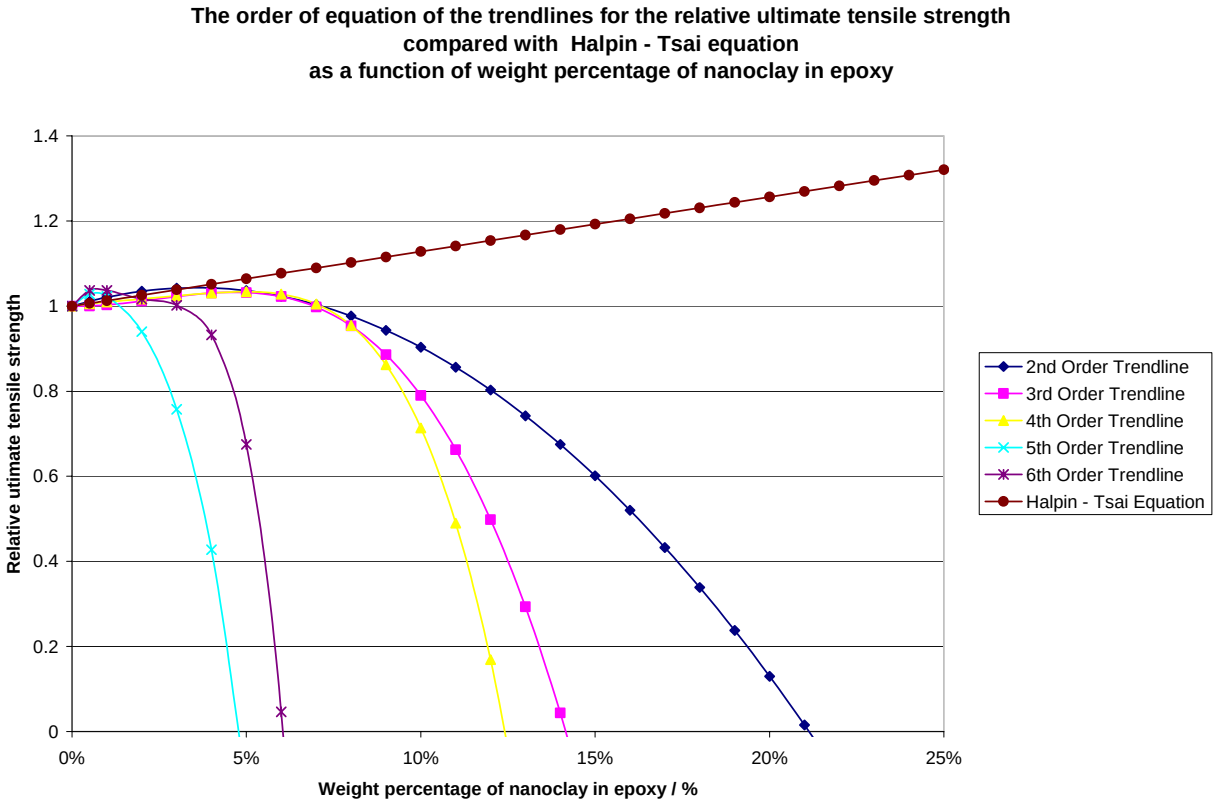

Figure 7.4 The order of equation of the trendlines for the relative ultimate tensile strength compared with Halpin-Tsai equation as a function of weight percentage of nanoclay in epoxy from 0wt% to 25wt%.

7.4 Conclusions

Casting method was employed to produce the dog-bone shape samples for tensile and other tests. The epoxy resin Araldite®GY 251 and the hardener HY 956 from CIBA-GEIGY were used and mixed in the ratio of 4:1 by weight. The nanoclay was courtesy from Southern Clay Product Garamite 1958. Totally 10 different nanoclay-epoxy compositions were prepared in order to show a gradual trend of changes upon mechanical, thermal and microstructural investigations. These compositions were pure epoxy, that is 0wt% nanoclay, 0.5wt%, 1wt%, 2wt%, 3wt%, 4wt%, 5wt%, 6wt%, 7wt% & 8wt% nanoclay in epoxy. Three different areas of characterization instruments were employed to study the mechanical, thermal and microstructural behaviors of the nanoclay-epoxy samples. From the mechanical instruments such as MTS tensile loading machine and Vickers' hardness tester, the ultimate tensile strength, flexural strength and Vickers' hardness value was obtained. From the thermal analyzers such as Dynamic Mechanical Analyzer (DMA), Thermomechanical Analyzer (TMA) and Thermogravimetric Analyzer (TGA), the glass transition temperature, linear coefficient of thermal expansion and decomposition temperature was obtained. From the microstructural analysis instruments such as X-Ray Diffractometry (XRD) and Scanning Electron Microscopy (SEM), the positions of the diffraction peaks and the microstructure of the samples fractured cross-sections was obtained.

From the stress-extension curves of the epoxy samples in tensile tests, the ultimate tensile strength of all the samples from 0wt% to 8wt% nanoclay was ranged from 42MPa to 46MPa. As the nanoclay content of the epoxy samples increased, the ultimate tensile strength also increased. The epoxy samples with 1wt%, 4wt%, 5wt% & 6wt% nanoclay had an increment by 5% in the ultimate tensile strength when compared with pure epoxy sample. In general, samples with

nanoclay content below 1wt% were ductile, while samples with nanoclay content from 2wt% to 6wt% were in between ductile and brittle transition and developed strength better than pure epoxy sample. However, samples with nanoclay content above 7wt% were brittle and the ductility was drastically dropped by more than 70% for 8wt% nanoclay sample and the failure was catastrophic. That is the ductility of the nanoclay-epoxy samples decreased while the nanoclay content increased.

From the stress-deflection curves of the epoxy samples from 0wt% to 8wt% nanoclay content, they all showed the same pattern with the compressive strength ranged from 61MPa to 67MPa. Samples from 0wt% to 6wt% nanoclay content bended with a permanently deformed "V" shape, while samples of 7wt% & 8wt% nanoclay content were completely torn apart. The epoxy sample of 6wt% nanoclay showed the largest flexural strength with an increment by 4.3% when compared with that of pure epoxy sample.

From the Vickers' hardness results of the nanoclay-epoxy samples, the 5wt% nanoclay sample was the hardest among all the compositions with the largest HV value of 11.3 when compared with that of pure epoxy sample of HV 9.8, the increment was 15% in Vickers' hardness value. And 2wt% nanoclay sample showed a drop in the hardness with value of HV 10.1 and was consistent in the ultimate tensile strength and flexural strength that 2wt% nanoclay sample was softer. However, the reason for the drop in strength in sample with 2wt% nanoclay content was unknown, or 2wt% nanoclay is the critical exfoliated clay content above which matrix transcrystallization percolates [43].

When combining with the tensile test, 3-point bending test and Vickers' hardness test results together, the compositions at 4wt%, 5wt% & 6wt% nanoclay content showed a feasible production in nanoclay reinforced epoxy composites regarding their enhanced mechanical

properties. However, in accounting for the ease of casting in order to mold samples with good mechanical properties, the nanoclay content should be kept below 5wt% to avoid the nanoclay-epoxy mixture too viscous to be cast [46]. Therefore, 5wt% nanoclay-epoxy sample seems to show better properties and ease of fabrication. Moreover, it agrees with the results in open literature [1].

From the tensile testing module in DMA, the glass transition temperature T_g of the epoxy samples took place at 45^{o}C. All 10 curves followed the same pattern with 5wt% nanoclay sample showed the highest elastic modulus when compared with all other compositions after the T_g, while 2wt% nanoclay sample showed the lowest elastic modulus. Therefore, 5wt% nanoclay sample was stiffer, while 2wt% nanoclay sample was softer at elevated temperature. However, the increased in nanoclay content in the epoxy samples didn't make much difference on the shift of the T_g. On the other hand, the increased in the nanoclay content in the epoxy samples contributed to higher strength of the materials at elevated temperature.

From the TMA results, the glass transition in all the 10 compositions showed at around 45^{o}C to 50^{o}C. They had about the same slope of thermal expansion with an average value of 210x10^{-6}/^{o}C. Again, the increased in the nanoclay content in the epoxy samples didn't make much difference on the coefficient of thermal expansion CTE.

From the TGA results, the nanoclay-epoxy samples seemed to be burnt out at about 450^{o}C. They had their first 10% weight loss at about 285^{o}C. Again, the increased in the nanoclay content in the epoxy samples didn't change much of the decomposition rate.

When combining with the DMA, TMA and TGA results together, the introduction of nanoclay content inside the epoxy samples seemed do not make change in the thermal properties such as the T_g, CTE and decomposition temperature.

From the XRD results, it was found that as the nanoclay content in the epoxy samples increased, the height of the main diffraction peak of nanoclay in the epoxy samples also increased, and the increase was linearly with the nanoclay content from 1wt% to 8wt%, but the peak positions of nanoclay diffraction peaks in all the epoxy samples remained unchange as if they were the pure nanoclay diffraction peaks. This indicated that the nanoclay acted like a nanodispenser all over the whole epoxy matrix as there was no peak shifting, no expansion of gallery in the nanoclay structure, thus no interaction between the nanoclay and the epoxy matrix.

From the SEM images, nanoclay was shown as nano-ribbon with about several microns in length and about 100 nm in width with aspect ration about 500.By EDX, the nano-ribbon was identified as Hectorite, a species of Smectite clay with strip morphology. It was trivial to imagine when this kind of nano-ribbon was evenly distributed across the matrix, it would easily inter-lock and entangle with the polymer chains in the matrix. There was a trend that as the nanoclay content in the epoxy samples increased, the fracture surfaces were broken down into rougher, smaller and irregular in shape tiny pieces with stress whitened edges, a lot of white spots or white lines, which believed to be the nanoclay (the nano-ribbon), were found coming out from the fracture surfaces. It was not the case for pure epoxy sample, where the fracture surface was clear-cut and mirror-plane.

As a conclusion, a model is deduced from all the experimental results to try to explain the phenomena taken place in the nanoclay-epoxy samples, which is called a “net” model.

A net model is when the nano-ribbons are evenly distributed inside the epoxy matrix, they will interlock and entangle with the polymer chains in the epoxy matrix, the high aspect ratio of nano-ribbon will follow the polymer chains and will be directed by the polymer cross-

linked structure to align in a regular pattern in a 3 dimensional network. The situation is like the platelets in our blood stream, trying to form a net to block the blood cells from bleeding out.

When the nanoclay-epoxy sample is under tension, the closely packed regular nano-ribbon pattern will direct the cross-linked polymer chains of epoxy to the vertical tensile force. The situation is looks like a bundle of polymer chains are being pulled rather than of a whole cross-linked structure. Due to the rigidity in the horizontal direction pinned by the nano-ribbon, the sample cannot contract the same amount as in the pure epoxy sample under the same tensile force. Therefore, an imaginary force is set up to compress both sides of the sample. If however, a crack exists in the horizontal direction, the horizontal force will follow the crack propagating direction and tear down the sample easily, that's why the ductility will decrease when nanoclay is introduced inside the epoxy matrix. Moreover, the fracture surface is rough for the nanoclay-epoxy sample because of the debonding or dis-entanglement between the increased interfaces of the epoxy polymer chains and the nano-ribbon surfaces. As a net in the matrix, there is no interaction with the epoxy, so there is no peak shifting in XRD, no significant glass transition difference in DMA, not much difference in thermal expansion in TMA, not much change in decomposition temperature in TGA among all the nanoclay-epoxy samples. But the net strengthen the samples to become more rigid, so samples were stiffer at elevated temperature in the elastic modulus in DMA and showed higher tensile strength, bending strength and Vickers' hardness value. But the rigidity of the net caused the decreased in the ductility and the shear failure of these regular pattern interfaces lead to the rough fracture surfaces with sharp stress whitened edges in the SEM results.

In general, the bonding or the adhesive force between the polymer chains and the nanoclay plays an important role in the enhancement properties of the nanocomposites.

7.5 Future Work

The decrease in ductility seems to be the main shortcoming of the nanoclay epoxy composites in application. Since the strength of the nanoclay epoxy sample has been increased by the introduction of nanoclay inside the epoxy matrix. The problem to deal with is to eliminate the horizontal alignments of nano-ribbons inside the epoxy matrix, which will direct the crack to propagate through the sample to cause catastrophic failure. The solution is to make all the alignments of nano-ribbons in one direction in order to strengthen this direction, and at the same time block the propagation of crack in the horizontal direction. This may be one of the directions of another future research.

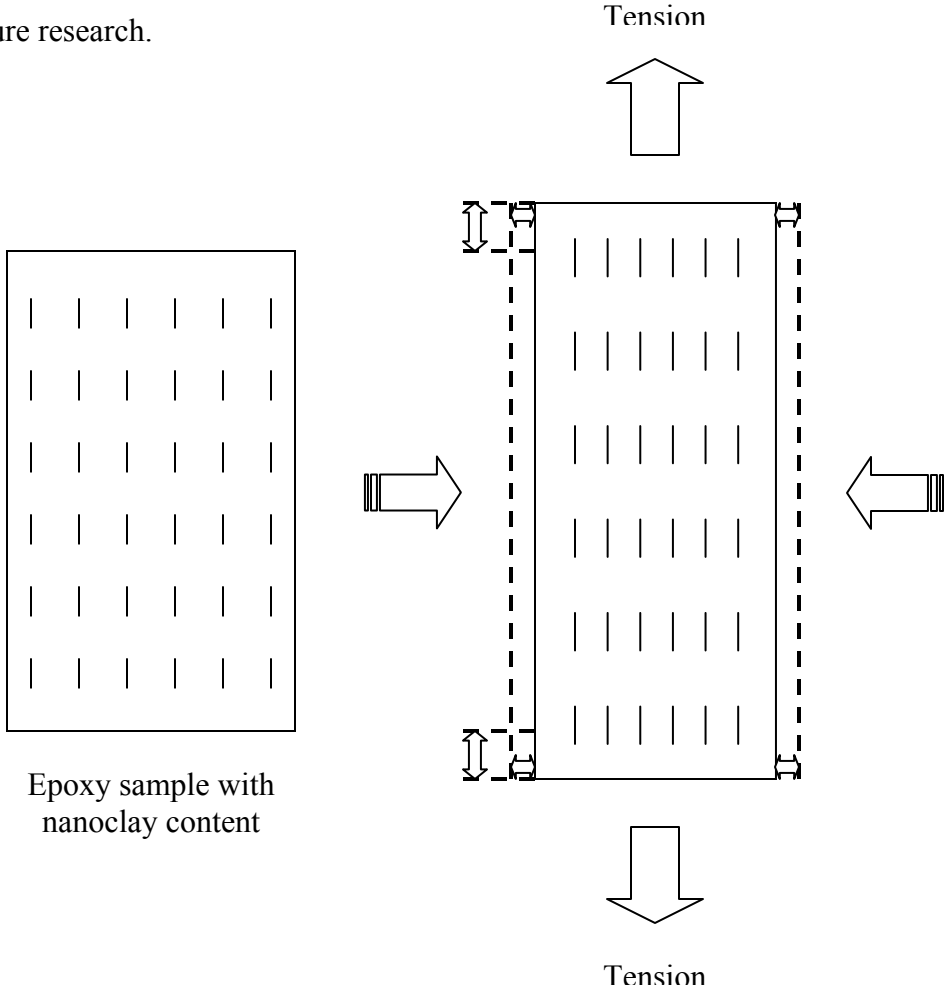

Figure 7.5 A schematic sketch of a nanoclay epoxy sample, the nano-ribbons align in one direction (left). When under tension (right), it will elongate and contract, but the horizontal force seems do not affect much in the ductility.

On the other hand, the introduction of nanoclay should be applied on soft polymer such as elastomer. S. Balakrishnan et al. introduced rubber into organoclay epoxy nanocomposites [51]. They found that as the concentration of elastomer phase increased, the fracture energy also increased when compared with unmodified nanoclay epoxy composites. Moreover, when rubber dispersants were added into organoclay epoxy resin, the ductility of the composite was enhanced without considerable reduction in the modulus and tensile strength.

Since epoxy is too rigid, which is a thermoset, a 3-dimension network system, the strong bridging behavior between resin and hardener may block the expansion of nanoclay. When compare with thermoplastic such as nylon, polybutene etc, the enhancement is greater in softer polymer as R. Hadal et al. had demonstrated the increment in the tensile properties of nanoclay reinforced polybutene and polymethylpentene nanocomposites [52]. Therefore, the direction of nanoclay should be applied on soft polymer, preferable use organo-modified nanoclay to enhance the bonding or the adhesive force between the polymer chains and the nanoclay surface.

Furthermore, the hot topic of Bio-materials composites research will be conducted in two areas of applications, one in medical application and the other one in environmental friendly application. In medical application, since bones in our body are one of the most important and most complex biomaterials, the replacement of bones or other tissues by biomaterials can bring fortune to patients with bones related diseases [53]. This kind of biomaterials for the replacement of bones should be biocompatible, and also bioactive, otherwise, this kind of foreign materials might be regarded as alien materials by human bodies and caused rejection or even fetal to human lives. Moreover, these biomaterials should be machinable, increase in mechanical strength and chemical resistance against body cell fluid. Beside replacement of bones, there is a kind of bioactive glass ceramic nails to replace the traditional metallic nails [54]. These bioactive

ceramic nails can intergrow with the bones to eliminate the operation to take out the metallic nails.

In environmental friendly application, composites with bio-degradable plastic such as biodegradable polyester and agricultural raw materials such as fibers, starch, cellulose and nanoclay will be studied. Since these agricultural raw materials are abundance, inexpensive, a natural resource from Earth, they are environmental friendly and disposed without negatively impacting the environment or the health of people [55]. Biodegradable polyesters are of great interest in the development of products from both synthetic and bio-based raw materials. These agricultural materials are expected to reinforce the strength of the bio-degradable plastic in a certain extent. Biodegradable polyesters allow agricultural-based raw materials to be used in the development of products with improved water-resistance while maintaining its excellent biodegradability. They also allow synthetic materials to be developed into products with improved biocompatibility and biodegradability, without impairing their excellent water-resistance and other properties. Therefore, biodegradable polyesters have become critical ingredients in the development of a variety of products including biocomposites, medical devices and packaging products.

Recently, Lau et al. demonstrated the precipitation of $Co(OH)_2$ colloidal particles on the nanoclay layer surfaces by physical adsorption and chemical adsorption in alkaline medium. The formation of $Co(OH)_2$ - nanoclay hybrid promoted the growth of carbon nanotubes (CNTs) by chemical vapor deposition (CVD). Pieces of nanoclay flakes served as growing sites for CNT that twisted with the other CNT to form a network-like structure connecting between the nanoclay flakes. This novel CNTs–nanoclay composite structure possesses high application potentials in advanced composites materials [56].

References

[1] M. Alexandre, P. Dubois, Polymer-layered silicate nanocomposites: preparation, properties and uses of a new class of materials, Mater. Sci. and Eng. 28 (2000) 1-63.

[2] D. M. Lincoln, R. A. Vaia, Z. G. Wang, B. S. Hsiao, Secondary structure and elevated temperature crystallite morphology of nylon-6/layered silicate nanocomposites, Polymer 42 (2001) 1621-1631.

[3] D. M. Lincoln, R. A. Vaia, Z. G. Wang, B. S. Hsiao, R. Krishnamoorti, Temperature dependence of polymer crystalline morphology in nylon 6/montmorillonite nanocomposites, Polymer 42 (2001) 9975-9985.

[4] T. B. Tolle, D. P. Anderson, Morphology development in layered silicate thermoset nanocomposites, Composites Science and Technology 62 (2002) 1033-1041.

[5] T. McNally, W. R. Murphy, C. Y. Lew, R. J. Turner, G. P. Brennan, Polyamide-12 layered silicate nanocomposites by melt blending, Polymer 44 (2003) 2761-2772.

[6] T. X. Liu, K. P. Lim, W. C. Tjiu, K. P. Pramoda, Z. K. Chen, Preparation and characterization of nylon 11/organoclay nanocomposites, Polymer 44 (2003) 3529-3535.

[7] A. Usuki, M. Kawasumi, Y. Kojima, A. Okada, T. Kurauchi, O. Kamigaito, Swelling behavior of montmorillonite cation exchanged for ω-amino acids by ε-caprolactam, J. Mater. Res., Vol. 8, No. 5, May (1993) 1174-1178.

[8] A. Usuki, Y. Kojima, M. Kawasumi, A. Okada, Y. Fukushima, T. Kurauchi, O. Kamigaito, Synthesis of nylon 6-clay hybrid, J. Mater. Res., Vol. 8, No. 5, May (1993) 1179-1184.

[9] Y. Kojima, A. Usuki, M. Kawasumi, A. Okada, Y. Fukushima, T. Kurauchi, O. Kamigaito, Mechanical properties of nylon 6-clay hybrid, J. Mater. Res., Vol. 8, No. 5, May (1993) 1185-1189.

[10] T. D. Fornes, D. R. Paul, Modeling properties of nylon 6/clay nanocomposites using composite , Polymer 44 (2003) 4993-5013.

[11] B. K. G. Theng, The Chemistry of Clay-Organic Reactions, Wiley, New York, 1974.

[12] M. Kawasumi, N. Hasegawa, M. Kato, A. Usuki, A. Okada, Preparation and mechanical properties of polypropylene-clay hybrids, Macromolecules 30 (1997) 6333-6338.

[13] G. Lagaly, Introduction: from clay mineral-polymer interactions to clay mineral-polymer nanocomposites, Appl. Clay Sci. 15 (1999) 1-9.

[14] G. Lagaly, Smectitic clays as ionic macromolecules. In: A. D. Wilson, H. J. (Eds) Prosser, Developments in Ionic Polymers, Vol. 2, Elsevier, London, (1986) 77-140.

[15] K. A. Carrado, P. Thiyagarajan, D. L. Elder, Polyvinyl alcohol-clay complexes formed by direct synthesis, Clays Miner. 44 (1996) 506-514.

[16] K. A. Carrado, L. Xu, In situ synthesis of polymer-clay nanocomposites from silicate glass, Chem. Mater. 10 (1998) 1440-1445.

[17] H. S. Jeon, J. K. Rameshwaram, G. Kim, D. H. Weinkauf, Characterization of polyisoprene-clay nanocomposites prepared by solution blending, Polymer 44 (2003) 5749-5758.

[18] J. H. Park, S. C. Jana, The relationship between nano- and micro-structures and mechanical properties in PMMA-epoxy-nanoclay composites, Polymer 44 (2003) 2091-2100.

[19] J. Wu, M. M. Lerner, Structural, thermal and electrical characterization of layered nanocomposites derived from sodium-montmorillonite and polyethers, Chem. Mater. 5 (1993) 835-838.

[20] Y. Fukushima, A. Okada, M. Kawasumi, T. Kurauchi, O. Kamigaito, Swelling behavior of montmorillonite by poly-6-amide, Clay Mineral, 23 (1988) 27-34.

[21] R. A. Vaia, E. P. Giannelis, Polymer melt intercalation in organically-modified layered silicates: model predictions and experiment, Macromolecules 30 (1997) 8000-8009.

[22] R. A. Vaia, H. Ishii, E. P. Giannelis, Synthesis and properties of two-dimensional nanostructures by direct intercalation of polymer melts in layered silicates, Chem. Mater. 5 (1993) 1694-1696.

[23] Y. Kojima, A. Usuki, M. Kawasumi, A. Okada, T. Kurauchi, O. Kamigaito, Synthesis of nylon-6-clay hybrid by montmorillonite intercalated with ε-caprolactam, J. Polym. Sci. Part A: Polym. Chem. 31 (1993) 983-986.

[24] Y. Kojima, A. Usuki, M. Kawasumi, A. Okada, T. Kurauchi, O. Kamigaito, One-pot synthesis of nylon-6-clay hybrid, J. Polym. Sci Part A: Polym. Chem. 31 (1993) 1755-1758.

[25] L. M. Liu, Z. N. Qi, X. G. Zhu, Studies on nylon-6 clay nanocomposites by melt-intercalation process, J. Appl. Polym. Sci. 71 (1999) 1133-1138.

[26] A. Okada, A. Usuki, The chemistry of polymer-clay hybrids, Mater. Sci. Eng. C3 (1995) 109-115.

[27] M. W. Noh, D. C. Lee, Synthesis and characterization of PS-clay nanocomposite by emulsion polymerization, Polym. Bull. 42 (1999) 619-626.

[28] P. B. Messersmith, E. P. Giannelis, Synthesis and characterization of layered silicate-epoxy nanocomposites, Chem. Mater. 6 (1994) 1719-1725.

[29] S. D. Burnside, E. P. Giannelis, Synthesis and properties of new poly(dimethylsiloxane) nanocomposites, Chem. Mater. 7 (1995) 1597-1600.

[30] S. J. Wang, C. F. Long, X. Y. Wang, Q. Li, Z. N. Qi, Synthesis and properties of silicone rubber organomontmorillonite hybrid nanocomposites, J. Appl. Polym. Sci. 69 (1998) 1557-1561.

[31] Y. Yang, Z.-K. Zhu, J. Yin, X.-Y. Wang, Z.-E. Qi, Preparation and properties of hybrids of organo-soluble polyimide and montmorillonite with various chemical surface modifications methods, Polymer 40 (1999) 4407-4414.

[32] S. Zhang, A. R. Horrocks, A review of flame retardant polypropylene fibres, Prog. Polym. Sci. 28 (2003) 1517-1538.

[33] J. W. Gilman, Flammability and thermal stability studies of polymer layered-silicate (clay) nanocomposites, Appl. Clay Sci. 15 (1999) 31-49.

[34] J. W. Gilman, T. Kashiwagi, S. Lomakin, E.P. Giannelis, E. Manias, J.D. Lichtenhan, P. Jones, Nanocomposites: radiative gasification and vinyl polymer flammability, in: Proceedings of the 6th European Meeting on Fire Retardancy of Polymeric Materials (FRPM'97), University of Lille, France, 24-26 September 1997, pp. 203-221.

[35] J. W. Gilman, T. Kashiwagi, J. E. T. Brown, S. Lomakin, Flammability studies of polymer layered silicatenanocomposites, SAMPE J. 43 (1998) 1053-1066.

[36] S. Duquesne, C. Jama, M. Le Bras, R. Delobel, P. Recourt, J. M. Gloaguen, Elaboration of EVA-nanoclay systems – characterization, thermal behavior and fire performance, Composites Science and Technology 63 (2003) 1141-1148.

[37] T. Lan, P. D. Kaviratna, T. J. Pinnavaia, On the nature of polyimide-clay hybrid composites, Chem. Mater. 6 (1994) 573-575.

[38] K. Yano, A. Usuki, A. Okada, Synthesis and properties of polyimide-clay hybrid films, J. Polym. Sci. Part A: Polym. Chem. 35 (1997) 2289-2294.

[39] J. F. Timmerman, B. S. Hayes, J. C. Seferis, Nanoclay reinforcement effects on the cryogenic microcracking of carbon fiber/epoxy composites, Comp. Sci. and Tech. 62 (2002) 1249-1258.

[40] M. Kawasumi, N. Hasegawa, A. Usuki, A. Okada, Novel memory effect found in nematic liquid crystal/fine particle system, Liq. Cryst. 21 (1996) 769-776.

[41] M. Kawasumi, A. Usuki, A. Okada, T. Kurauchi, Liquid crystalline composite based on a clay mineral, Mol. Cryst. Liq. Cryst. 281 (1996) 91-103.

[42] Z. Wu, C. Zhou, N. Zhu, The nucleating effect of montmorillonite on crystallization of nylon 1212/montmorillonite nanocomposite, Polymer Testing 21 (2002) 479-483.

[43] N. Sheng, M. C. Boyce, D. M. Parks, G. C. Rutledge, J. I. Abes, R. E. Cohen, Multiscale micromechanical modeling of polymer/clay nanocomposites and the effective clay particle, Polymer 45 (2004) 487-506.

[44] T. X. Liu, Z. H. Liu, K. X. Ma, L. Shen, K. Y. Zeng, C. B. He, Morphology, thermal and mechanical behavior of polyamide 6/layered-silicate nanocomposites, Composites Science and Technology 63 (2003) 331-337.

[45] M. F. Lai, J. K. Kim, Effects of epoxy treatment of organoclay on structure, thermo-mechanical and transport properties of poly(ethylene terephthalate-co-ethylene naphthalate)/organoclay nanocomposites, Polymer 46 (2005) 4722–4734.

[46] J. Ren, Y. X. Huang, Y. Liu, X. Z. Tang, Preparation, characterization and properties of poly(vinyl chloride)/compatibilizer/organophilic-montmorillonite nanocomposites by melt intercalation, Polymer Testing 24 (2005) 316-323.

[47] V. G. Gregoriou, G. Kandilioti, S. T. Bollas, Chain conformational transformations in syndiotactic polypropylene/layered silicate nanocomposites during mechanical elongation and thermal treatment, Polymer 46 (2005) 11340–11350.

[48] S. G. Lei, S. V. Hoa, M.-T. Ton-That, Effect of clay types on the processing and properties of polypropylene nanocomposites, Composites Science and Technology 66 (2006) 1274–1279.

[49] J. Morawiec, A. Pawlak, M. Slouf, A. Galeski, E. Piorkowska, N. Krasnikowa, Preparation and properties of compatibilized LDPE/organo-modified montmorillonite nanocomposites, European Polymer Journal 41 (2005) 1115–1122.

[50] M. A. Osman, J. E. P. Rupp, U. W. Suter, Tensile properties of polyethylene-layered silicate nanocomposites, Polymer 46 (2005) 1653–1660.

[51] S. Balakrishnan, P. R. Start, D. Raghavan, S. D. Hudson, The influence of clay and elastomer concentration on the morphology and fracture energy of preformed acrylic rubber dispersed clay filled epoxy nanocomposites, Polymer 46 (2005) 11255–11262.

[52] R. Hadal, Q. Yuan, J. P. Jog, R. D. K. Misra, On stress whitening during surface deformation in clay-containing polymer nanocomposites: A microstructural approach, Materials Science and Engineering A 418 (2006) 268–281.

[53] G. E. Fantner et al., Hierarchical interconnections in the nano-composite material bone: Fibrillar cross-links resist fracture on several length scales, Composites Science and Technology 66 (2006) 1205-1211.

[54] W. Vogel, Perspective of the development of bioactive glass ceramics for biomedical applications, Journal of Non-Crystalline Solids 73 (1985) 593-597.

[55] G. Biresaw, C. J. Carriere, Compatibility and mechanical properties of blends of polystyrene with biodegradable polyesters, Composites: Part A 35 (2004) 313-320.

[56] K. T. Lau, M. Lu, J. Q. Qi, D. D. Zhao, H. Y. Cheung, C. K. Lam, H. L. Li, Cobalt hydroxide colloidal particles precipitation on nanoclay layers for the formation of novel nanocomposites of carbon nanotubes/nanoclay, Composites Science and Technology 66 (2006) 450-458.

Vita

Man-Wai Ho was born and raised in Hong Kong. He entered The Chinese University of Hong Kong in the Department of Physics in 1996. He gradually developed a love of science and the attitude to be a scientist. He graduated with a Bachelor of Science in Physics in 1999. In his final year project as an undergraduate, he found fascinating in doing experiments and materials research. Then, he decided to go to the graduate school to start his Master of Philosophy in the same place. After 2 years of hard research work, he learnt a lot of experimental skills and performed independent research. His attitude towards Physics helped him to struggle to do accurate, neat, delicate and precise experiments. He was proud to be able to build a hot-press furnace to complete his materials research in Aluminum-based composites.

However, after he graduated with a master degree in 2001, he couldn't go for his doctoral degree immediately, because he wanted to study oversea. Then, he spent 1 year worked as a graduate assistant for his supervisor and at the same time prepared for the necessary examinations required to study in USA.

Fortunately, he got accepted in the University of New Orleans in 2002 and began his Doctor of Philosophy in the Department of Mechanical Engineering at the age of 25. He explored himself and broadened his horizons both in academic and real life experiences during his stay in US. After 4 years of heavy coursework loads, examinations and research work, he was going to graduate in December 2006. By that time, he had been spending 10 years of life in the University. At the same time, it will be a great opportunity for him to start his own career.